The background image shows a complex solar flare simulation. It features intricate, swirling plasma filaments in shades of yellow, orange, and white against a darker, textured background. A prominent, bright white filament extends from the bottom left towards the center, with several smaller filaments branching off it. The overall effect is one of intense, turbulent energy release.

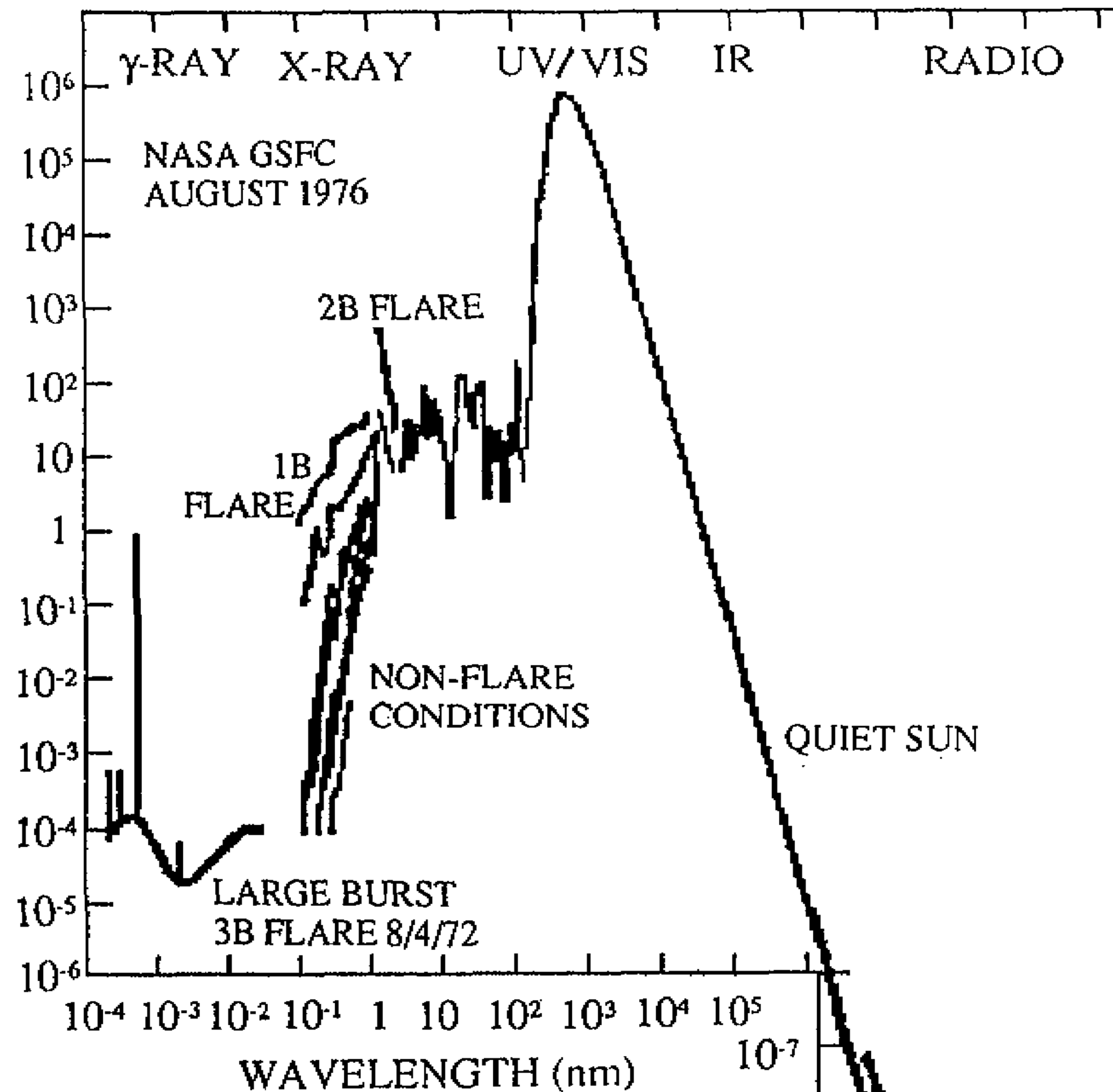
Testing the Physics of Solar and Stellar Flares with NASA's Solar Dynamics Observatory and Radiative MHD Simulations

Mark Cheung, Lockheed Martin Solar & Astrophysics Lab, Palo Alto, CA

Solar Astronomy 101

Most Salient Observational Features about the Sun

- It rotates, but not as a solid body. The equator rotates faster than the poles (use helioseismology to probe the interior).
- It has sunspots. The number of sunspots waxes and wanes with an eleven year cycle.
- Magnetic fields pervade the entire Sun.
- The Sun is a **panchromatic** astrophysical object.
- The hot corona consists of loops anchored at/near sunspots.
- Total eclipses are way cool (forget about partial ones). 😎



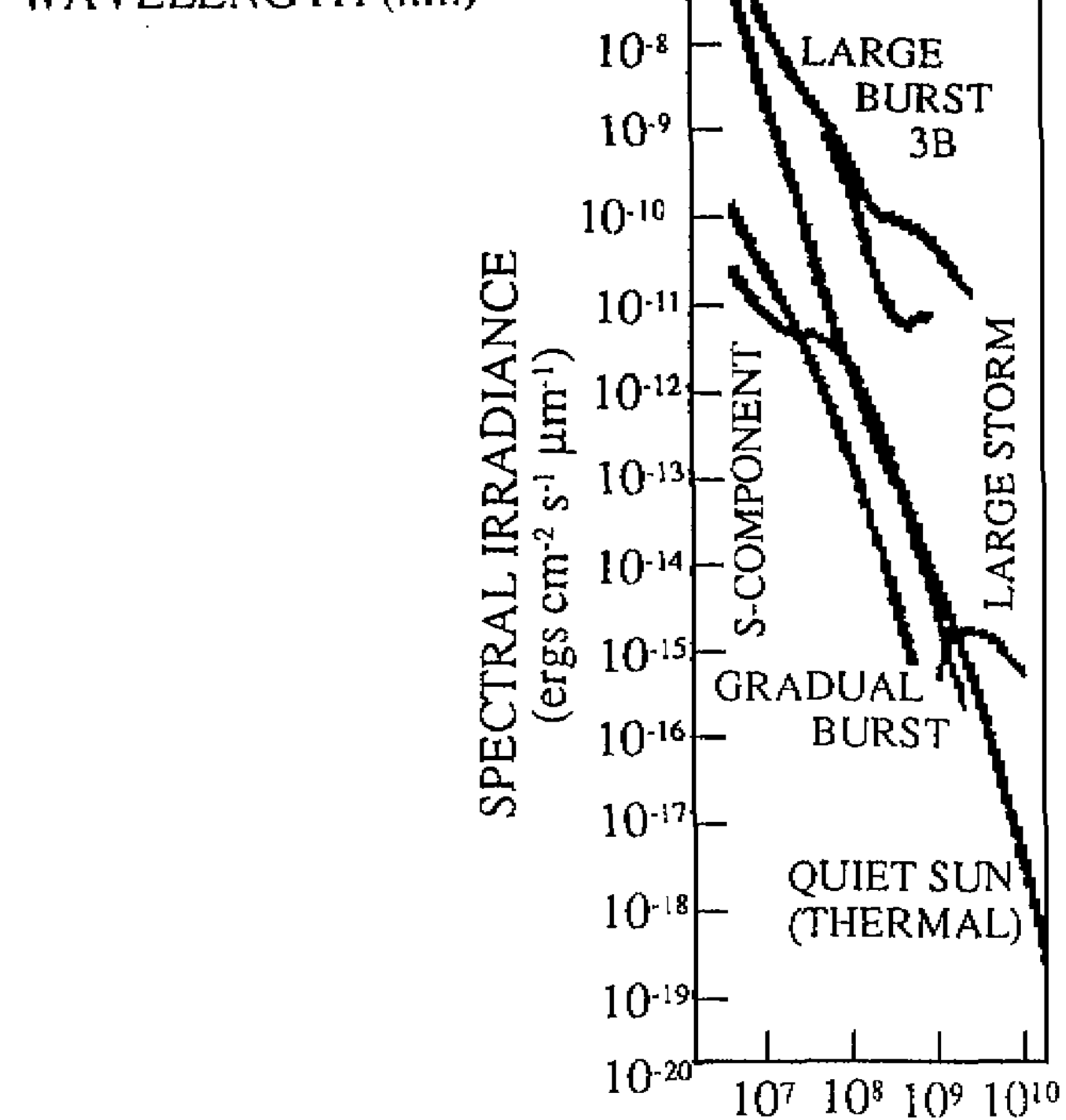
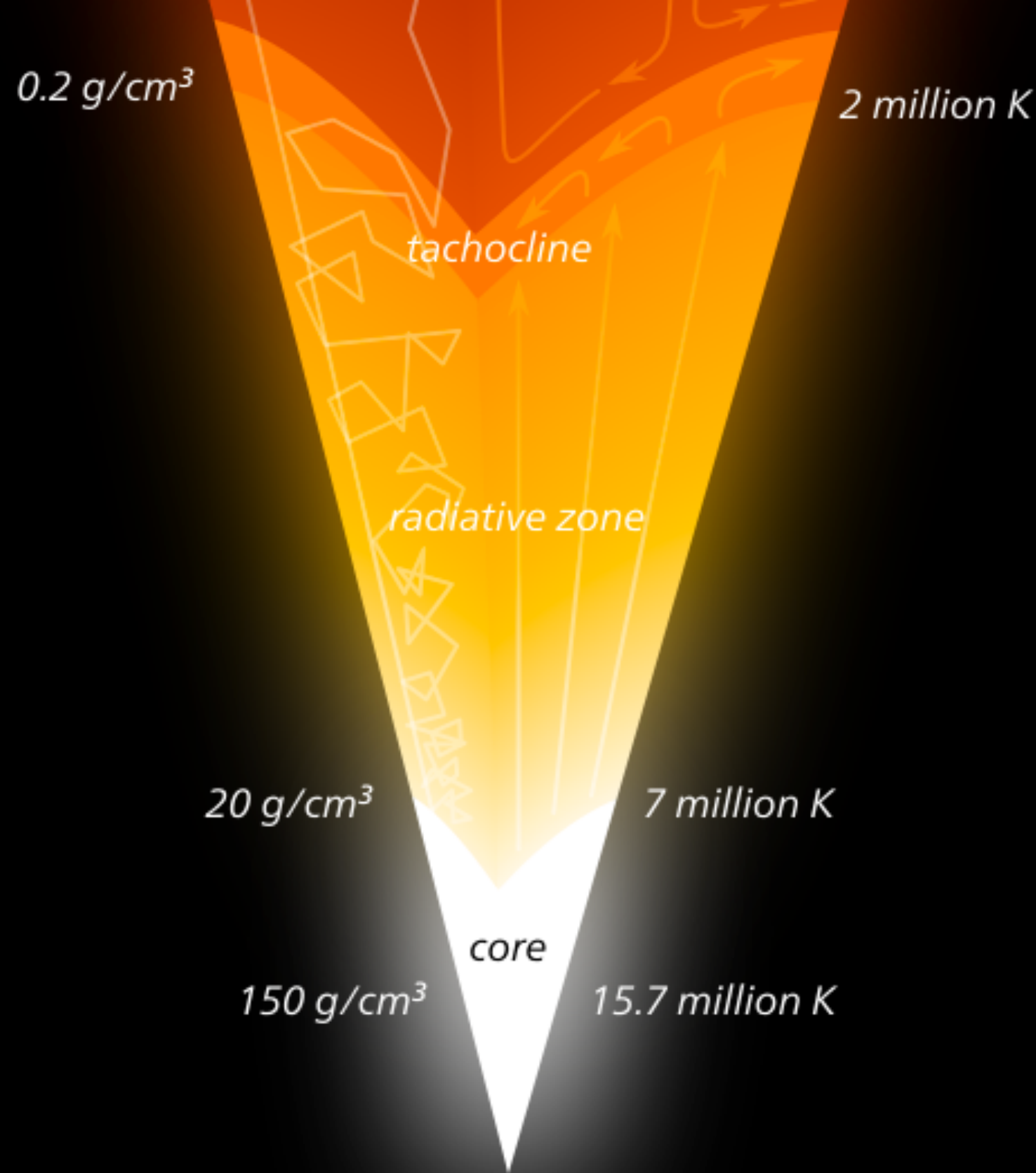


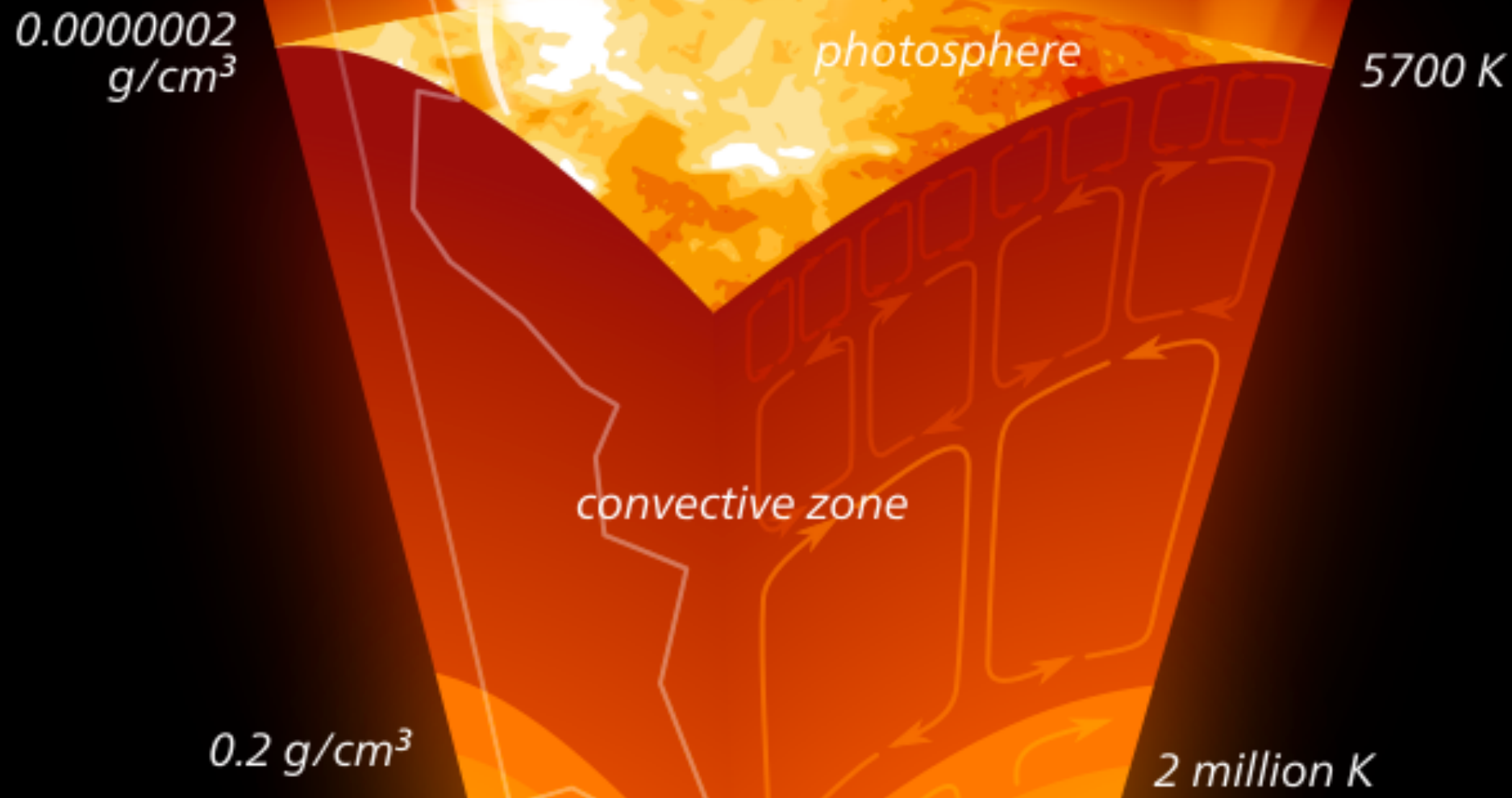
Fig. 3. The solar spectrum from gamma rays to radio wavelengths from *White* [1977].



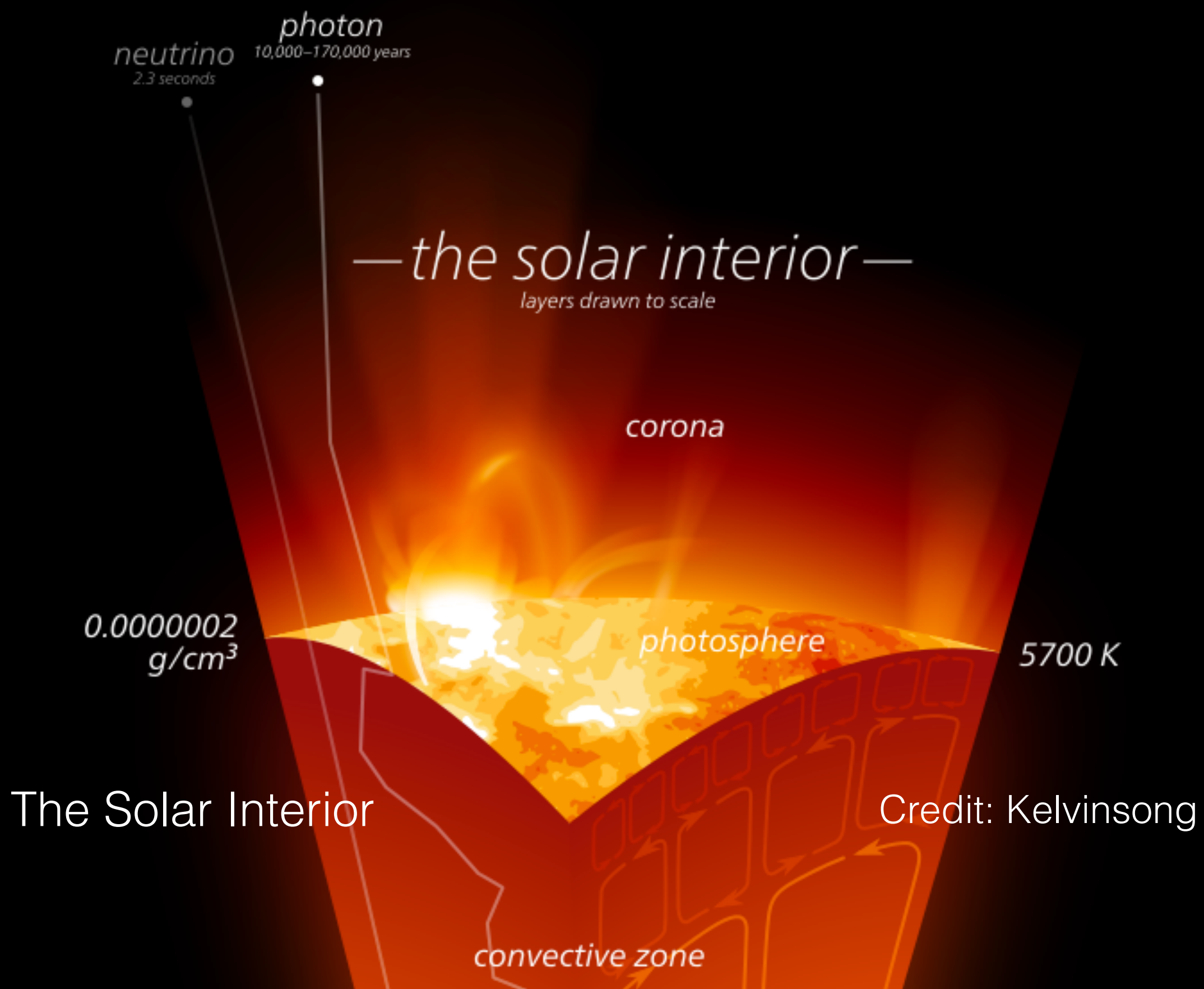
The Solar Interior

Credit: Kelvinsong

The Solar Interior



Credit: Kelvinsong



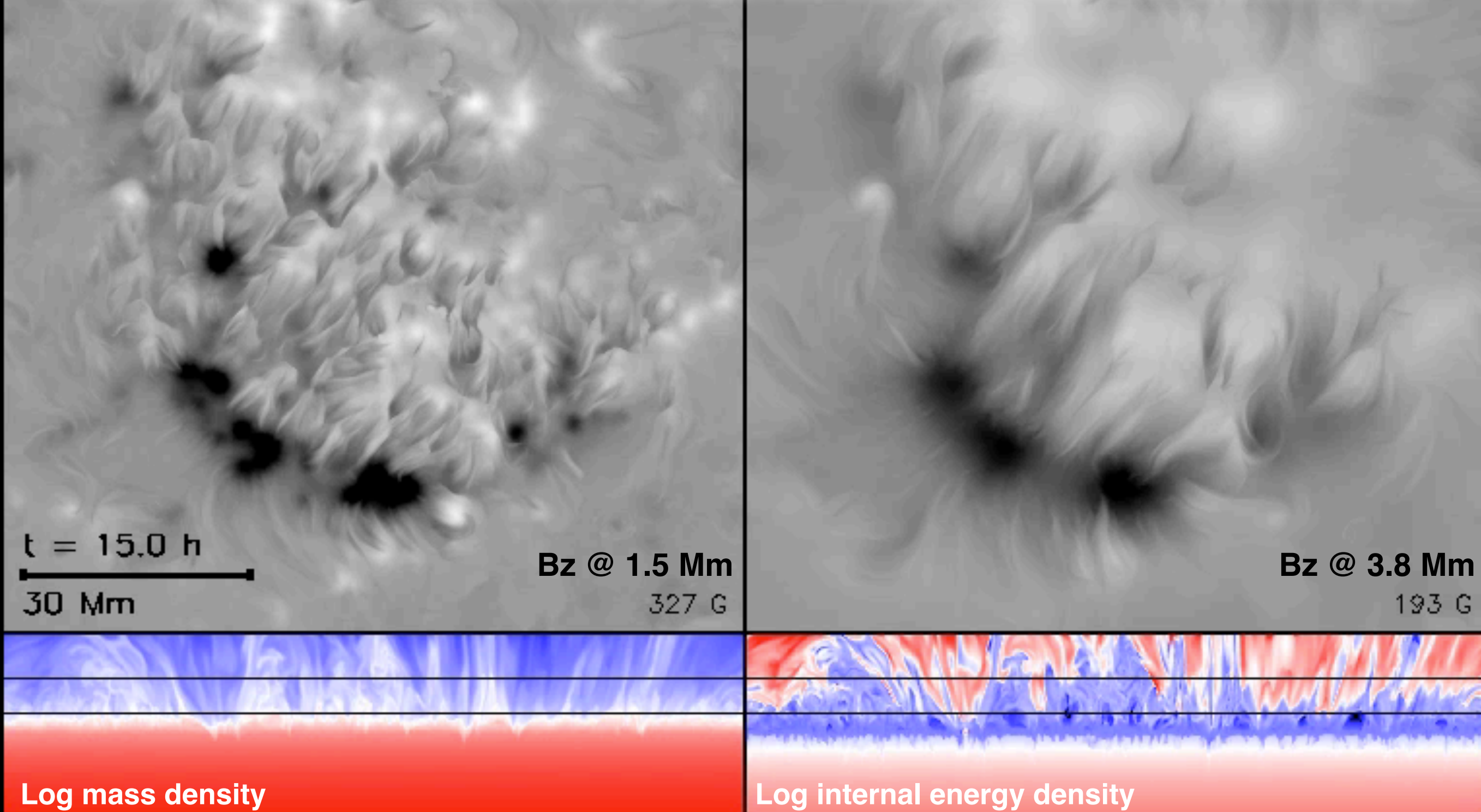
The Coronal Heating Conundrum

- There is lots of energy available.
- The solar atmosphere is strongly stratified.
- Radiative flux at photosphere $\sim 6 \times 10^{10} \text{ erg cm}^{-2} \text{ s}^{-1}$
- Power required to sustain the corona $\sim 10^{5-7} \text{ erg cm}^{-2} \text{ s}^{-1}$
- But that doesn't mean the coronal heating conundrum is uninteresting. Analogy: Food supply in the world.

15 million K	Temperature	1 million K
150 g cm ⁻³	Mass Density	1x10 ⁻¹⁵ g cm ⁻³
2x10 ¹⁷ erg cm ⁻³	Internal Energy Density/Pressure	0.1 erg cm ⁻³

Radiative MHD simulation of AR formation* (M. Rempel)

*work done for NASA's Heliophysics Grand Challenges Research project (LMSAL/NCAR/SAO/BAERI/U Oslo)

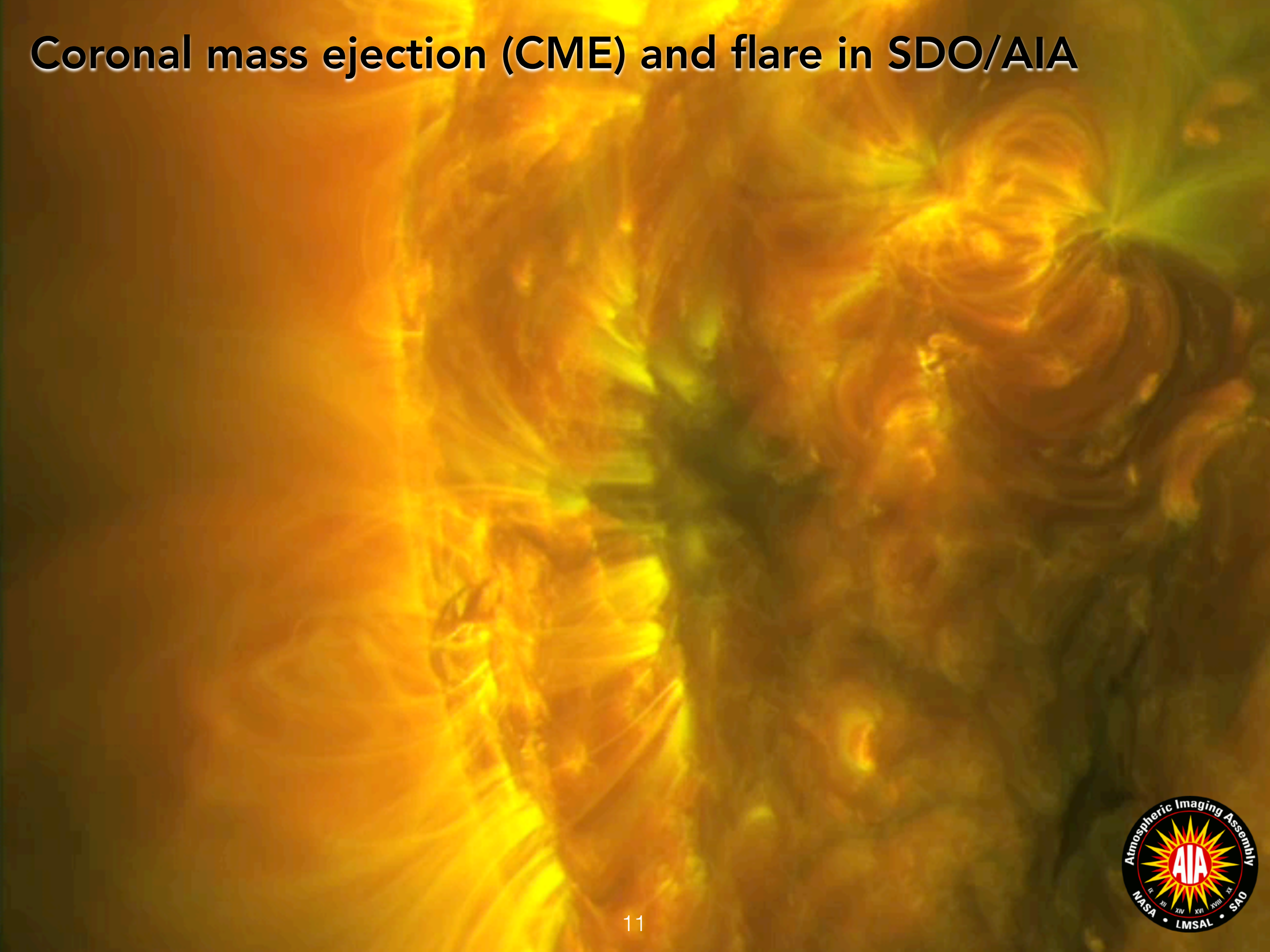


Radiatively-driven, turbulent, magnetoconvection generates magnetoacoustic fluctuations that dissipate to heat the chromosphere and corona and drives the solar wind. *c.f. MRI-driven turbulence causing disk winds; e.g. Miller & Stone 2000 ... many references ... Takasao et al. 2018*

Broad Science Questions

- What are the physical mechanisms that:
 - drive the build-up of magnetic energy in the solar corona to cause flares and eruptions?
 - channel the abrupt release of stored magnetic energy into other forms, which are ultimately responsible for the salient observational signatures common to flares (e.g. increase in X-ray and EUV fluxes by orders of magnitudes)?
- How, and what do we learn about the temperature structure and evolution of coronal (namely million K) plasma using EUV and X-ray observations?
- What lessons do we learn from studying the solar atmosphere that can be applied to other astrophysical systems, e.g. stellar activity?
- Heads-up: This talk does not cover particle acceleration.

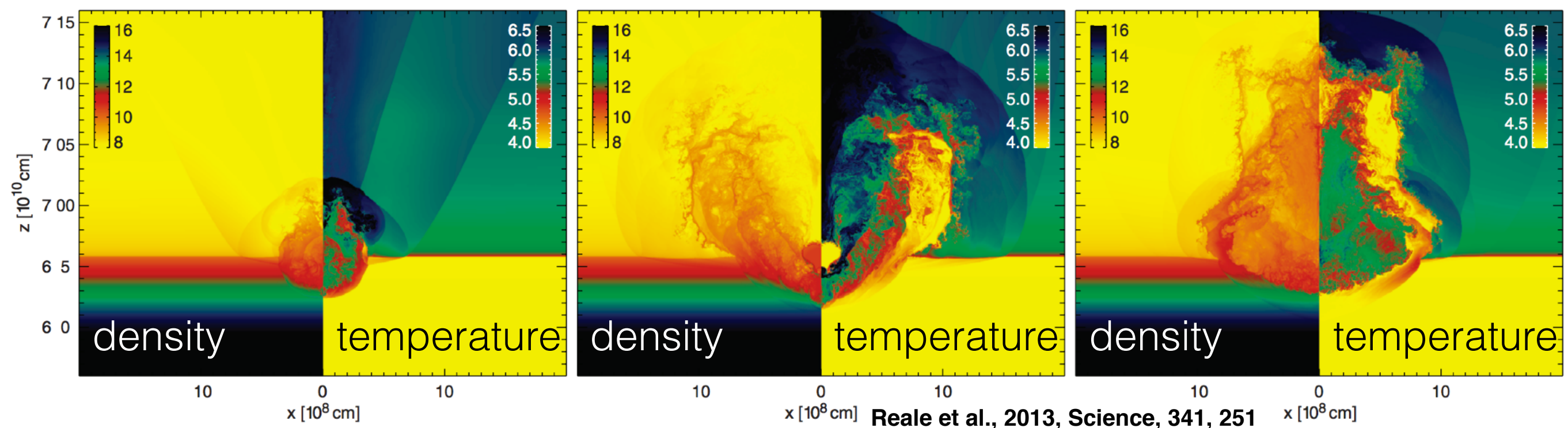
Coronal mass ejection (CME) and flare in SDO/AIA



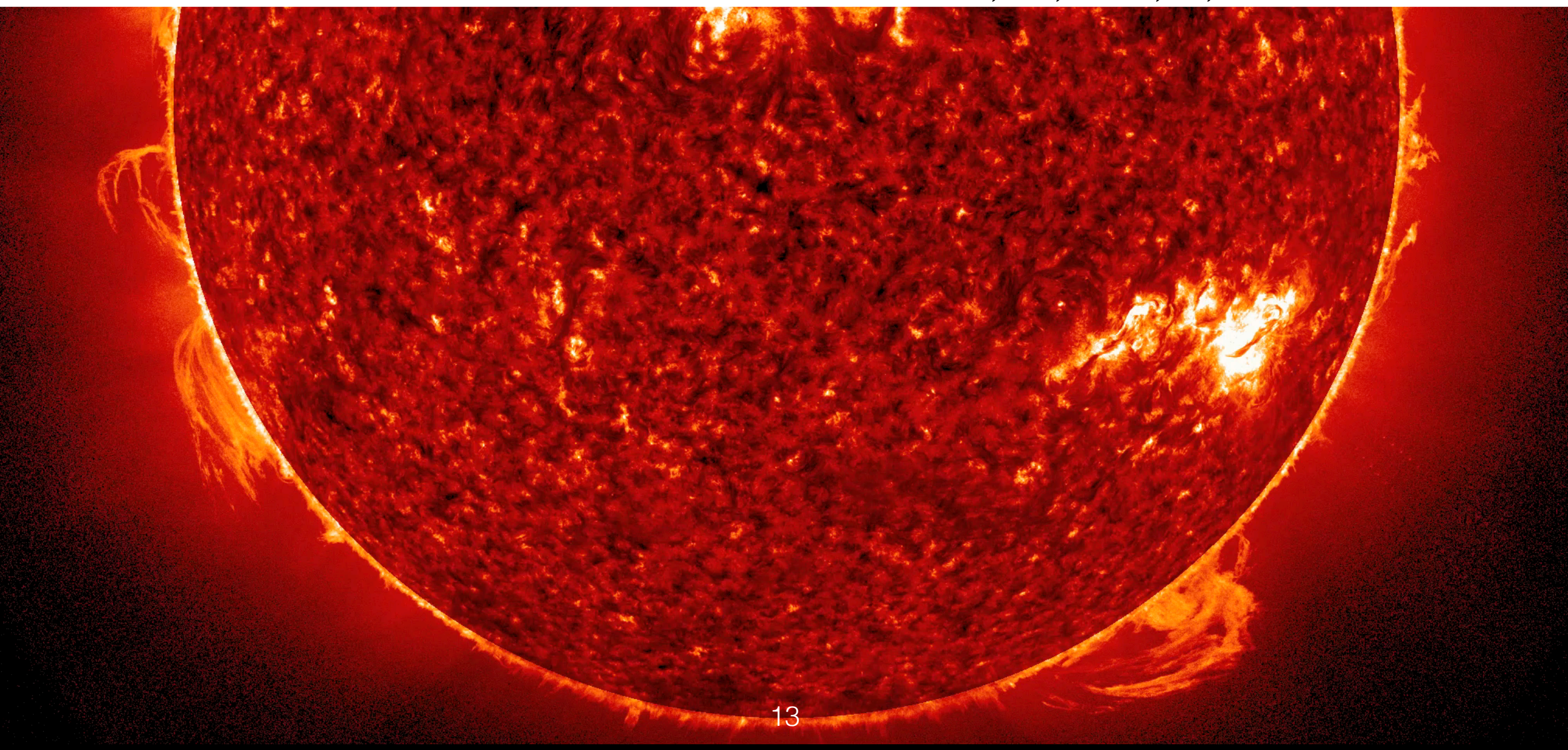
Downs et al.
"Probing the solar
magnetic field with
a sungrazing
comet", *Science*,
340, 1196 (2013)

NASA SDO and
STEREO EUV
observations of the
2011 swing-by of
Comet Lovejoy,
compared with
magnetic coronal
modeling.

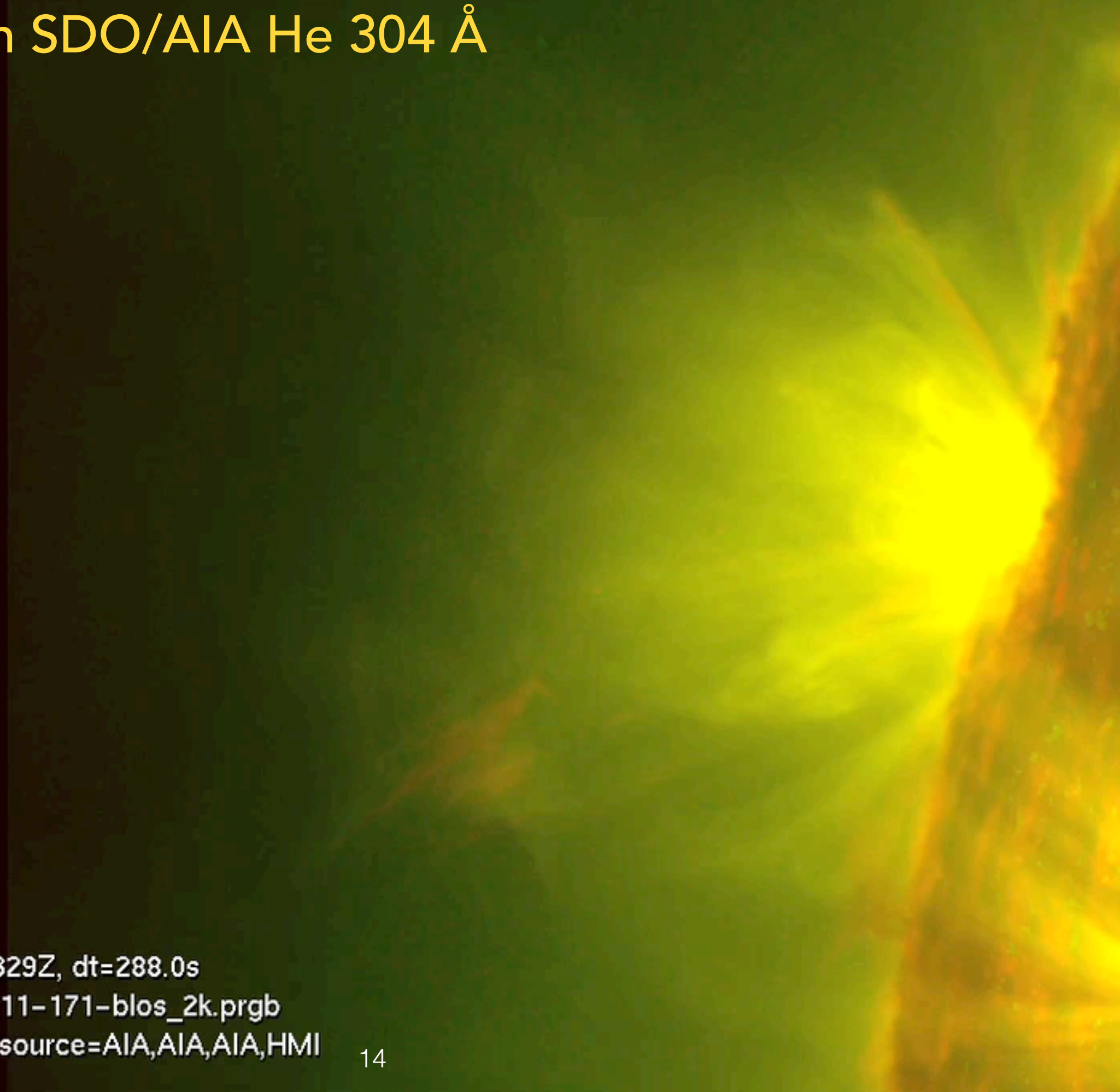
See also Bryans &
Pesnell (2012) and
McCauley et al.
(2013) for emission
mechanisms from
outgassed material.



Reale et al., 2013, Science, 341, 251



Coronal rain in SDO/AIA He 304 Å



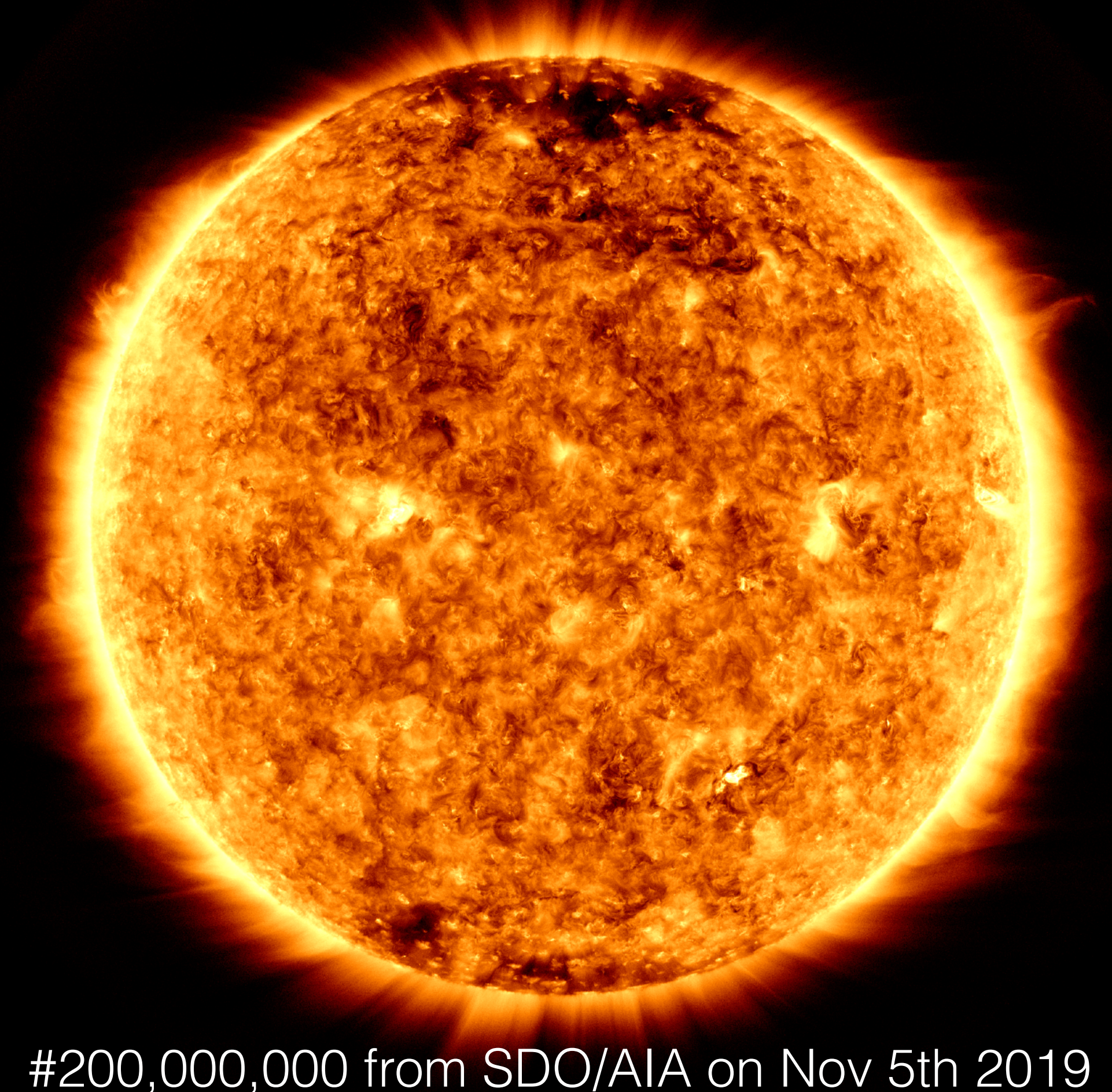
Time: 2014-04-11T18:00:03.329Z, dt=288.0s
aia_20140411T180003_304-211-171-blos_2k.prgb
channel=304, 211, 171, 6173, source=AIA,AIA,AIA,HMI

SDO's main goal is to understand, driving toward a predictive capability, the solar variations that influence life on Earth and humanity's technological systems.



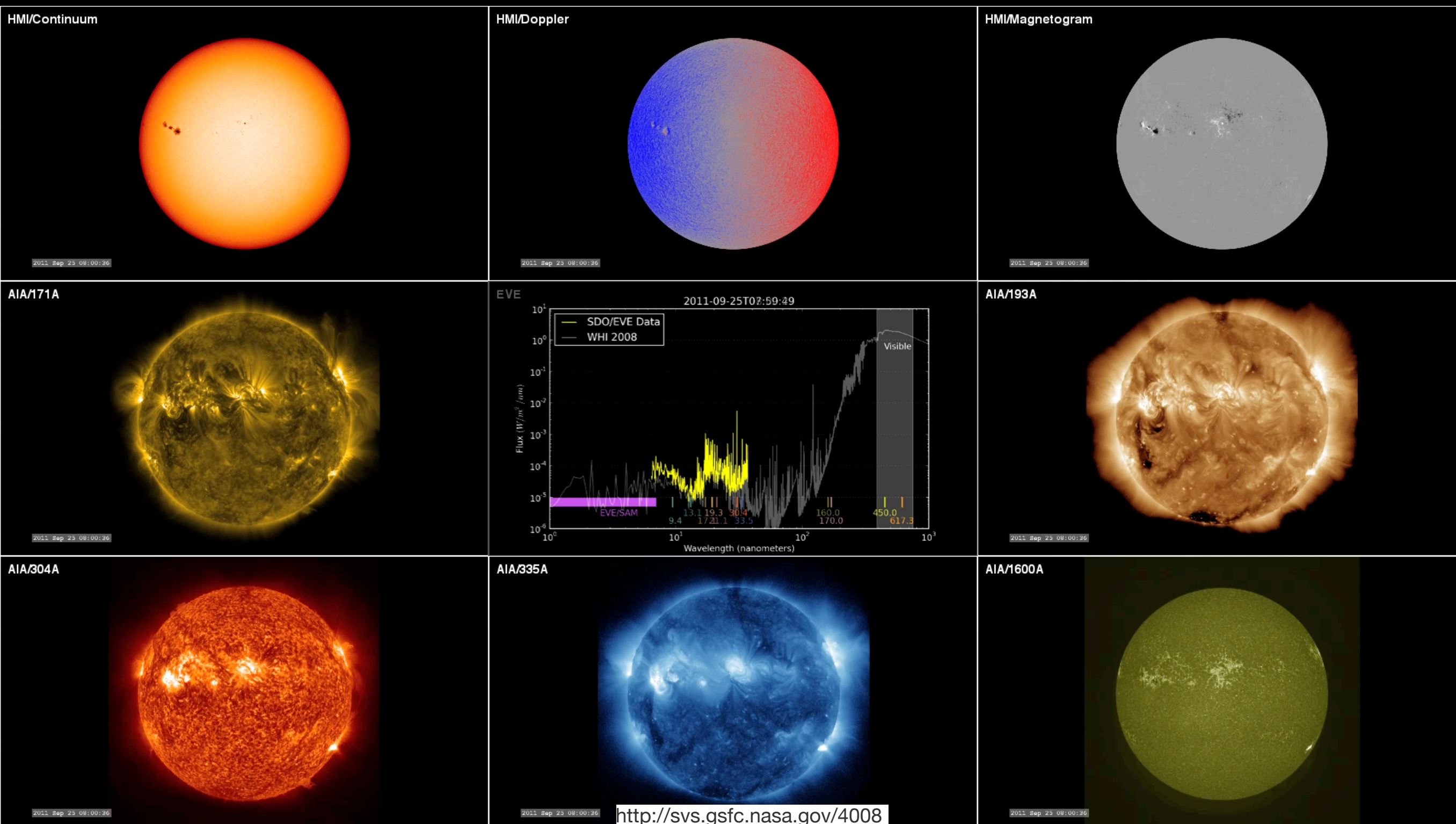
solar dynamics observatory

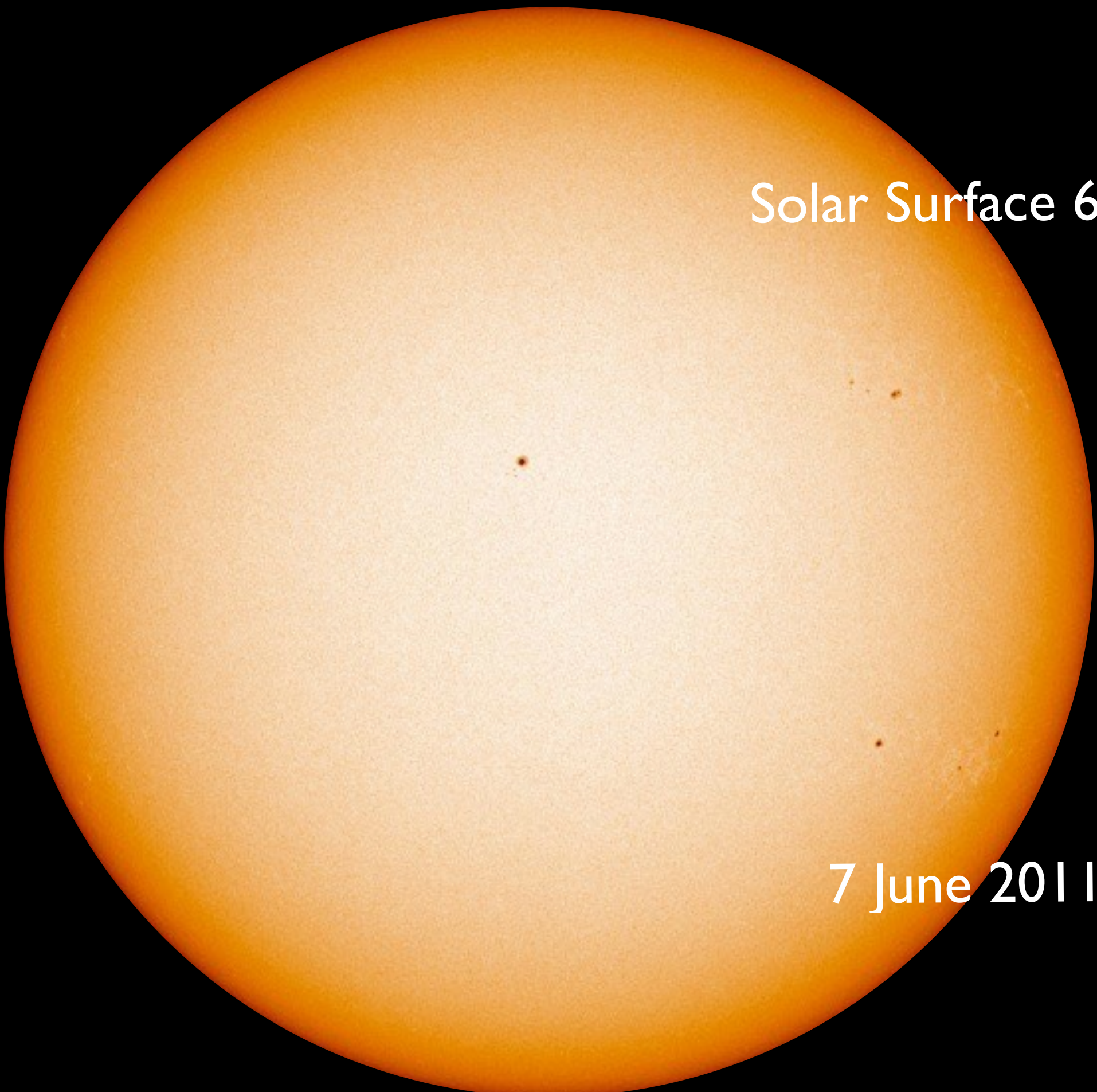
**SDO images the sun's surface, atmosphere and interior.
The mission generates 2 terabytes worth of science data everyday.**



#200,000,000 from SDO/AIA on Nov 5th 2019

NASA SDO Data: A treasure trove of information

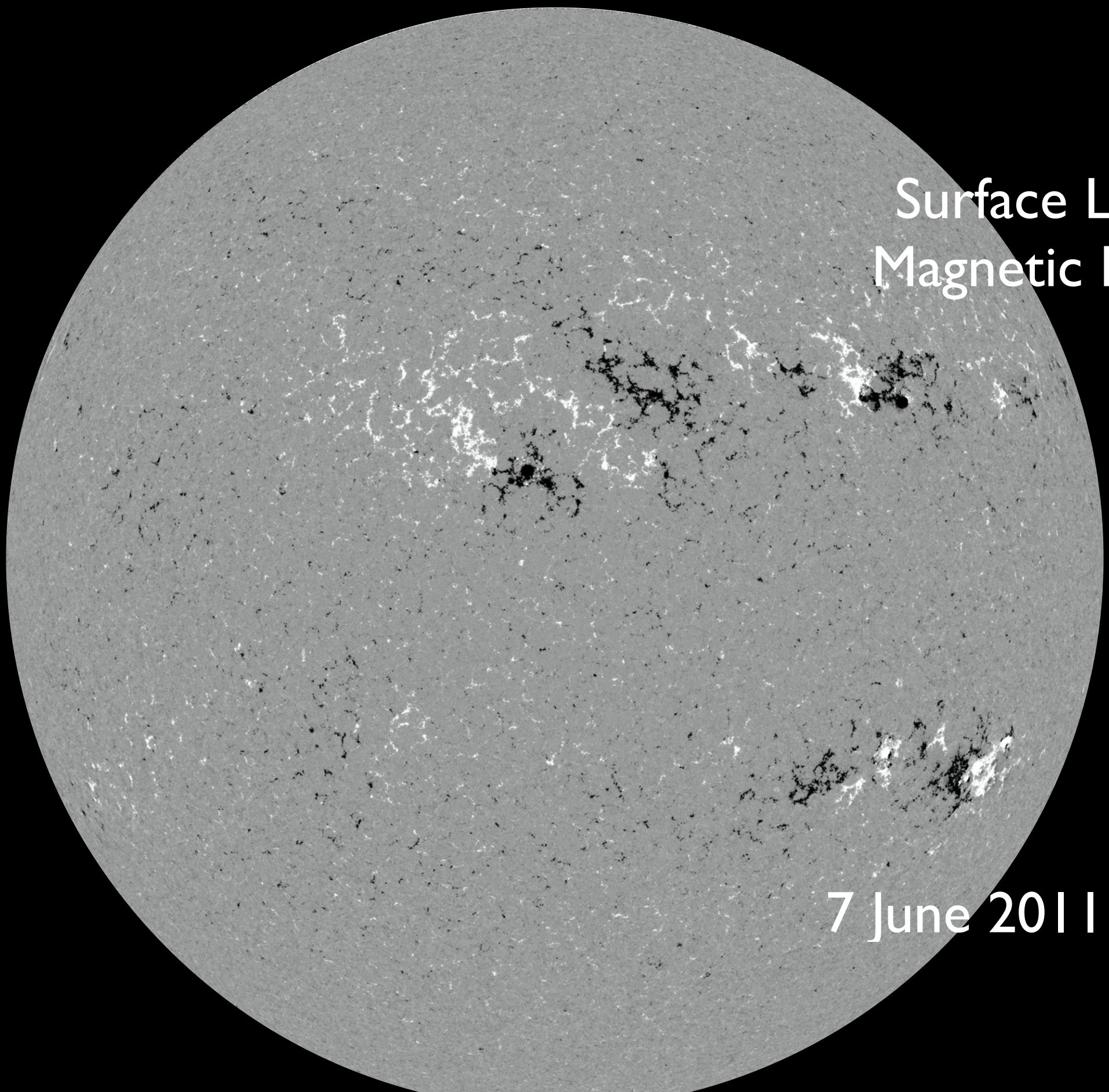




Solar Surface 6,000 K

7 June 2011 7:48:08

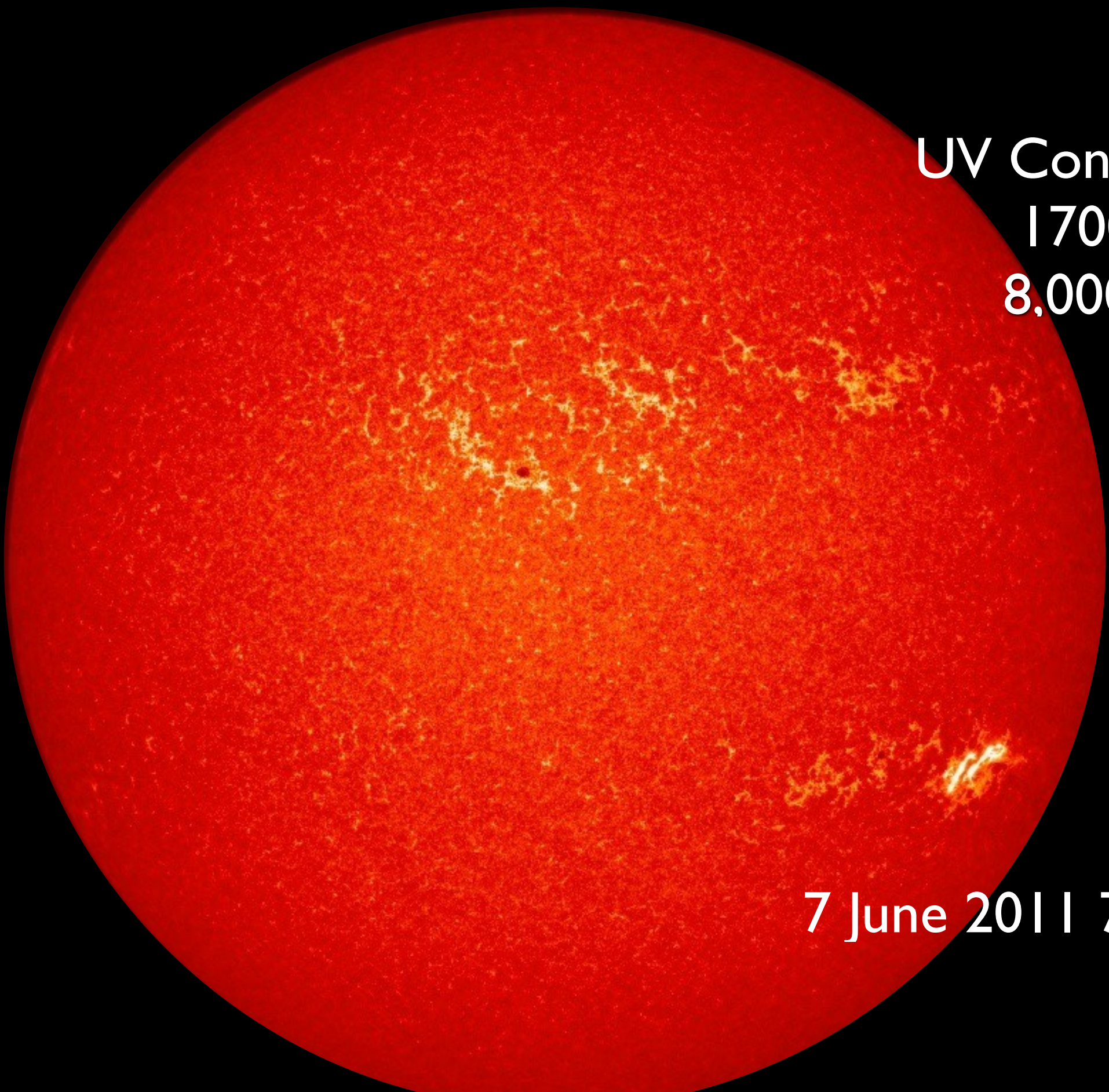
HMI/Stanford



Surface LOS
Magnetic Field

7 June 2011 7:48:08

HMI/Stanford



UV Continuum
1700Å
8,000 K

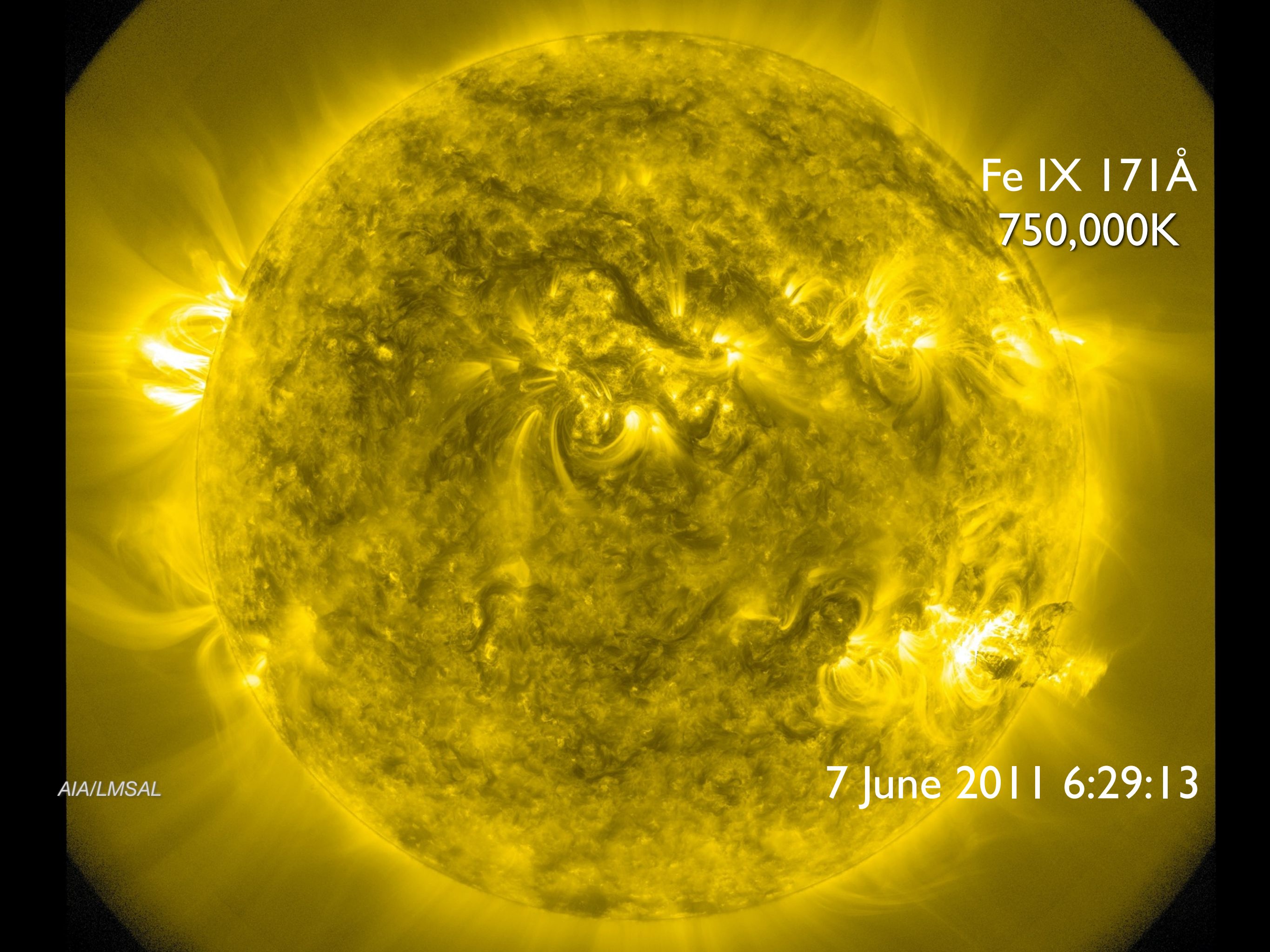
7 June 2011 7:29:20

AIA/LMSAL

He II 304Å
90,000 K

7 June 2011 6:29:33

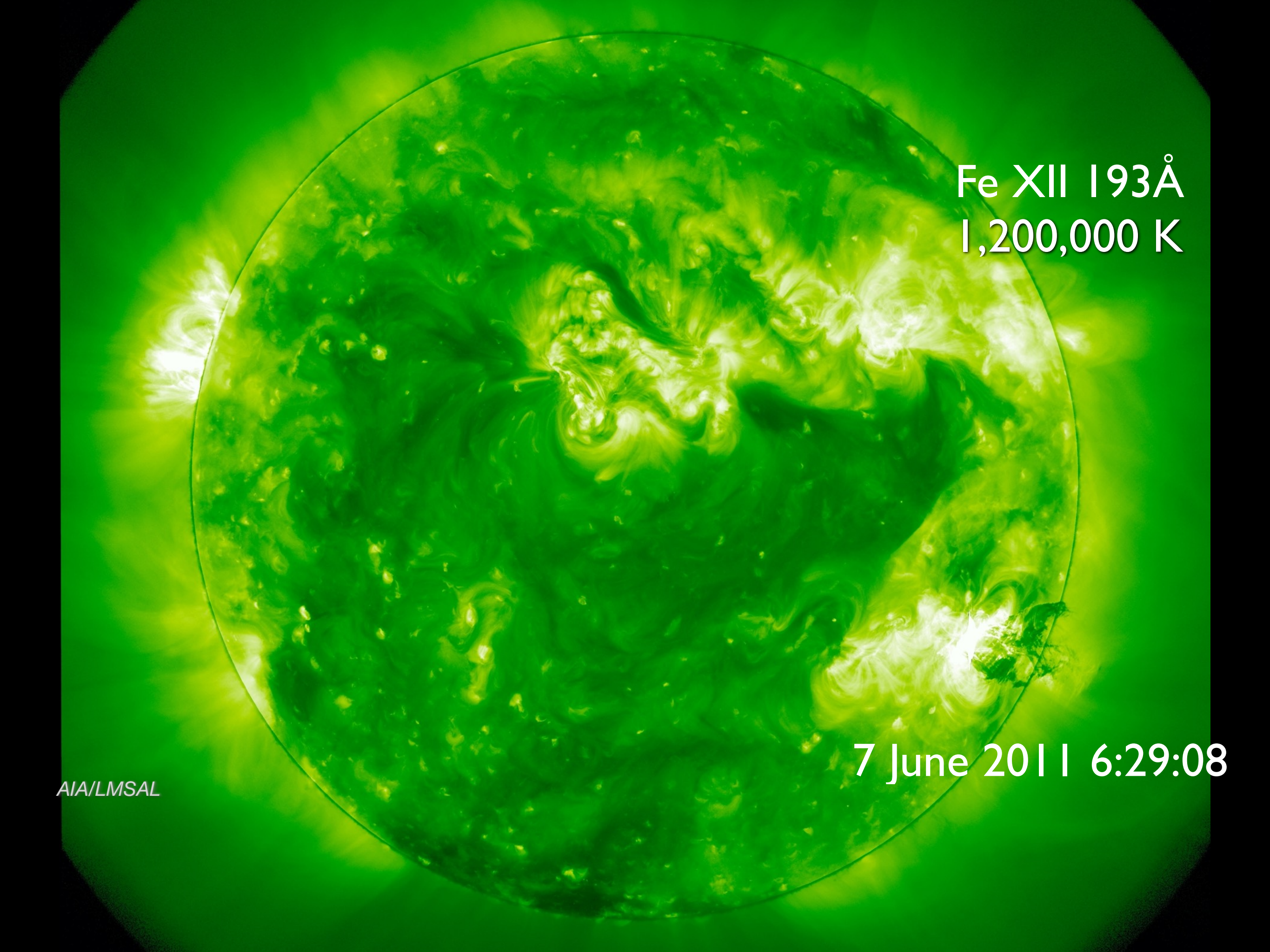
AIA/LMSAL



Fe IX 171Å
750,000K

AIA/LMSAL

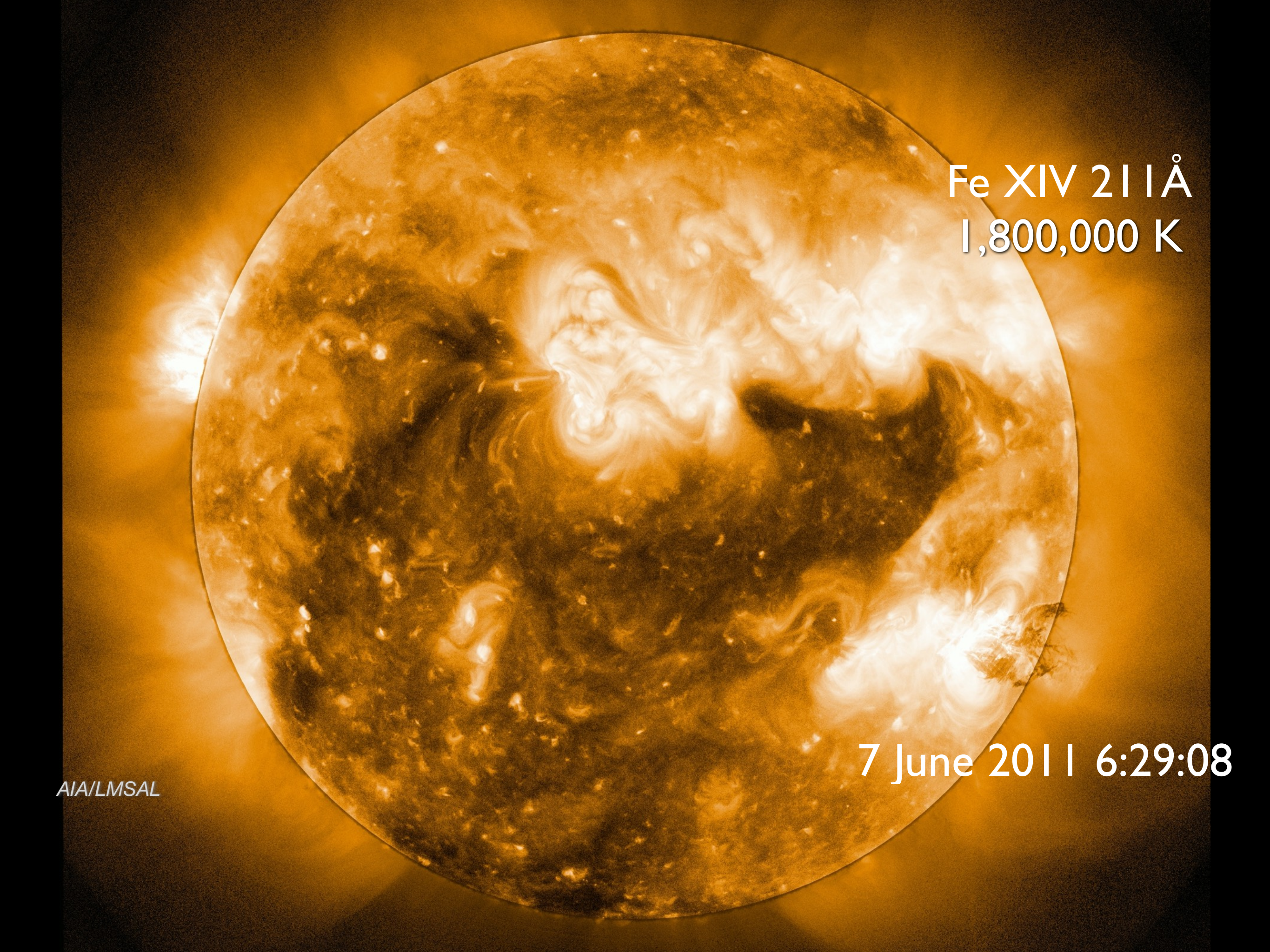
7 June 2011 6:29:13

A green-tinted solar image showing the Sun's surface and its surrounding atmosphere. Several bright, white and yellow solar flares are visible, particularly on the left and right sides. A large, complex solar prominence extends from the bottom right towards the center. The background is a dark green color.

Fe XII 193Å
1,200,000 K

7 June 2011 6:29:08

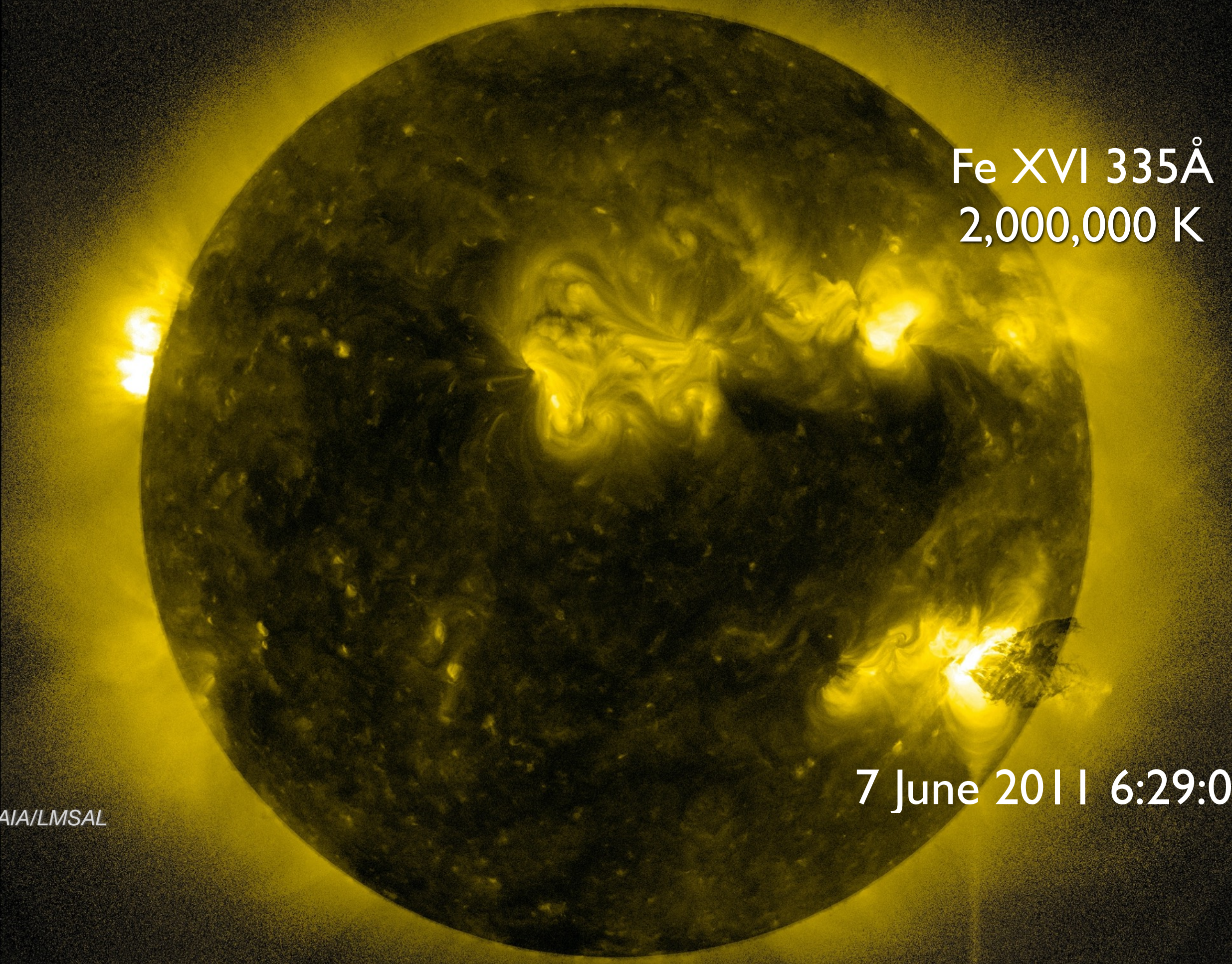
AIA/LMSAL



Fe XIV 211Å
1,800,000 K

7 June 2011 6:29:08

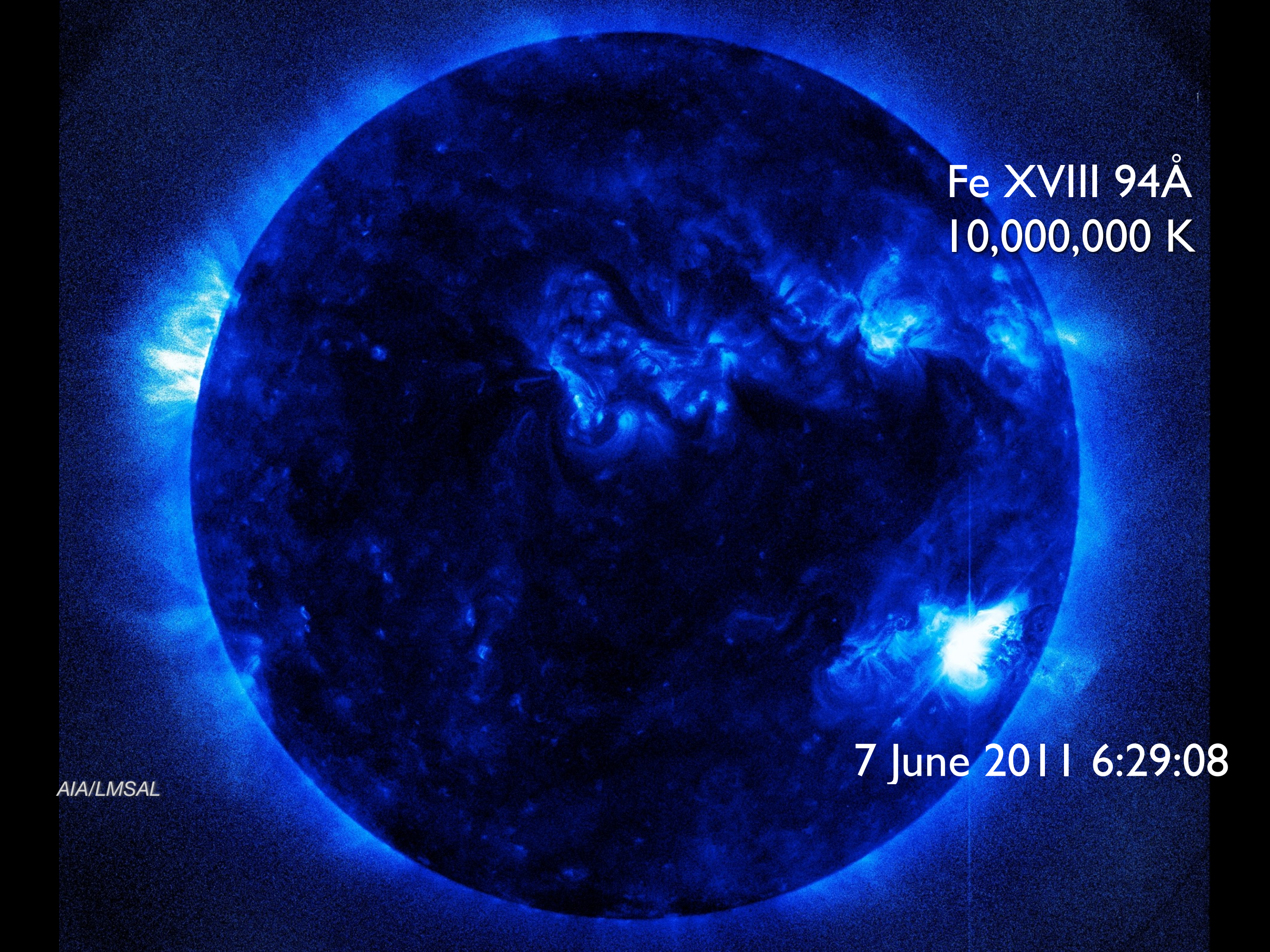
AIA/LMSAL

A solar flare is captured in a yellow-tinted image of the Sun's surface. The flare is located on the upper right quadrant of the Sun, showing a bright, turbulent plasma cloud expanding from a central bright point. The surrounding solar atmosphere is visible as a darker yellow glow.

Fe XVI 335Å
2,000,000 K

7 June 2011 6:29:08

AIA/LMSAL

A high-contrast, blue-toned image of the Sun's surface and atmosphere. The Sun's disk is mostly dark, with bright, glowing plasma filaments and loops visible against the black background of space. A large, intense white-light flare is visible on the left side of the Sun, with a bright, circular core and surrounding plasma. The overall scene is dynamic and energetic.

Fe XVIII 94Å
10,000,000 K

7 June 2011 6:29:08

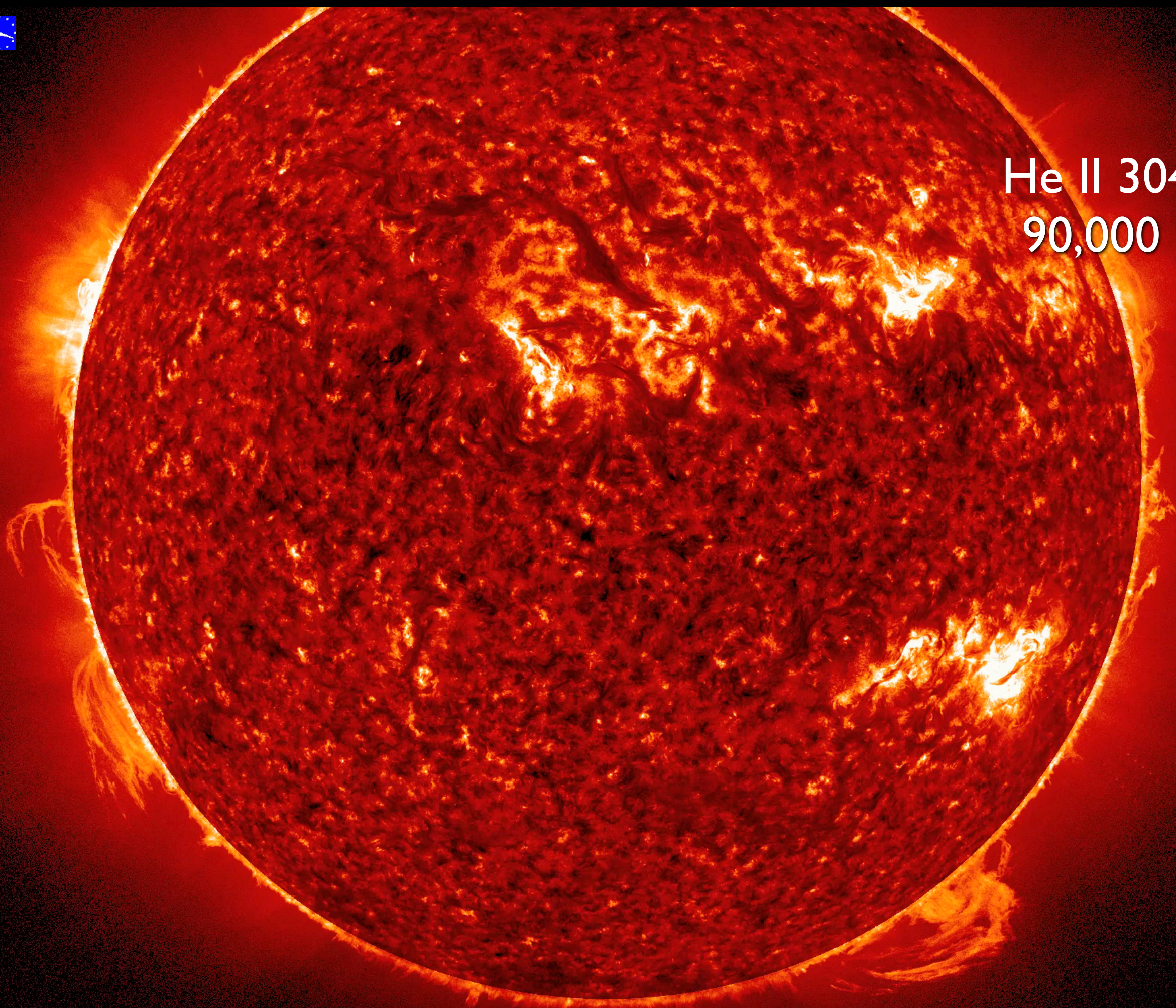
AIA/LMSAL

2011-Jun-07
06:18:34



AIA 304A

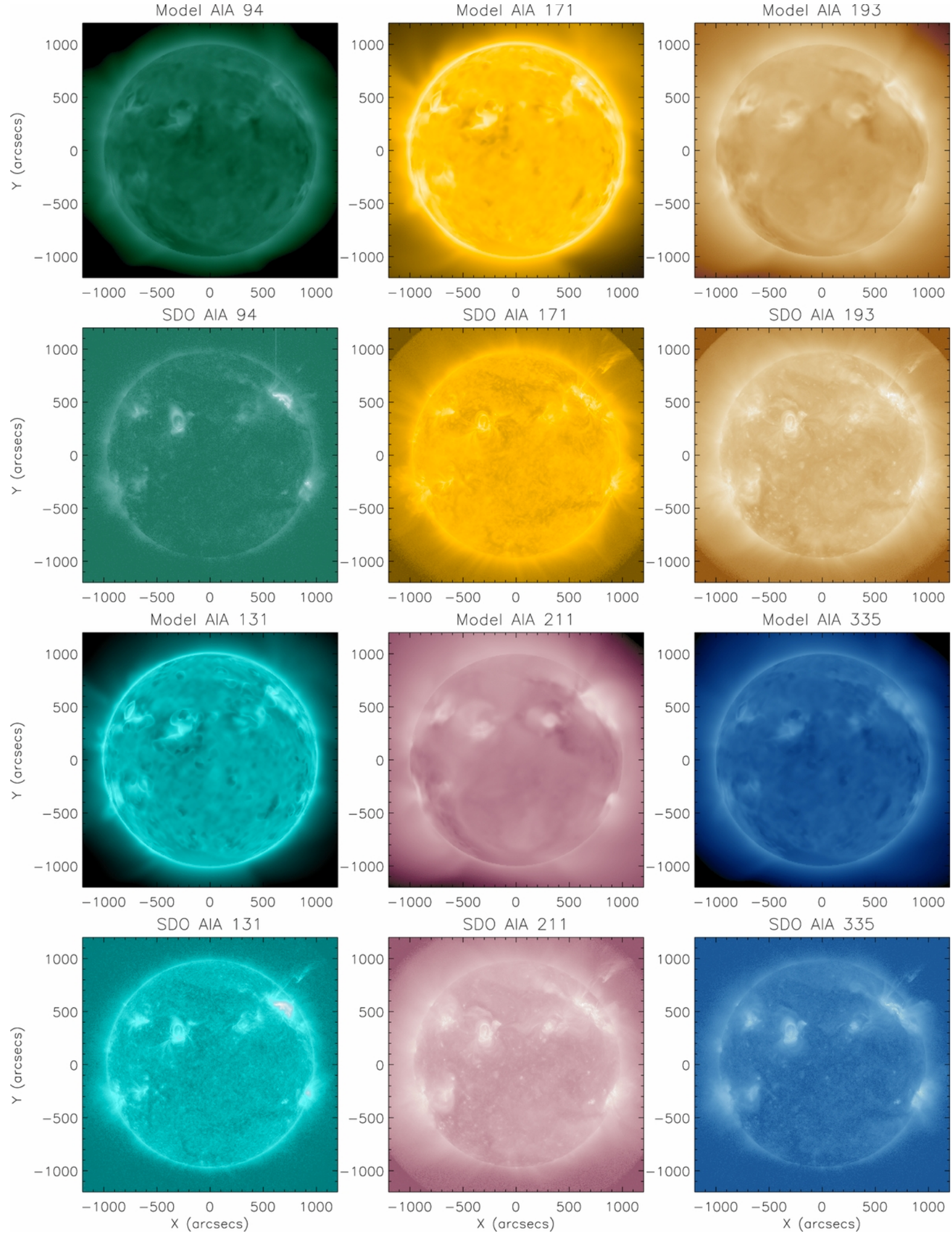
He II 304Å
90,000 K



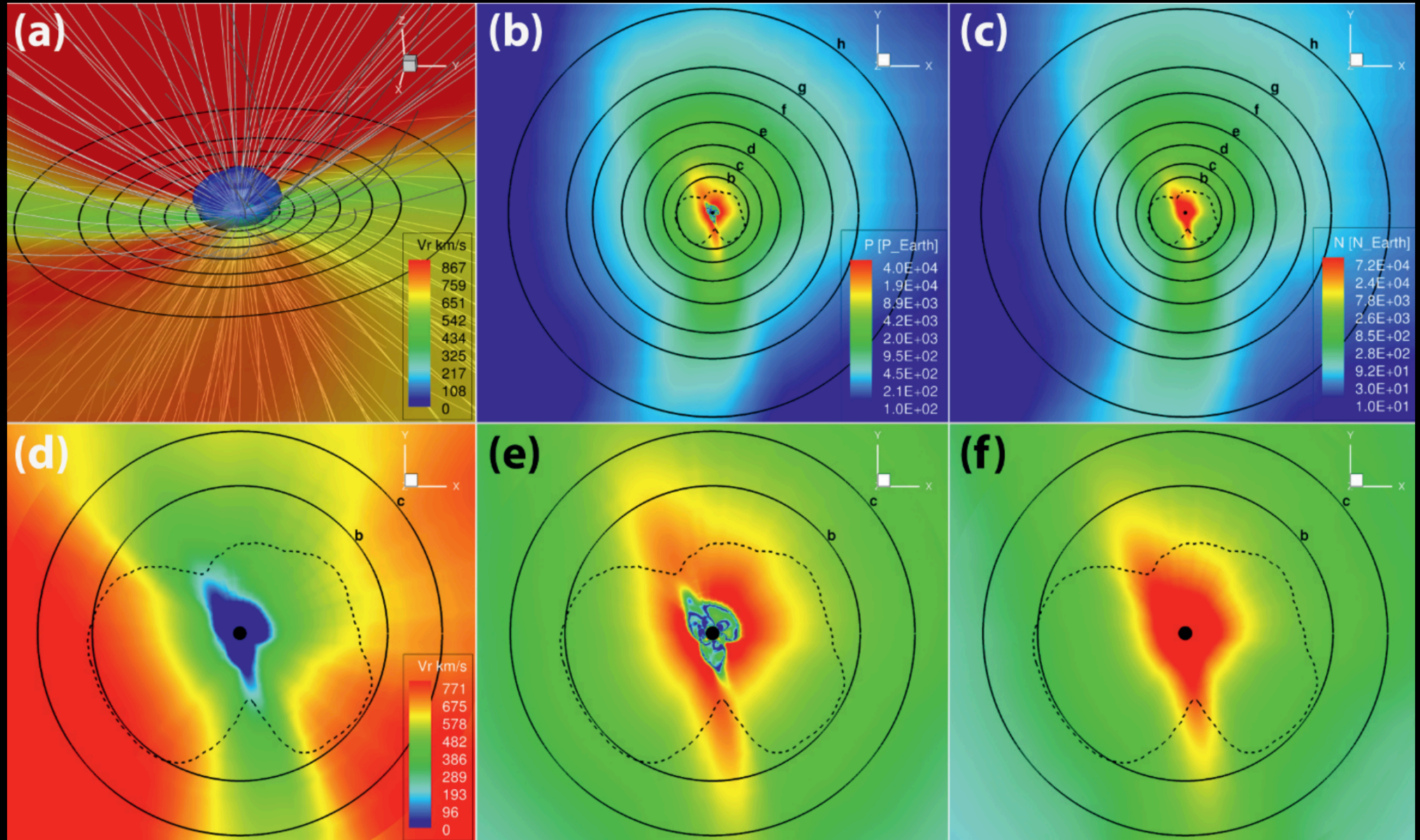
Alfvén Wave Solar Model (AWSOM)

van der Holst et al.
2014ApJ...782...81V

- Fully-compressible MHD equations + Alfvén wave propagation and dissipation.
- Used AIA (and STEREO) EUV images to validate the Alfvén wave heating model (as opposed to an analytical spatially-dependent heating model).
- See Alvarado-Gómez et al. (2016) for application to stellar winds of exoplanet host stars: HD 1237, HD 22049, and HD 147513.



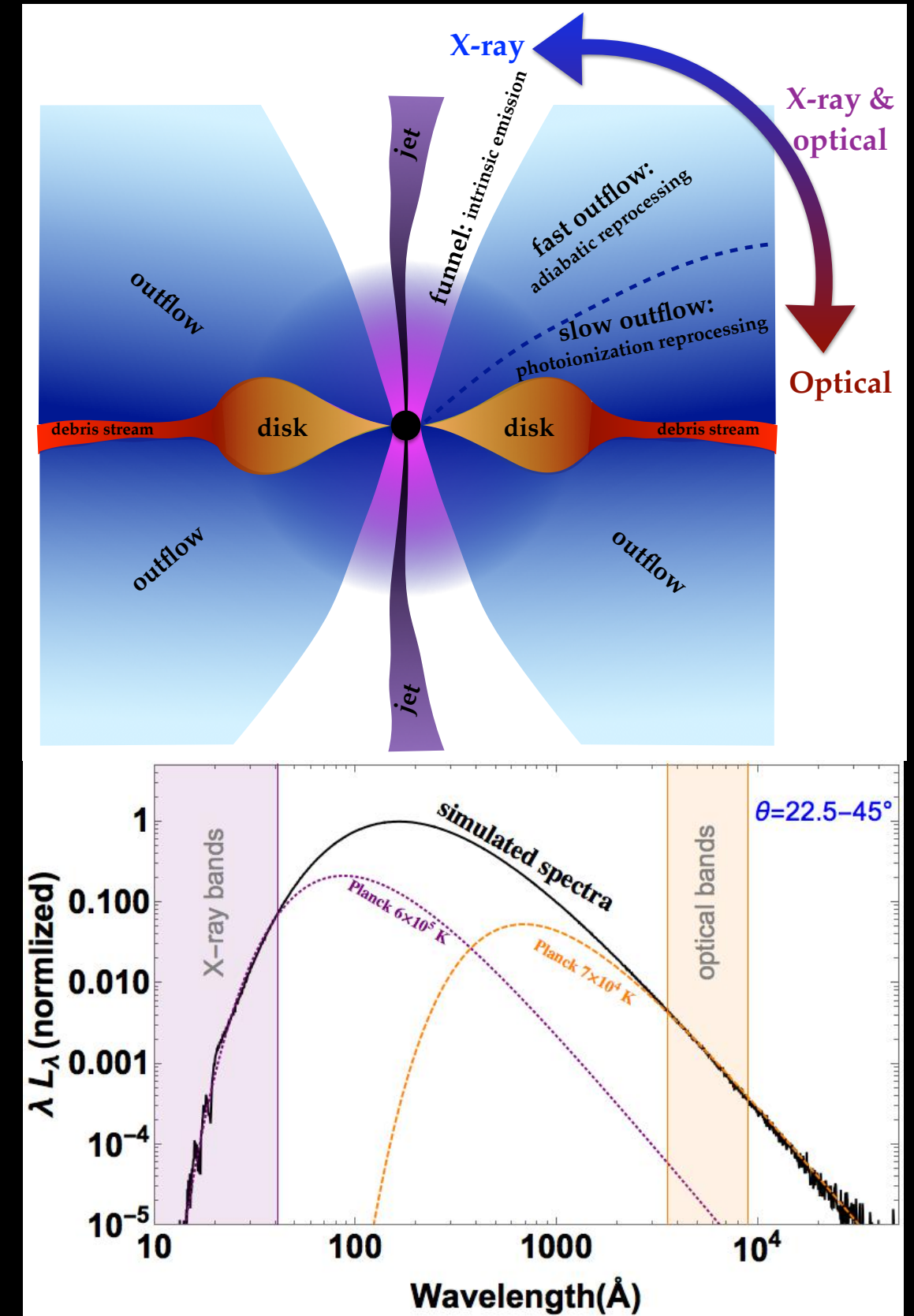
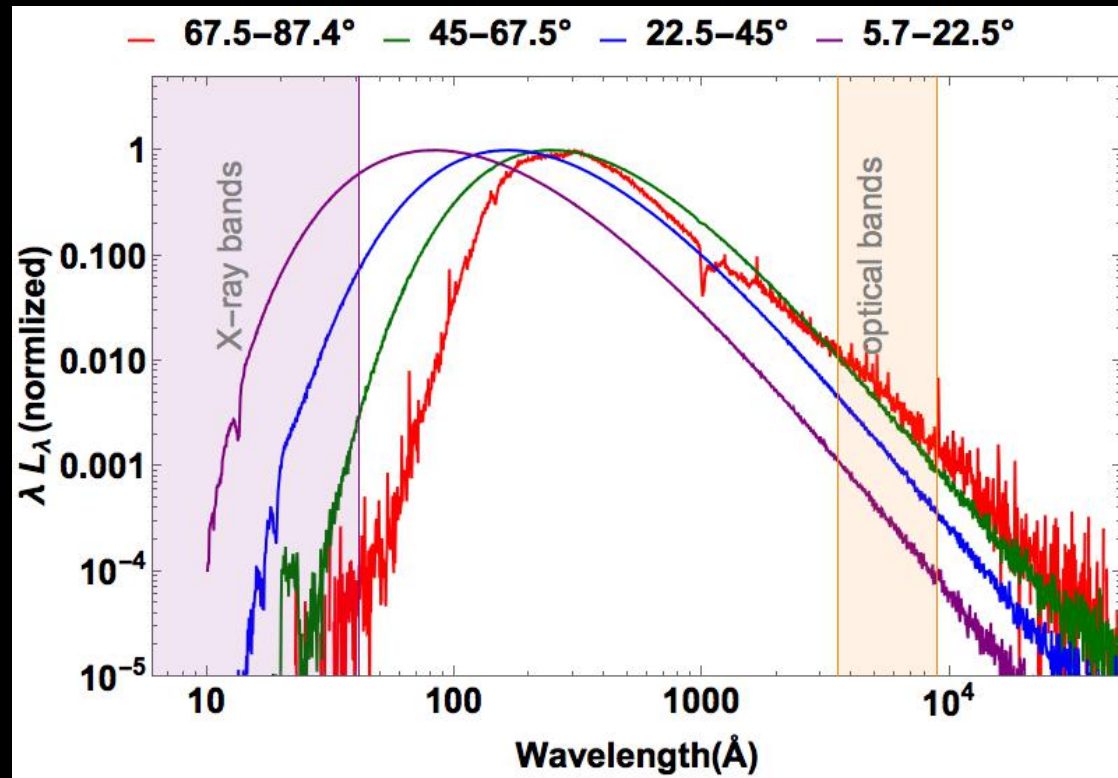
Space Weather @ Trappist-1



Dong + (PNAS, 2018)

Flares from Tidal Disruption Events (TDEs) around Supermassive Black Holes

Dai et al. 2018
([2018ApJ...859L..20D](#)): In GR Radiation MHD simulations of TDEs producing super-Eddington accretion, the synthetic spectrum from the disk peaks at EUV wavelengths.



What does the SDO/Atmospheric Imaging Assembly image?

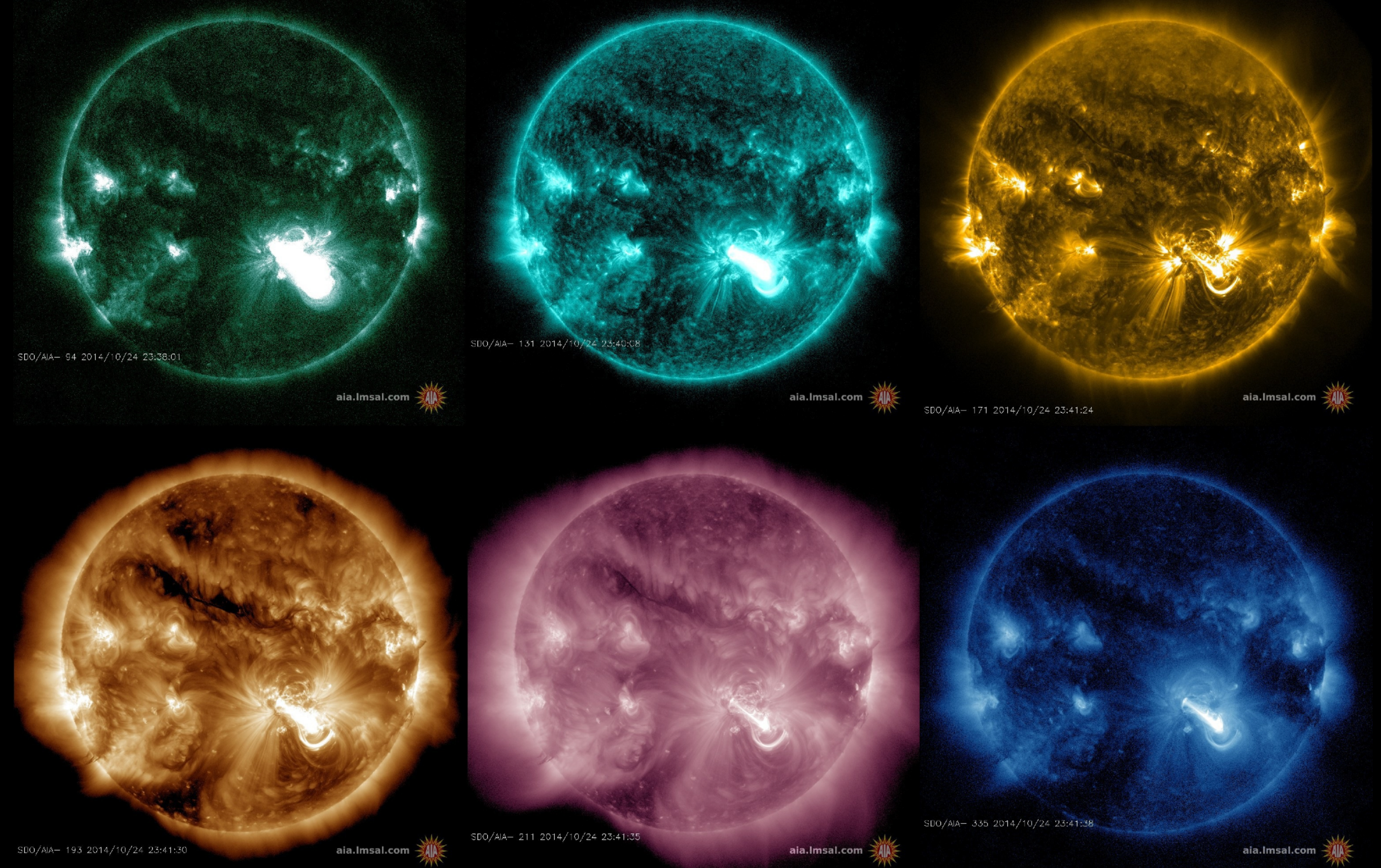


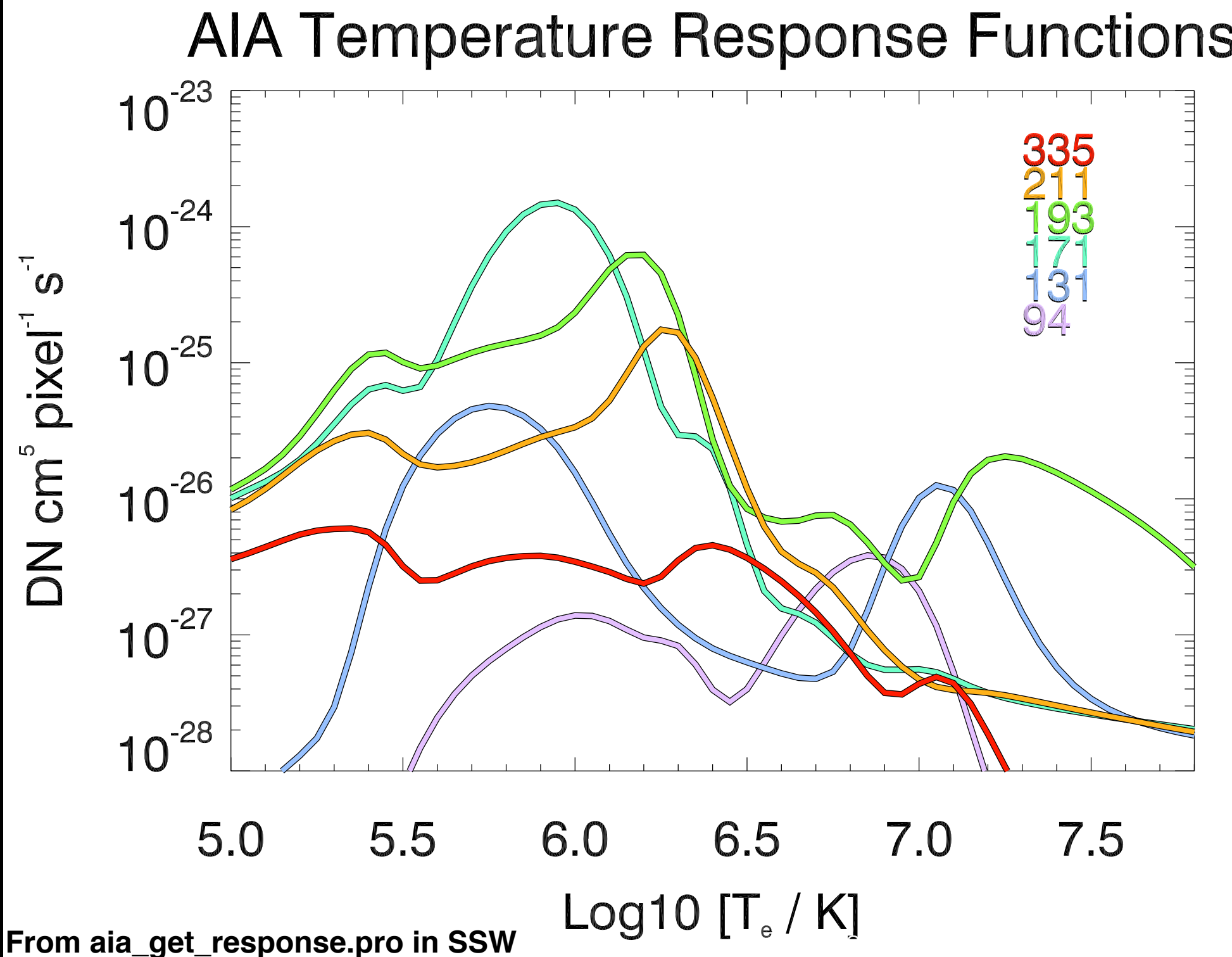
Table 1. Predicted AIA count rates.

Major EUV Lines in SDO/AIA passbands

	Ion	λ Å	T_p^a K	Fraction of total emission				211 Å	Cr IX	210.61	5.95	0.07	-	-	-	
				CH	QS	AR	FL									
94 Å	Mg VIII	94.07	5.9	0.03	-	-	-		Ca XVI	208.60	6.7	-	-	-	0.09	
	Fe XX	93.78	7.0	-	-	-	0.10		Fe XVII	204.67	6.6	-	-	-	0.07	
	Fe XVIII	93.93	6.85	-	-	0.74	0.85		Fe XIV	211.32	6.3	-	0.13	0.39	0.12	
	Fe X	94.01	6.05	0.63	0.72	0.05	-		Fe XIII	202.04	6.25	-	0.05	-	-	
	Fe VIII	93.47	5.6	0.04	-	-	-		Fe XIII	203.83	6.25	-	-	0.07	-	
	Fe VIII	93.62	5.6	0.05	-	-	-		Fe XIII	209.62	6.25	-	0.05	0.05	-	
	Cont.			0.11	0.12	0.17	-		Fe XI	209.78	6.15	0.11	0.12	-	-	
131 Å	O VI	129.87	5.45	0.04	0.05	-	-		Fe X	207.45	6.05	0.05	0.03	-	-	
	Fe XXIII	132.91	7.15	-	-	-	0.07		Ni XI	207.92	6.1	0.03	-	-	-	
	Fe XXI	128.75	7.05	-	-	-	0.83		Cont.		0.08	0.04	0.07	0.41		
	Fe VIII	130.94	5.6	0.30	0.25	0.09	-		304 Å	He II	303.786	4.7	0.33	0.32	0.27	0.29
	Fe VIII	131.24	5.6	0.39	0.33	0.13	-		He II	303.781	4.7	0.66	0.65	0.54	0.58	
	Cont.			0.11	0.20	0.54	0.04		Ca XVIII	302.19	6.85	-	-	-	0.05	
171 Å	Ni XIV	171.37	6.35	-	-	0.04	-		Si XI	303.33	6.2	-	-	0.11	-	
	Fe X	174.53	6.05	-	0.03	-	-		Cont.		-	-	-	-	-	
	Fe IX	171.07	5.85	0.95	0.92	0.80	0.54		335 Å	Al X	332.79	6.1	0.05	0.11	-	-
	Cont.			-	-	-	0.23		Mg VIII	335.23	5.9	0.11	0.06	-	-	
193 Å	O V	192.90	5.35	0.03	-	-	-		Mg VIII	338.98	5.9	0.11	0.06	-	-	
	Ca XVII	192.85	6.75	-	-	-	0.08		Si IX	341.95	6.05	0.03	0.03	-	-	
	Ca XIV	193.87	6.55	-	-	0.04	-		Si VIII	319.84	5.95	0.04	-	-	-	
	Fe XXIV	192.03	7.25	-	-	-	0.81		Fe XVI	335.41	6.45	-	-	0.86	0.81	
	Fe XII	195.12	6.2	0.08	0.18	0.17	-		Fe XIV	334.18	6.3	-	0.04	0.04	-	
	Fe XII	193.51	6.2	0.09	0.19	0.17	-		Fe X	184.54	6.05	0.13	0.15	-	-	
	Fe XII	192.39	6.2	0.04	0.09	0.08	-		Cont.		0.08	0.05	-	0.06		
	Fe XI	188.23	6.15	0.09	0.10	0.04	-		32							
	Fe XI	192.83	6.15	0.05	0.06	-	-									
	Fe XI	188.30	6.15	0.04	0.04	-	-									
	Fe X	190.04	6.05	0.06	0.04	-	-									
	Fe IX	189.94	5.85	0.06	-	-	-									
	Fe IX	188.50	5.85	0.07	-	-	-									
	Cont.			-	-	0.05	0.04									

O'Dwyer, Del Zanna,
 Mason & Weber
 (A&A 2010), using the
 CHIANTI atomic package

Problem Statement



$y = \mathbf{AIA}$ count rates

$\mathbf{x} = D\mathbf{m}$,
cols. of D = basis
funcs

m = emission
measure (EM) in
temperature bins

EM @ certain temperature = line-of-sight integral of n_e^2

Sparse Solution by Basis Pursuit

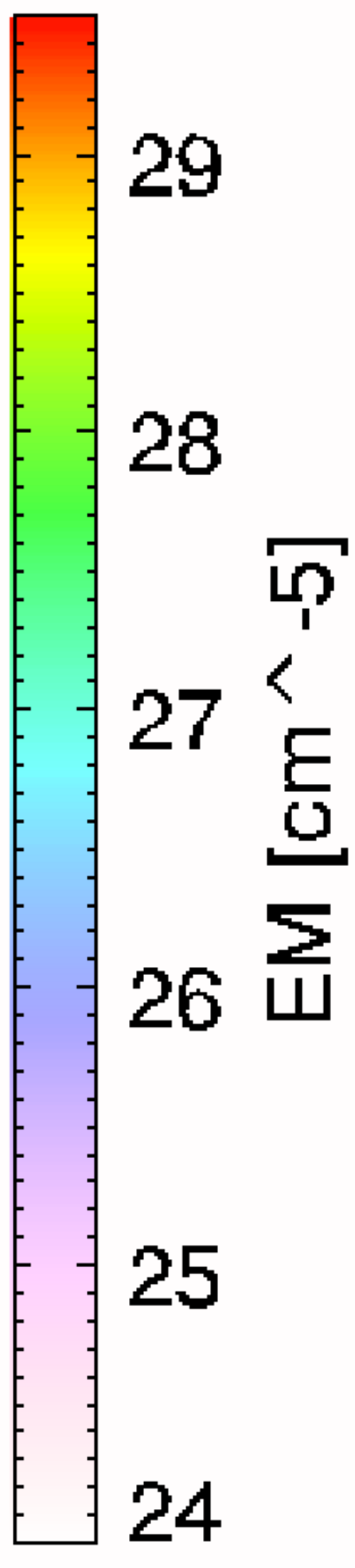
In practice, measurement uncertainties imply that the equality $\mathbf{y} = \mathbf{Kx}$ may not be satisfied. So our method solves the following linear program:

$$\begin{aligned} & \text{minimize} \sum_j^n \mathbf{x}_j \text{ subject to } \mathcal{K}\vec{x} \leq \vec{y} + \vec{\eta}, \\ & \quad \vec{x} \geq 0, \quad \mathcal{K}\vec{x} \geq \max(\vec{y} - \vec{\eta}, 0). \end{aligned}$$

The vector η is a measure of the uncertainty in the count rate and provides tolerance for the predicted counts (\mathbf{Kx}) to deviate from the observed values (\mathbf{y}). To enforce positive counts the lower bound is set to $\max(y-\eta, 0)$.

Cheung et al. (2015): This method has been validated on (1) simple log-normal DEM models, (2) 3D model of quasi-steadily heated loops in a non-linear force-free field and (3) 3D MHD model of an active region with field-aligned thermal conduction.

AR 11158 @ 2011-02-15T00:13:26



$E_M [\text{cm}^{-5}]$

29

28

27

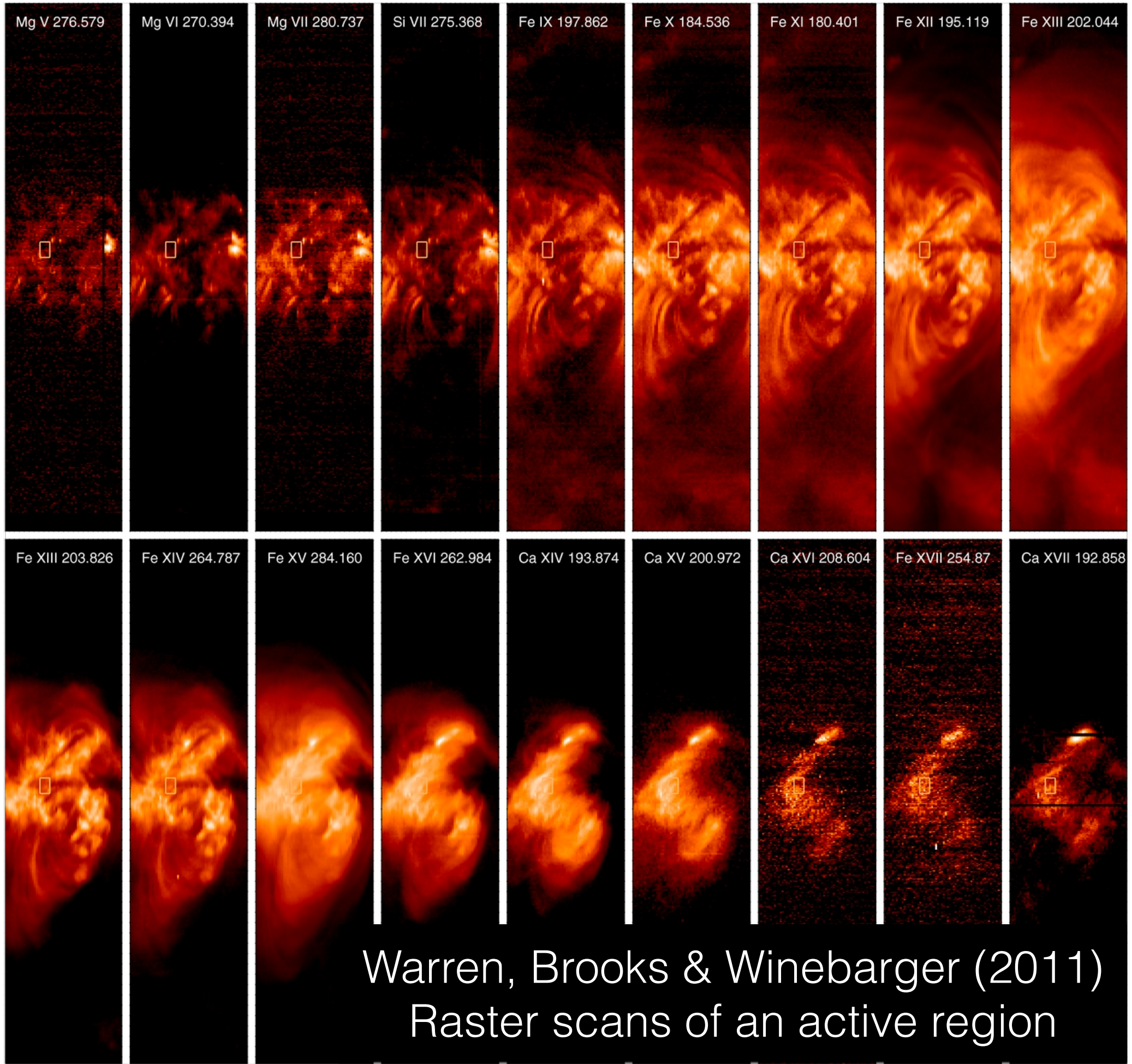
26

25

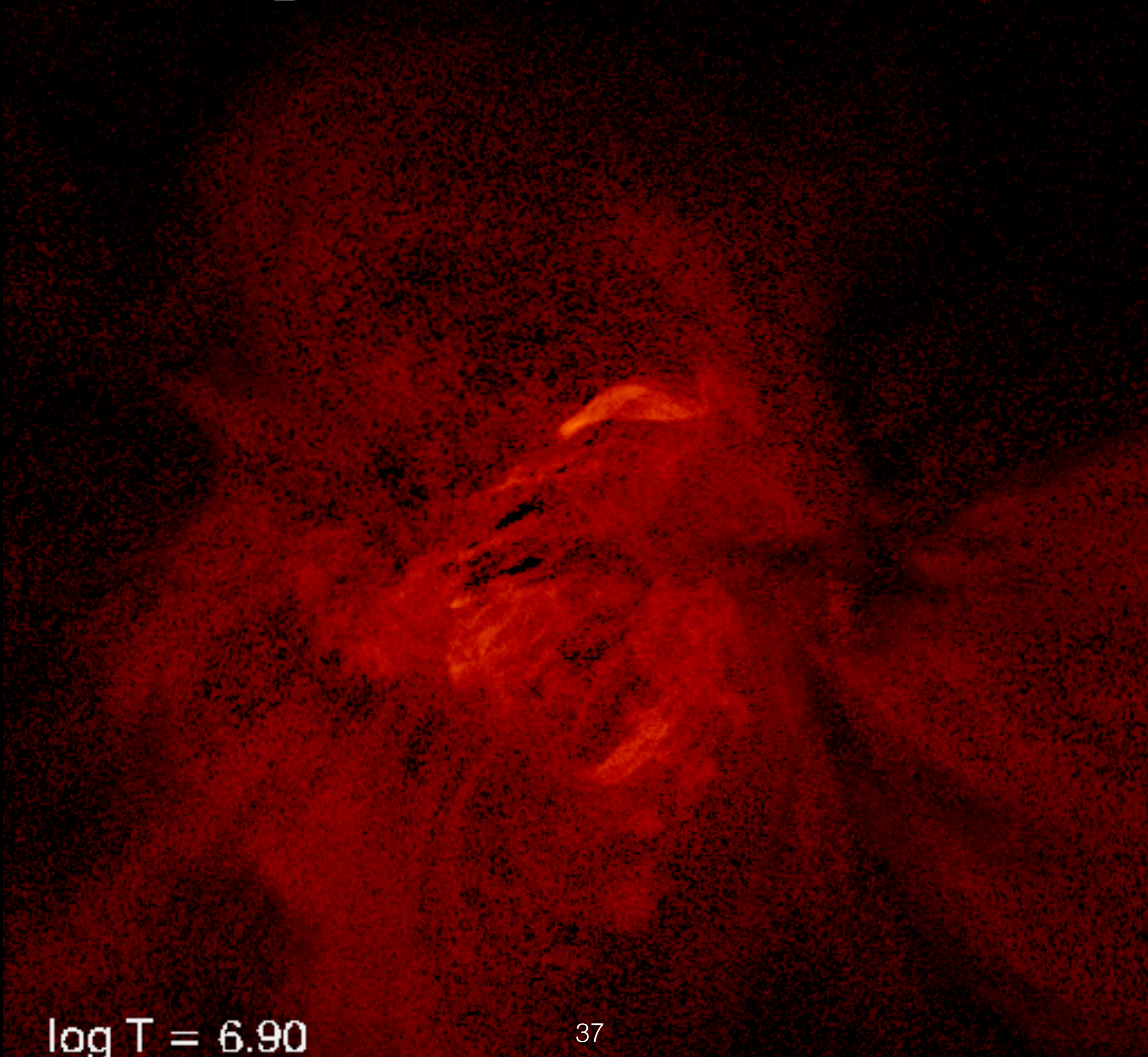
24

$\log T = 5.70$

35

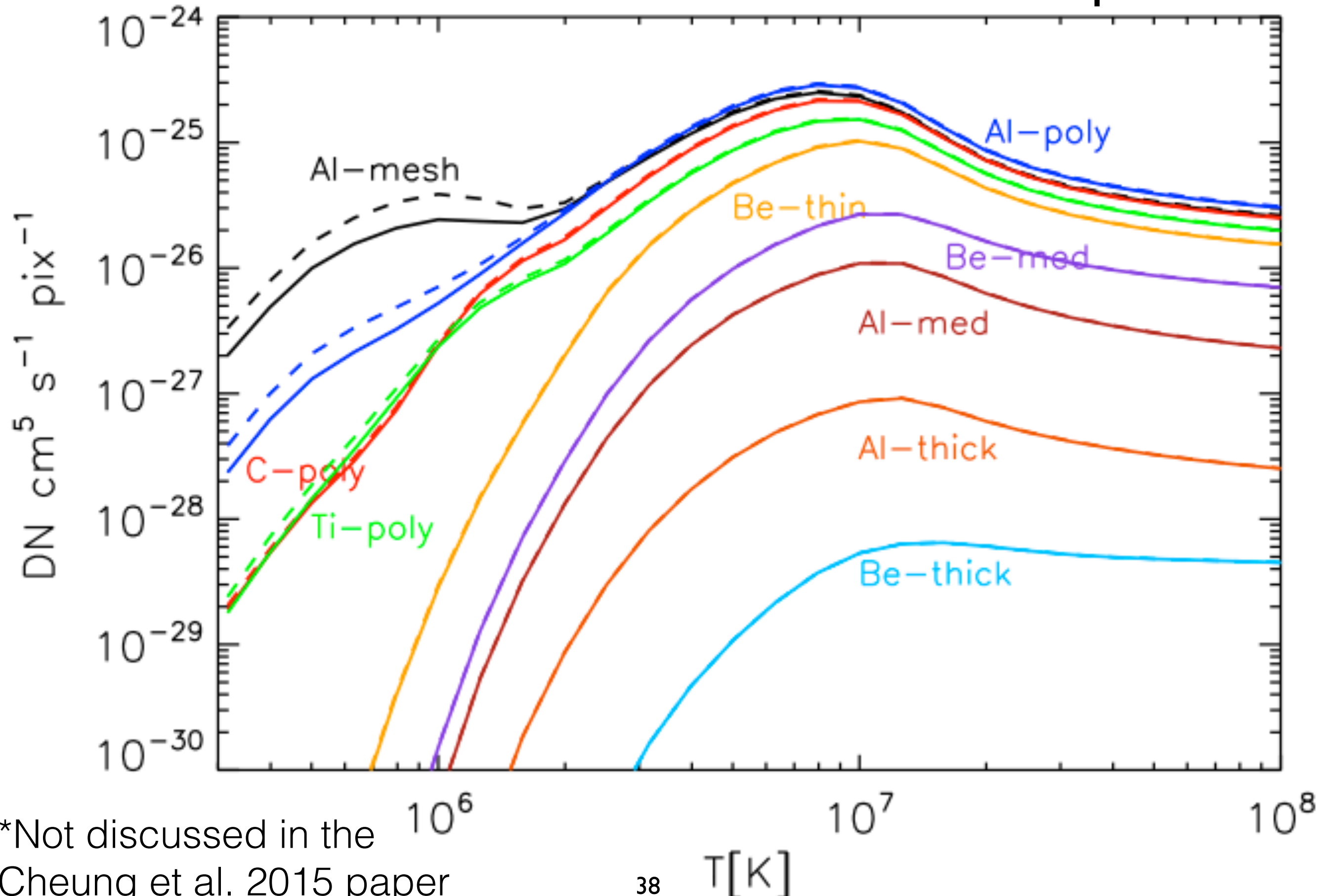


AR 11089 @ 2010-07-23T15:00:08



$\log T = 6.90$

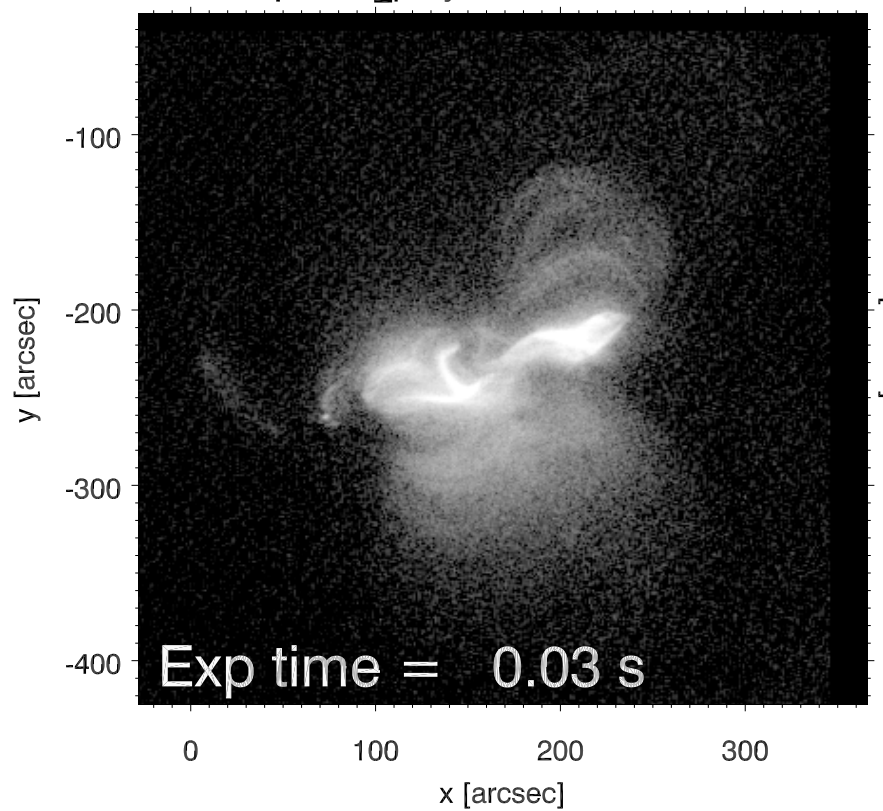
Validation Exercise: AIA-XRT Cross-Comparison



*Not discussed in the
Cheung et al. 2015 paper

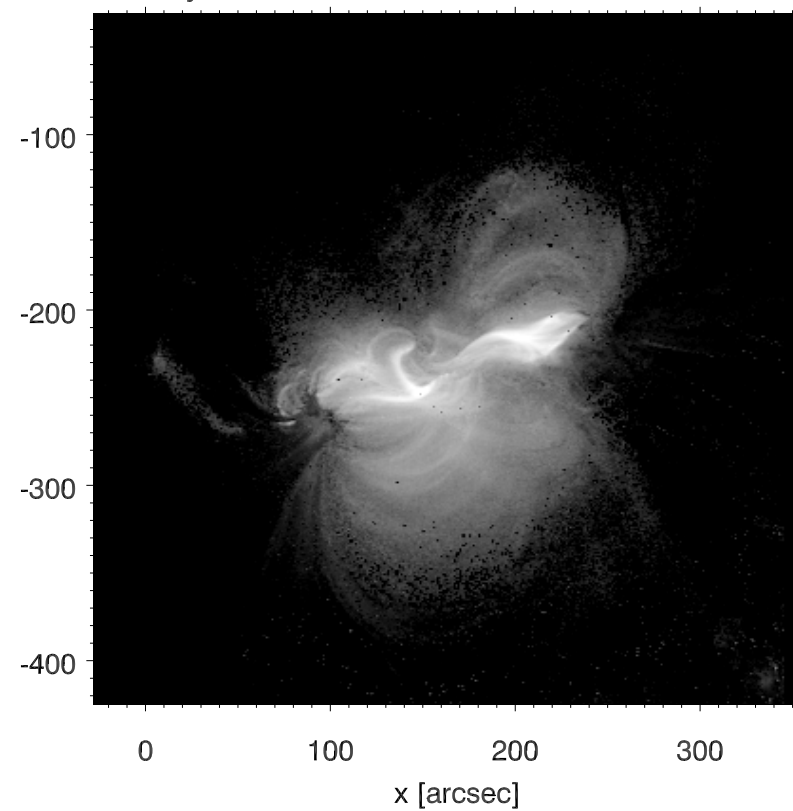
Hinode/XRT

XRT Open/Ti_poly@2011-02-14T23:31:19

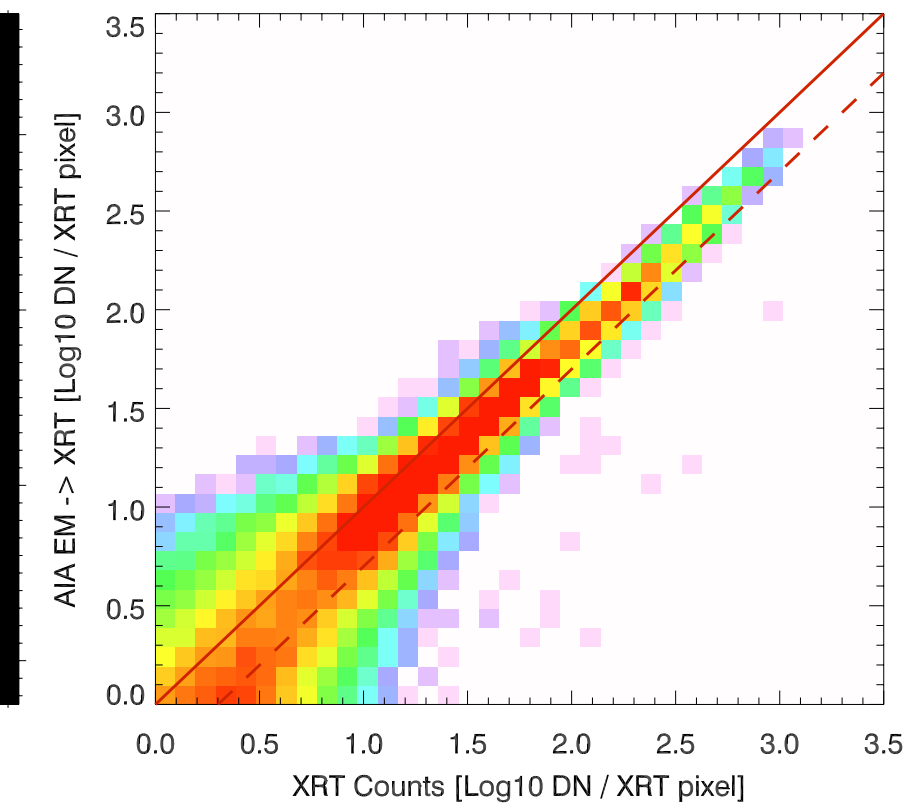


AIA DEM → Mock XRT

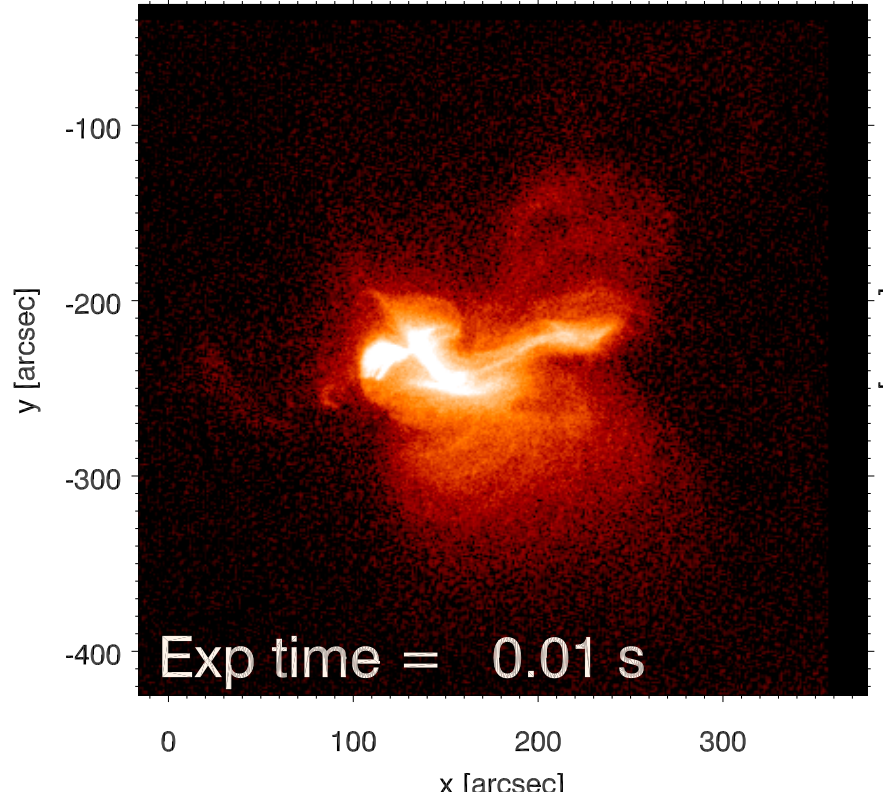
Synthesized from AIA 1x1 binned EM



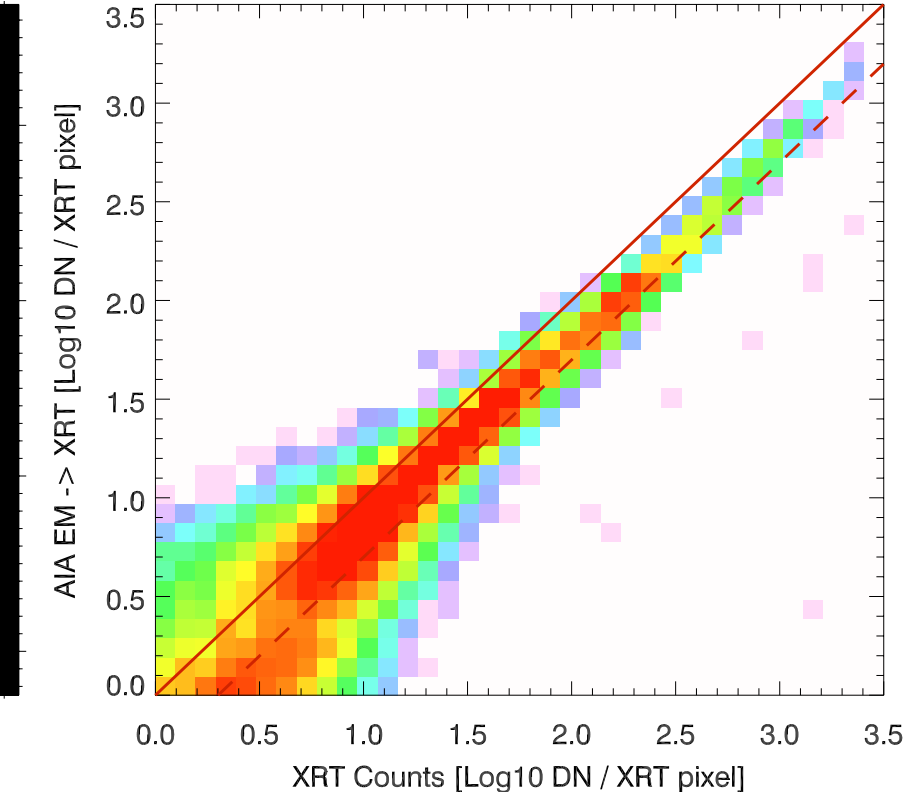
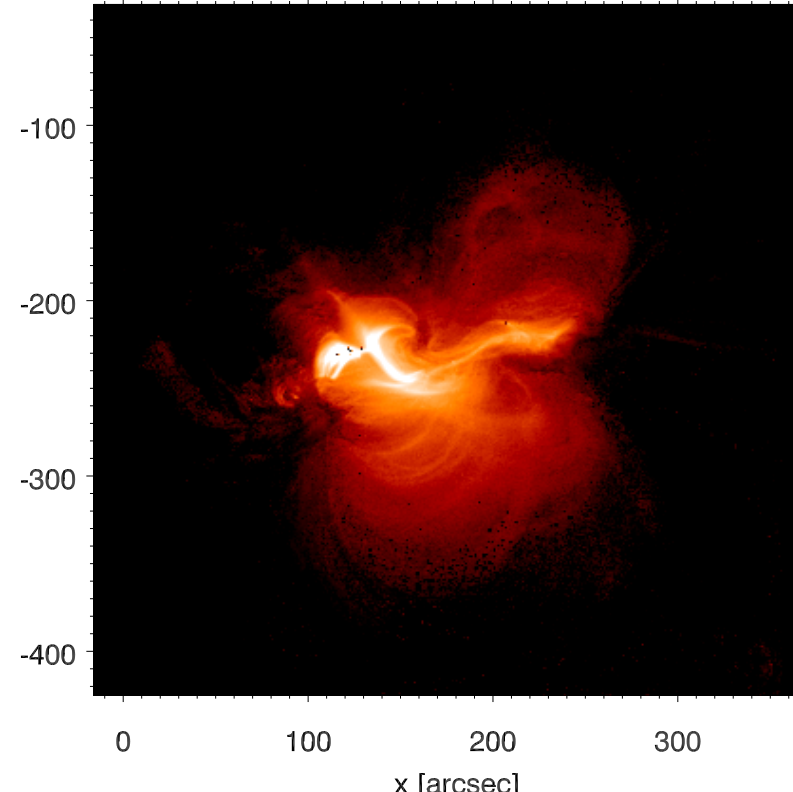
2D histograms



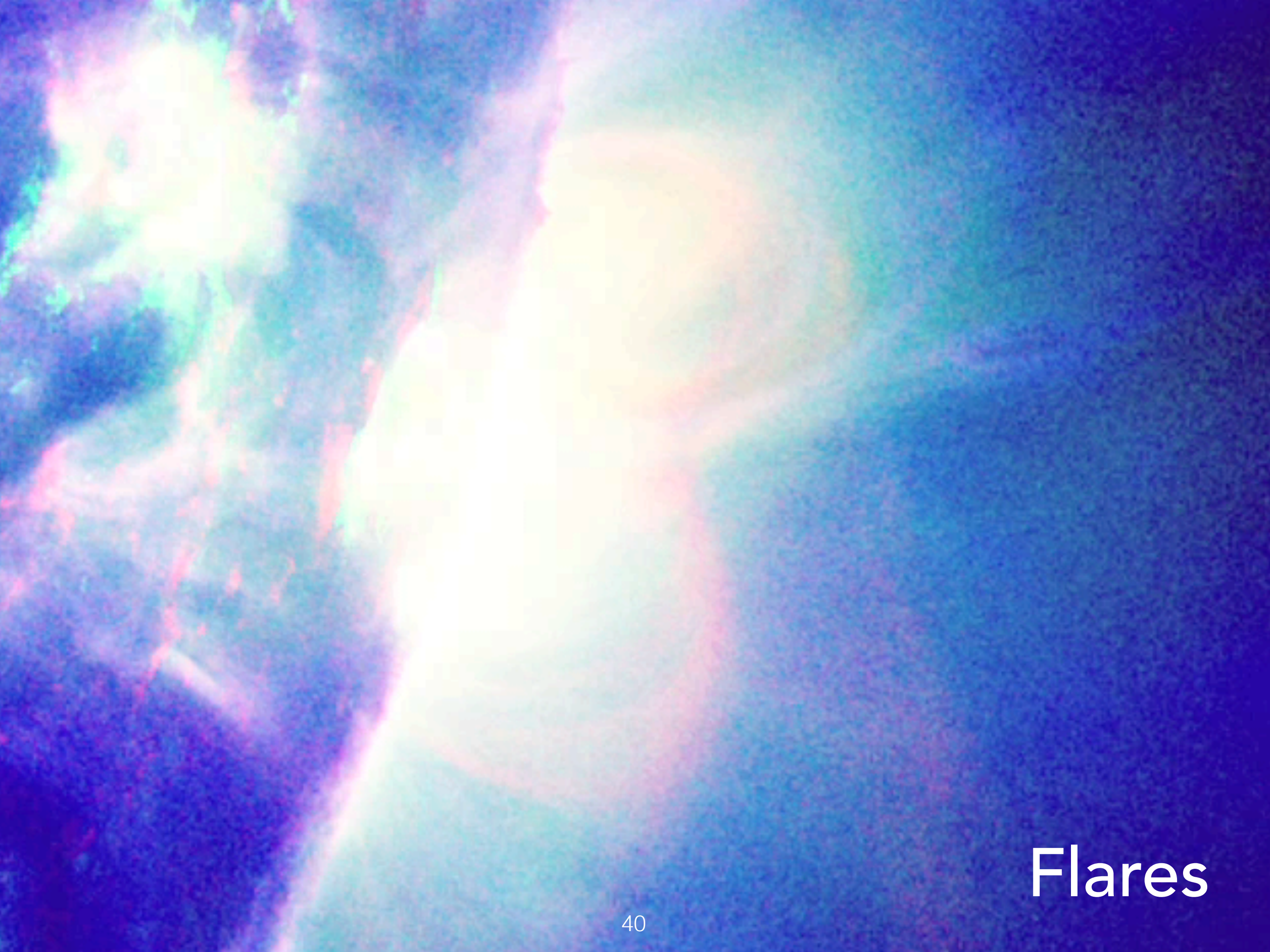
XRT AI_poly/Open@2011-02-15T00:56:07



Synthesized from AIA 1x1 binned EM



Also, see Su et al. (2018) for validation against RHESSI.

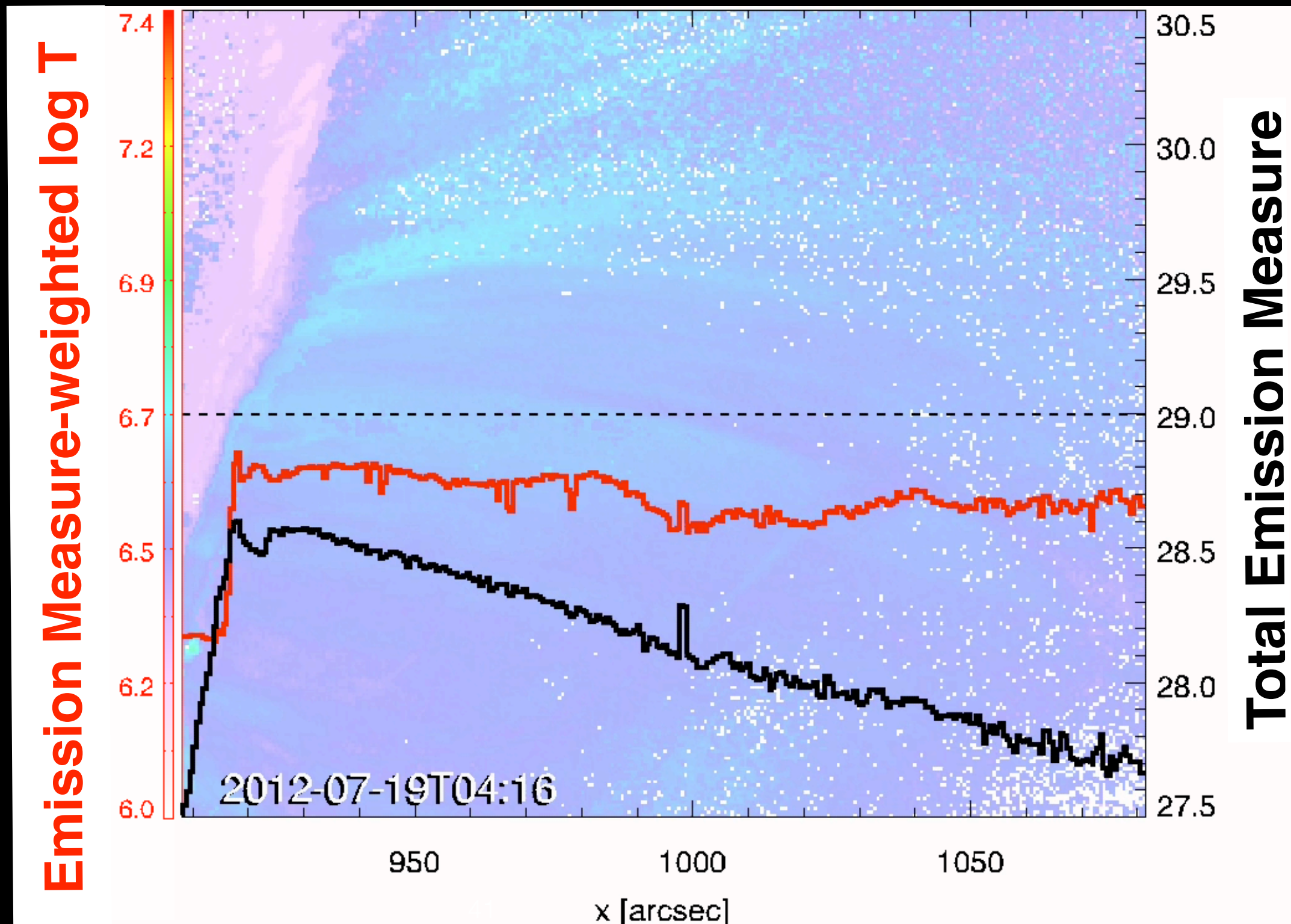


Flares

Application to a limb flare to track chromospheric evaporation

M7.7 limb flare

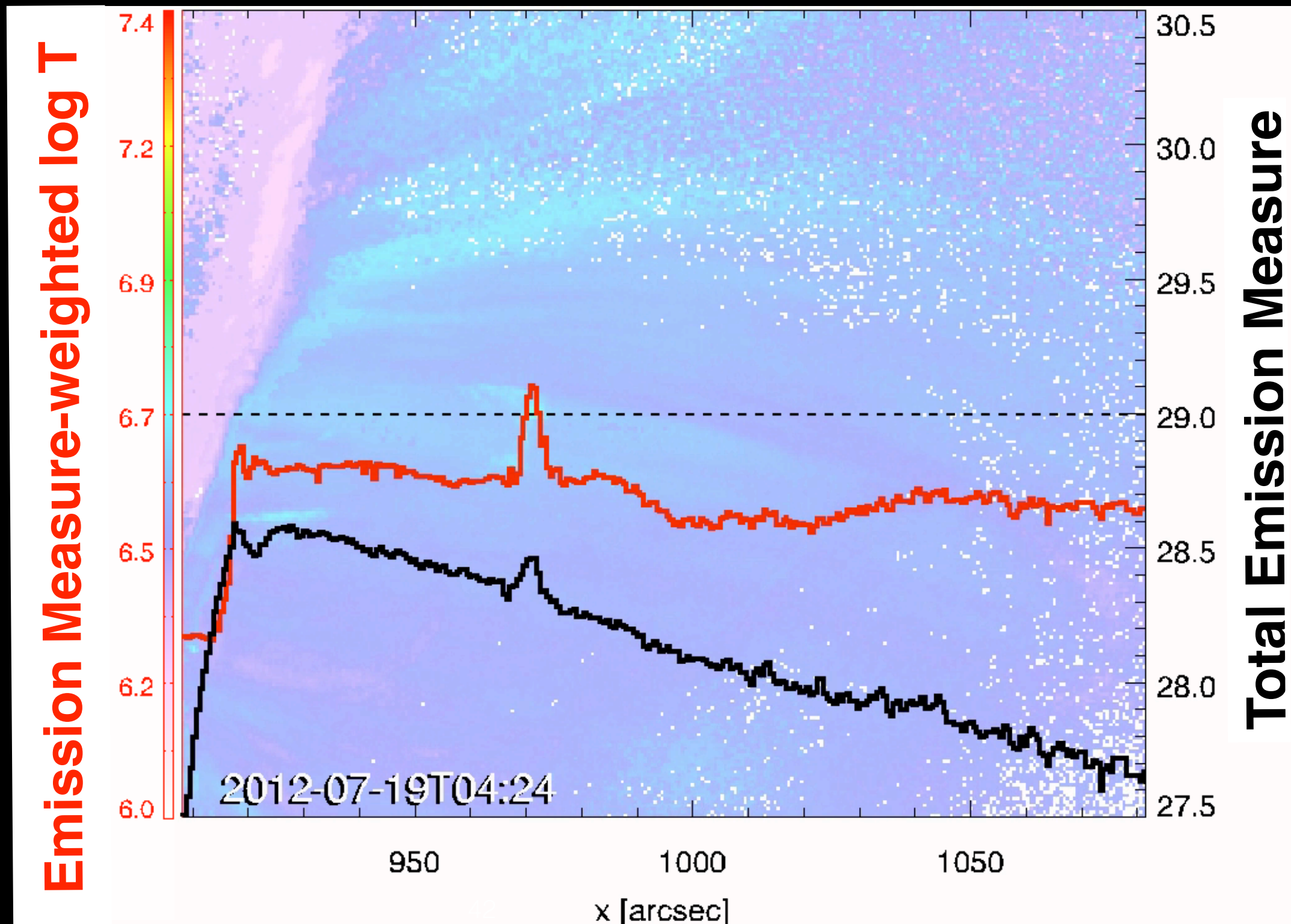
- Patsourakos, Vourlidas & Stenborg, 2013, ApJ, 764, 125
- Wei Liu, Chen & Petrosian, 2013, ApJ, 767, 168
- Rui Liu, 2013, MNRAS, 434, 1309
- Krücker & Battaglia, 2014, ApJ, 780, 107
- Sun, Cheng & Ding, 2014, ApJ, 786, 73
- Krücker et al., 2015, ApJ, 802, 19



Application to a limb flare to track chromospheric evaporation

M7.7 limb flare

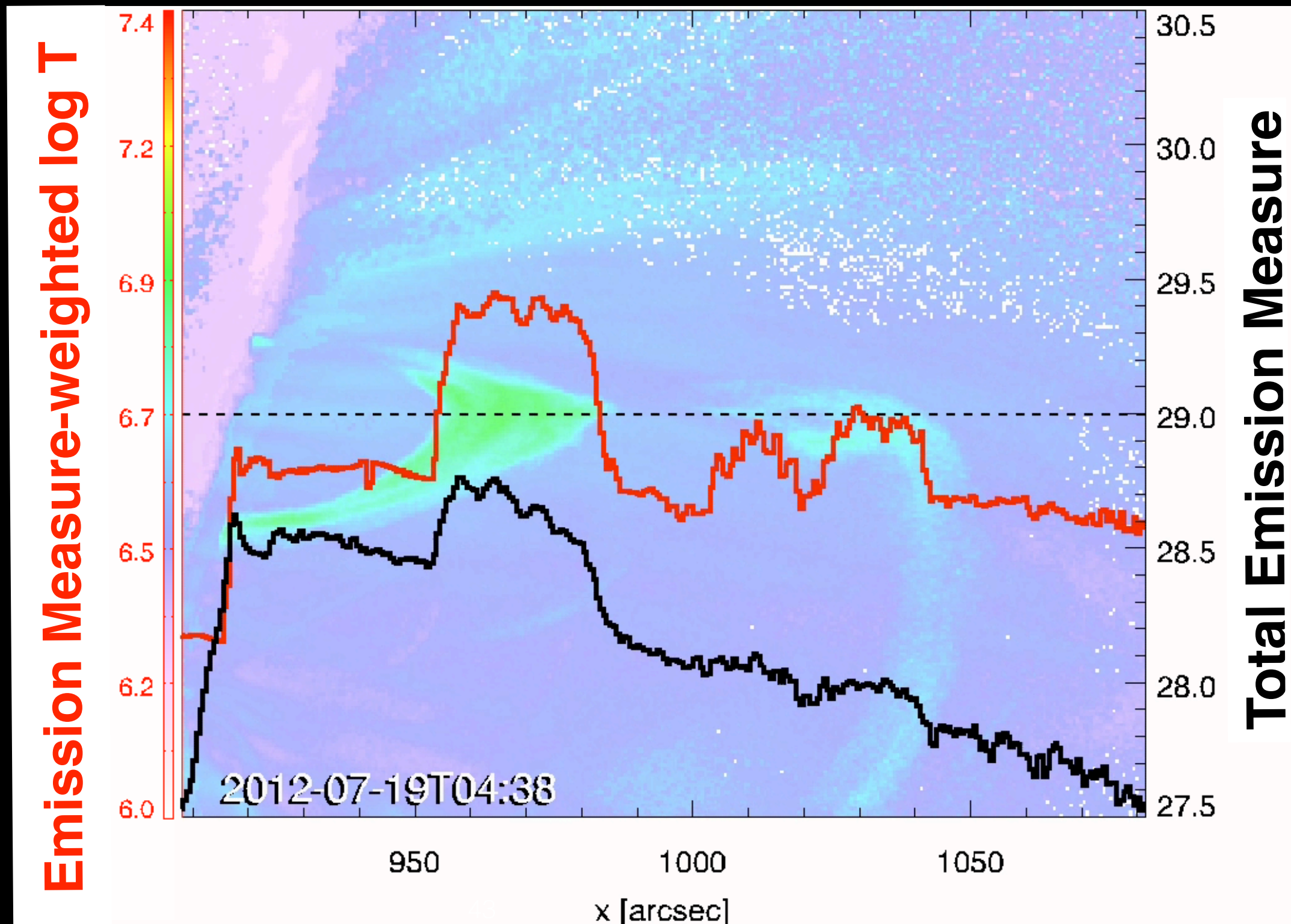
- Patsourakos, Vourlidas & Stenborg, 2013, ApJ, 764, 125
- Wei Liu, Chen & Petrosian, 2013, ApJ, 767, 168
- Rui Liu, 2013, MNRAS, 434, 1309
- Krücker & Battaglia, 2014, ApJ, 780, 107
- Sun, Cheng & Ding, 2014, ApJ, 786, 73
- Krücker et al., 2015, ApJ, 802, 19



Application to a limb flare to track chromospheric evaporation

M7.7 limb flare

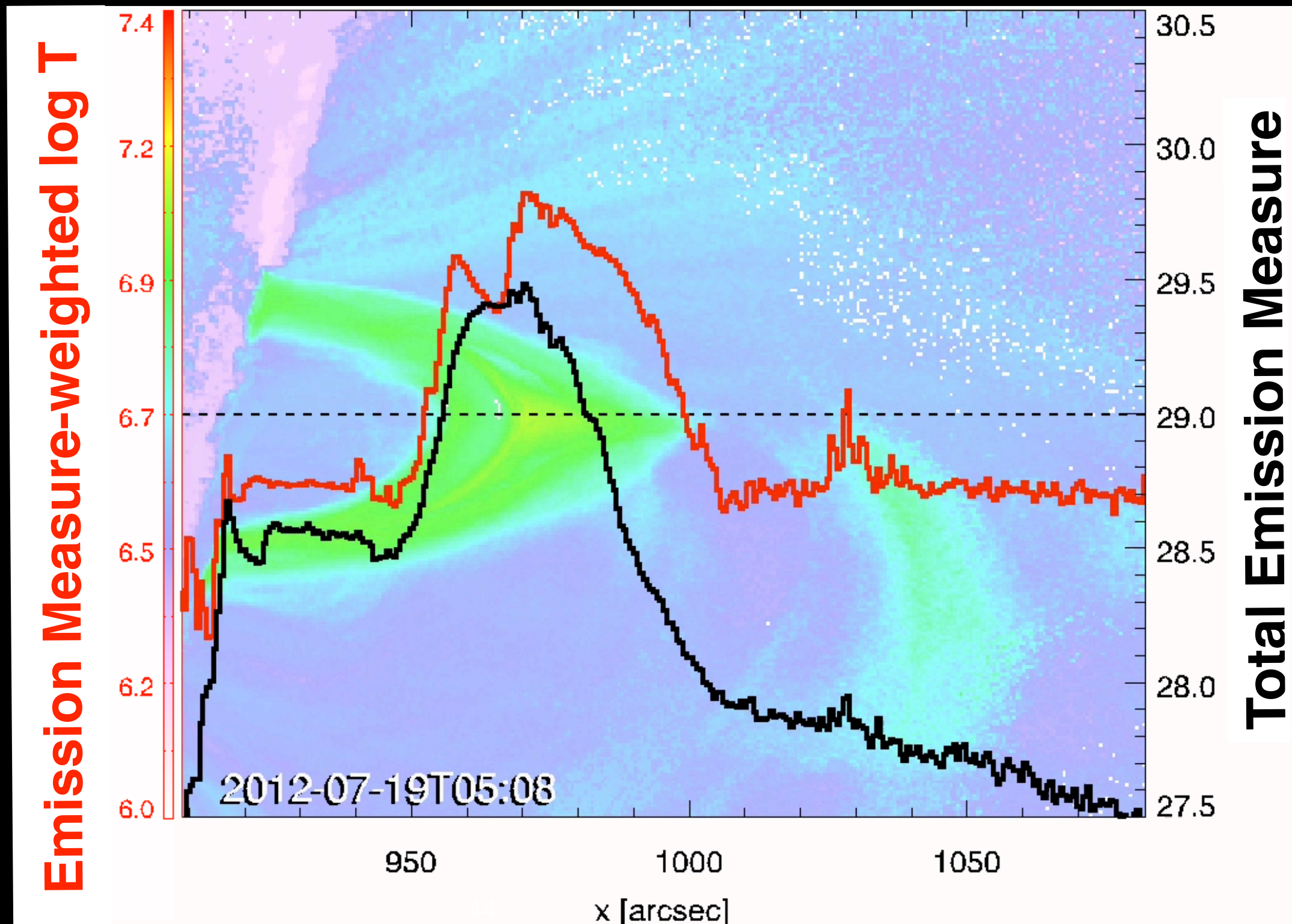
- Patsourakos, Vourlidas & Stenborg, 2013, ApJ, 764, 125
- Wei Liu, Chen & Petrosian, 2013, ApJ, 767, 168
- Rui Liu, 2013, MNRAS, 434, 1309
- Krücker & Battaglia, 2014, ApJ, 780, 107
- Sun, Cheng & Ding, 2014, ApJ, 786, 73
- Krücker et al., 2015, ApJ, 802, 19



Application to a limb flare to track chromospheric evaporation

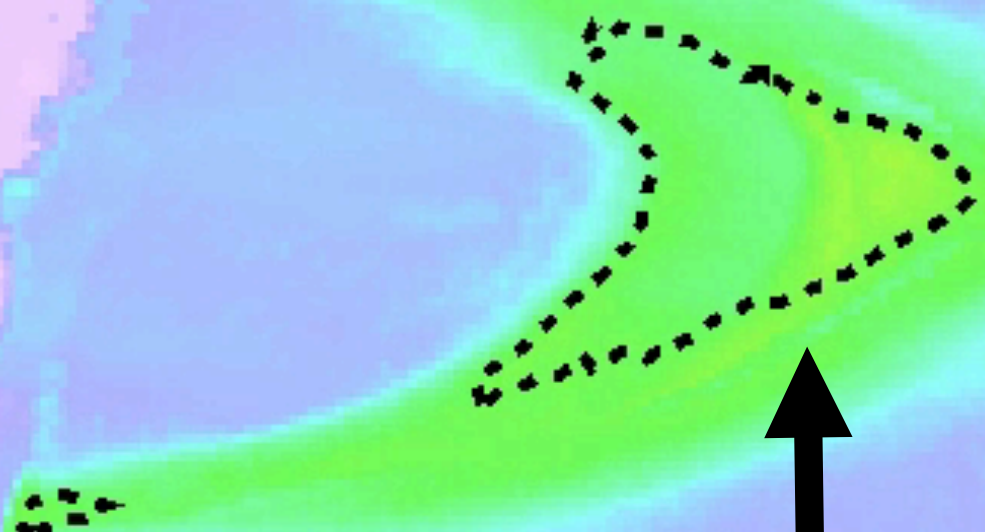
M7.7 limb flare

- Patsourakos, Vourlidas & Stenborg, 2013, ApJ, 764, 125
- Wei Liu, Chen & Petrosian, 2013, ApJ, 767, 168
- Rui Liu, 2013, MNRAS, 434, 1309
- Krücker & Battaglia, 2014, ApJ, 780, 107
- Sun, Cheng & Ding, 2014, ApJ, 786, 73
- Krücker et al., 2015, ApJ, 802, 19

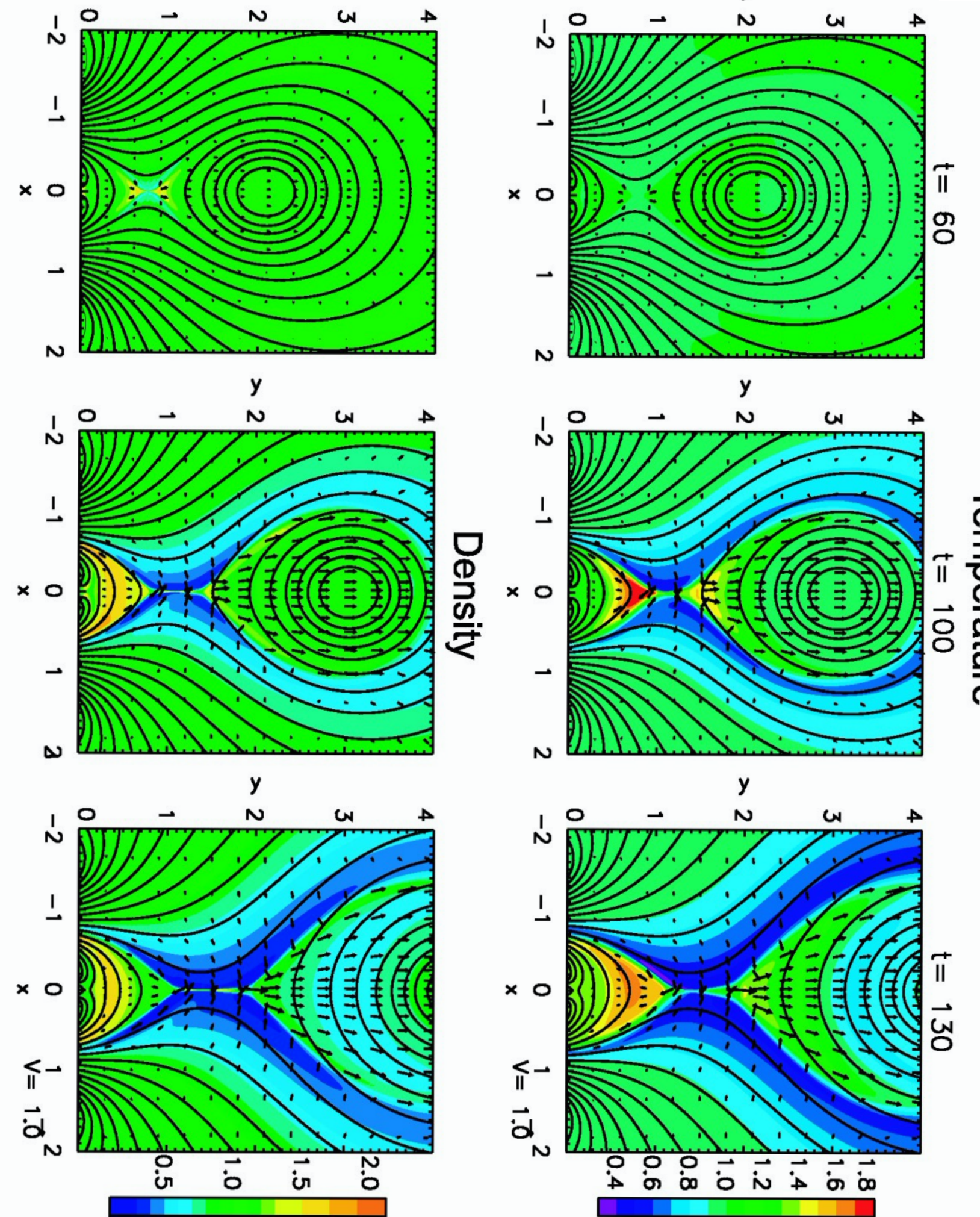


Dashed contours: Total EM = 10^{29} cm $^{-5}$
Solid contours: Total EM = 10^{30} cm $^{-5}$

Chromospheric evaporation

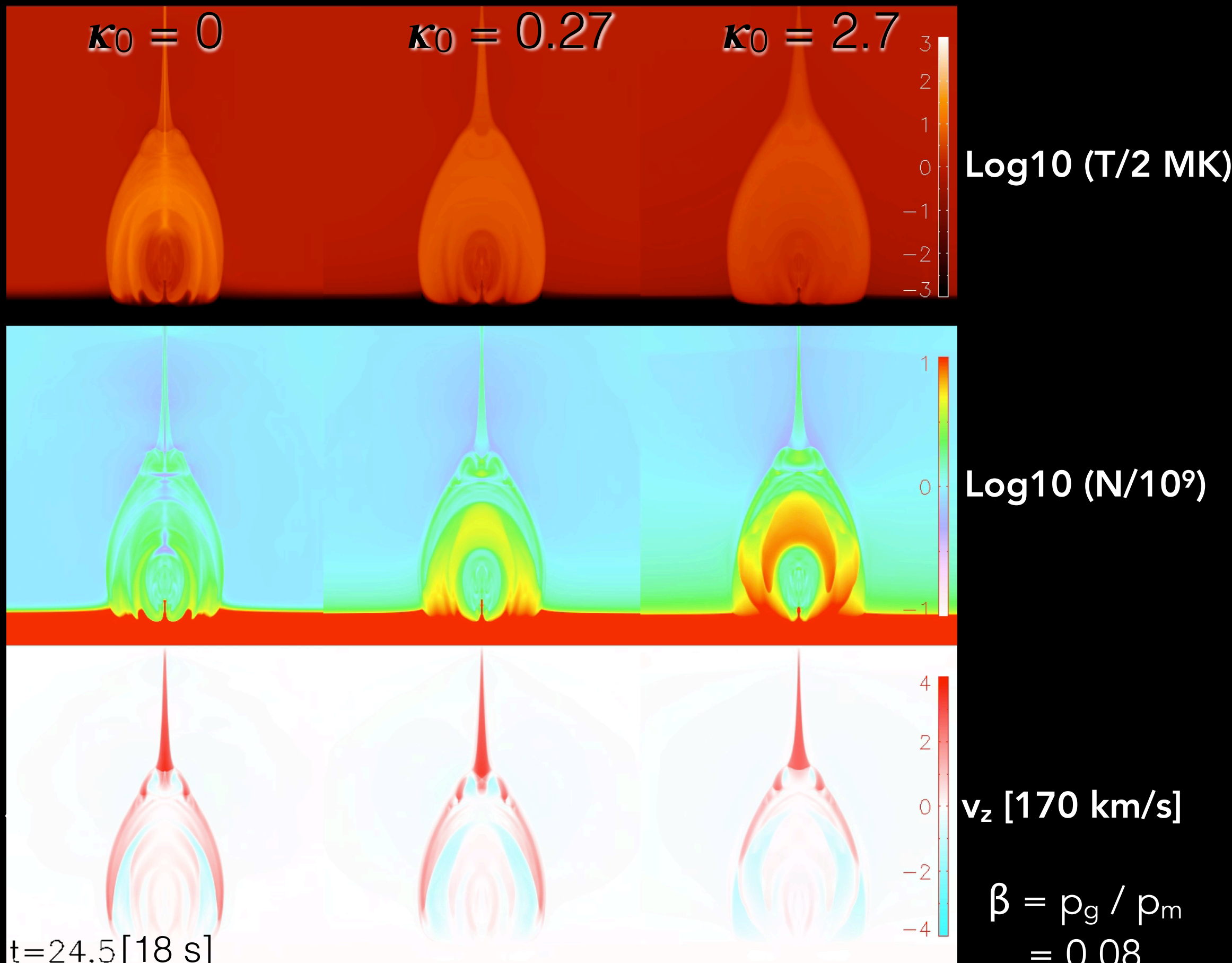


Downward mass pumping from reconnection outflow

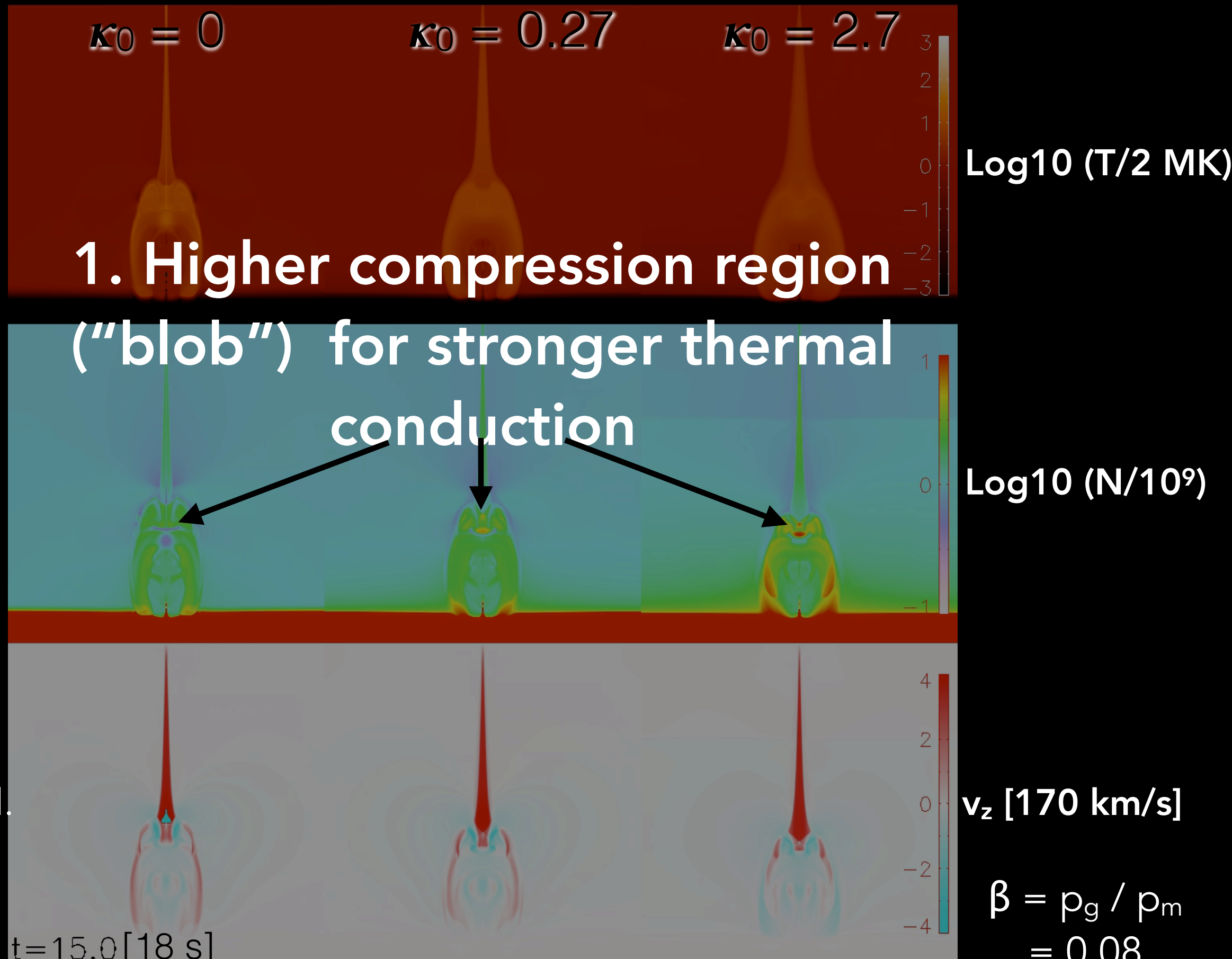


- Shiota et al. (2005, ApJ, 634, 663):
- 2.5D MHD simulation of the eruption of a pre-existing flux rope triggered by flux emergence.
 - Similar scenario as modeled by Chen & Shibata (2000, ApJ, 545, 524) but with field-aligned thermal conduction.
 - Both temperature and density are initially uniform (dimensionless value of unity).

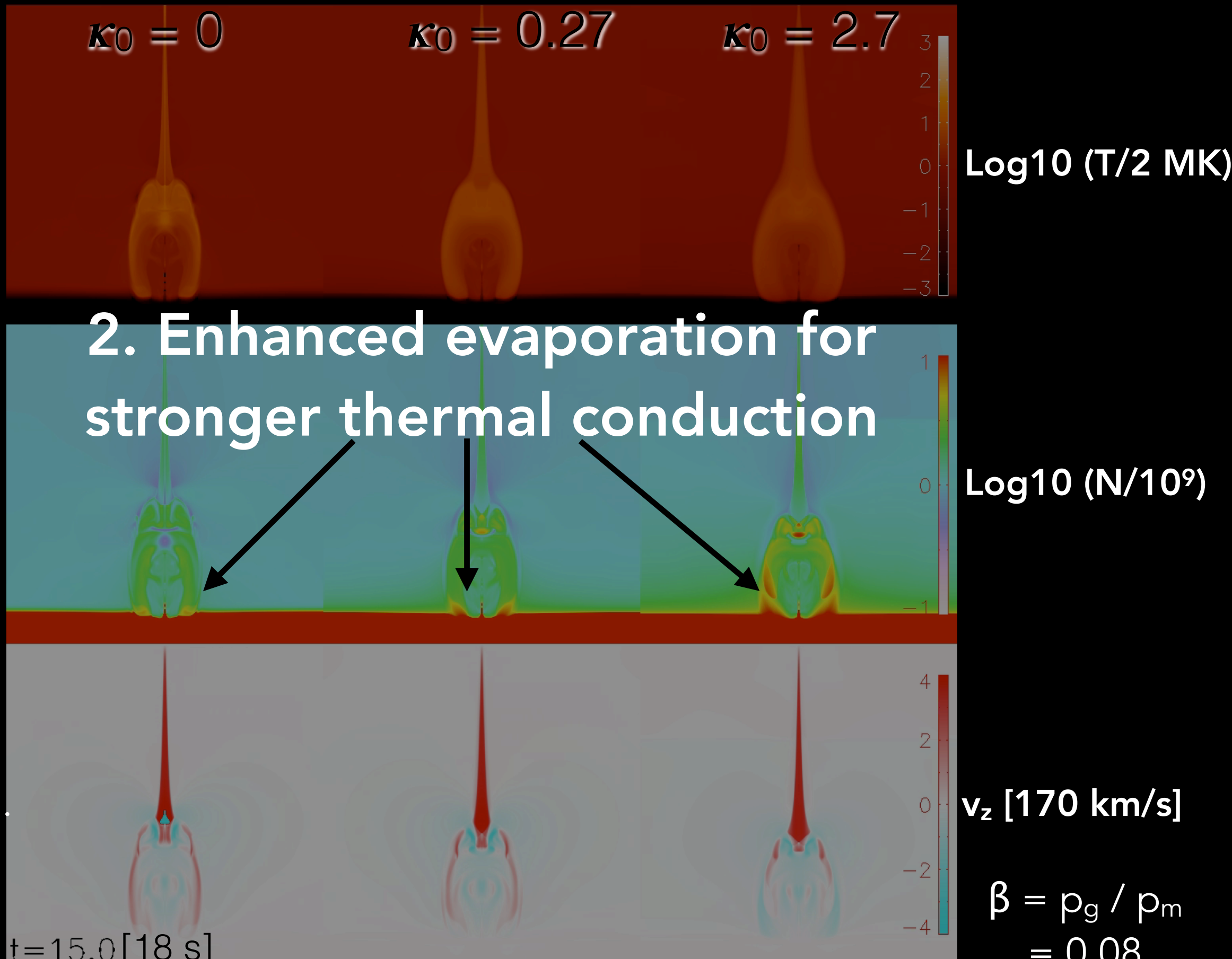
Influence of efficiency of thermal conduction / system size

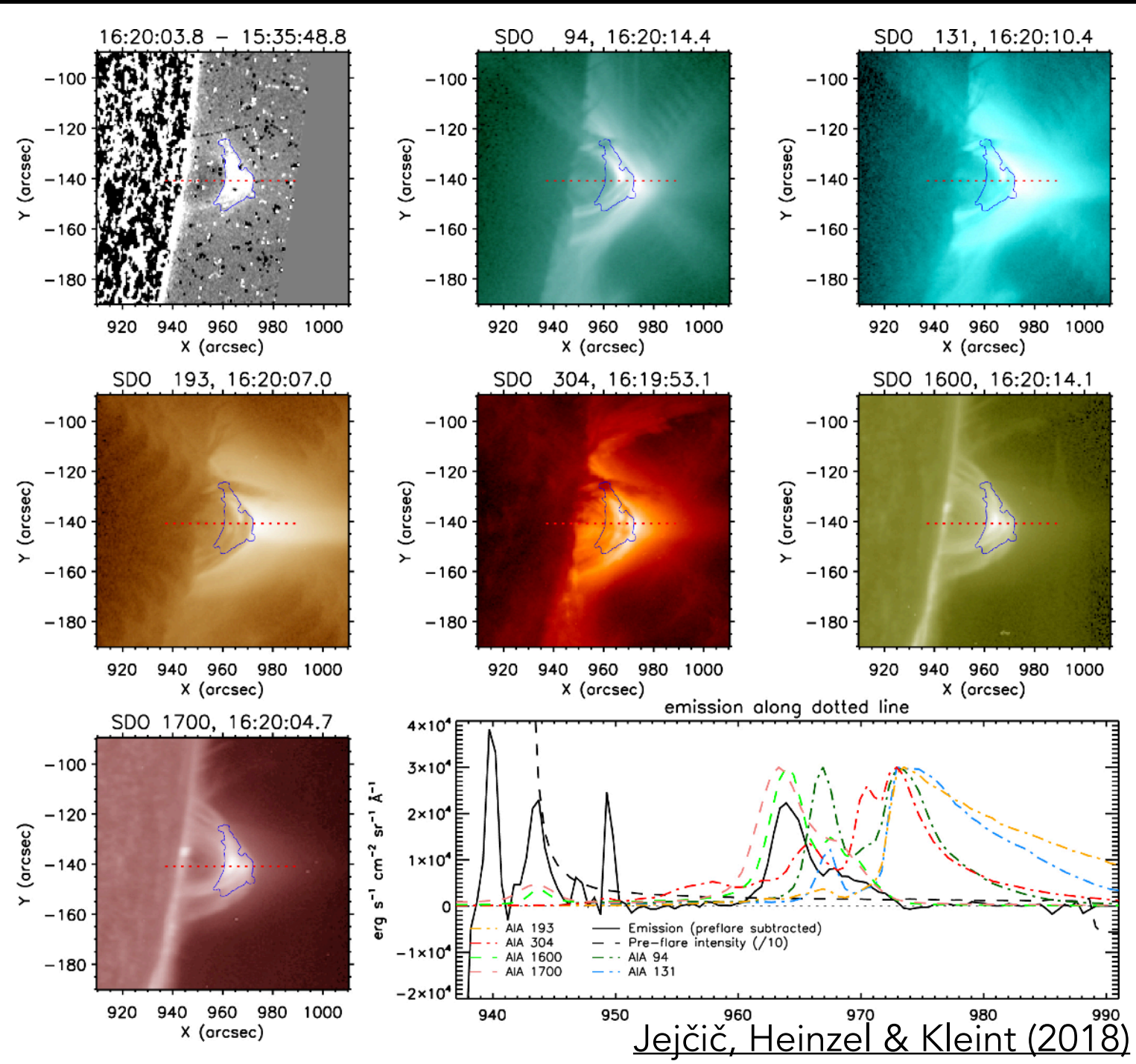


Influence of efficiency of thermal conduction / system size



Influence of efficiency of thermal conduction / system size





Shibayama et al. (2013) ...
Estimated energies of Kepler superflares assuming black-body radiation @ 10,000 K plasma at the base of flare loops (ribbons).

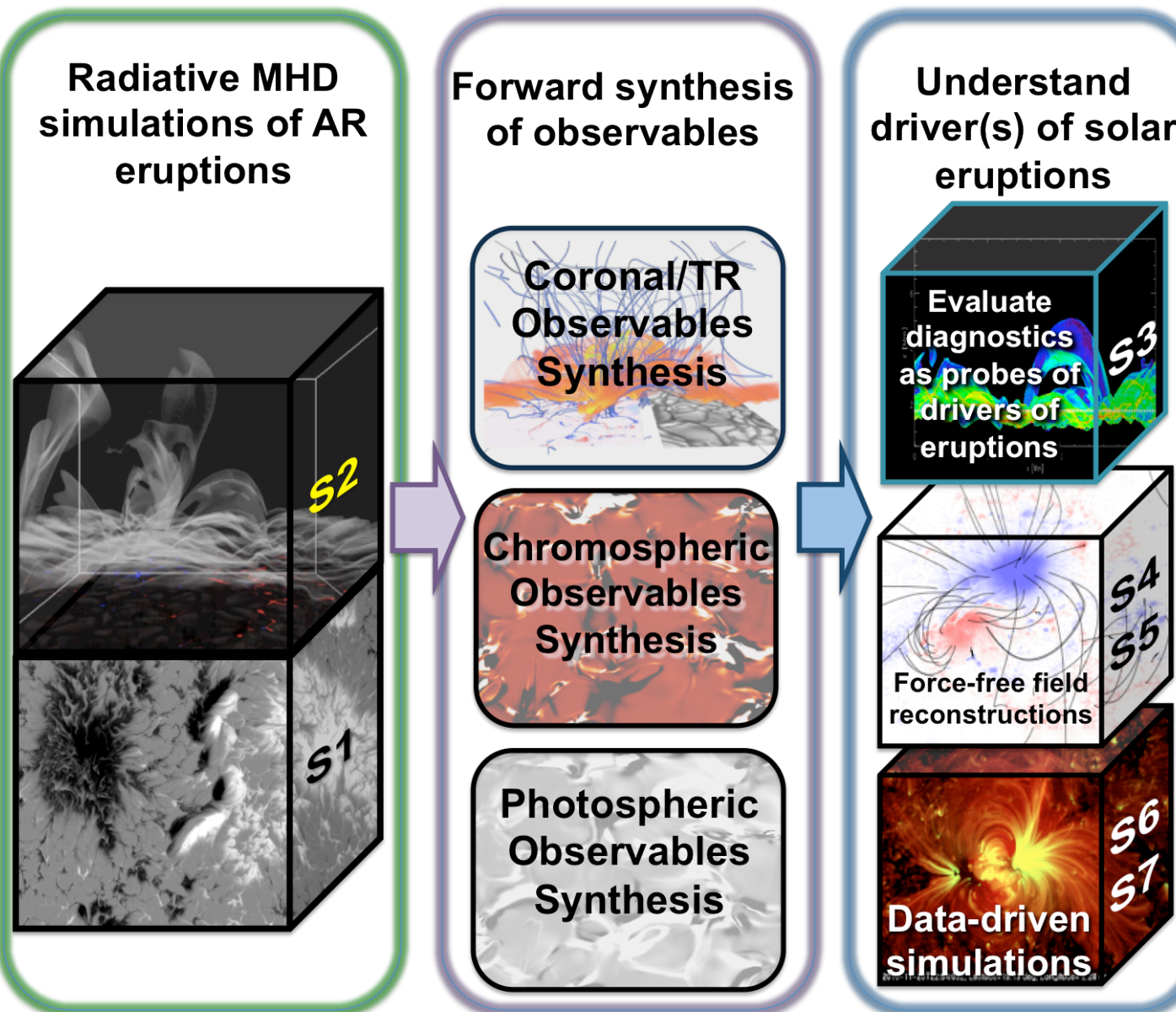
Jejčič, Heinzel & Kleint (2018): SDO Observations of X8.2 limb flare-loop emission detected in SDO/HMI.

Heinzel & Shibata (2018):

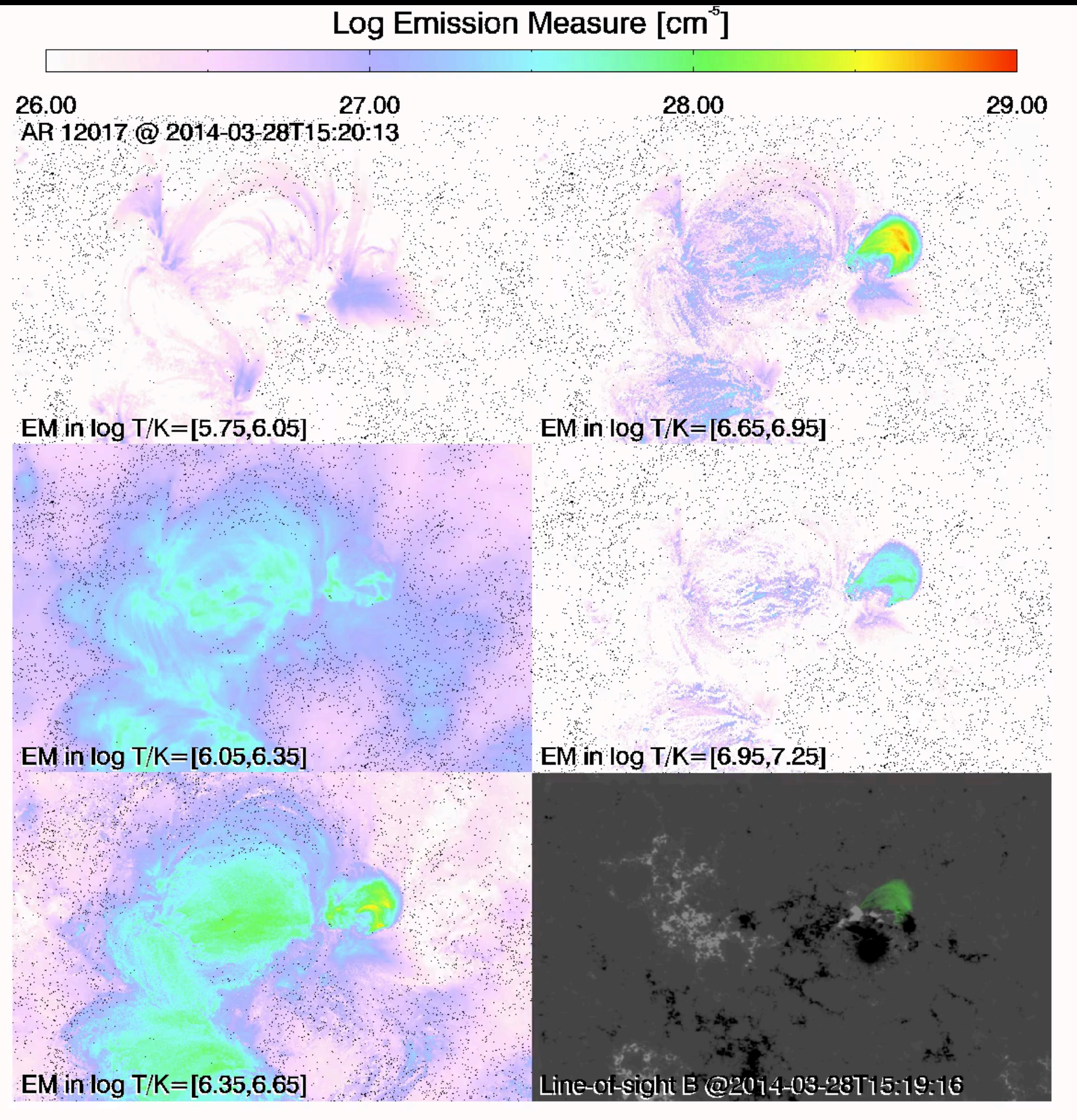
" This new scenario for interpreting superflare emission suggests that the observed WL flux is due to a mixture of the ribbon and loop radiation and can be even loop-dominated during the gradual phase of superflares."

NASA Heliophysics Grand Challenges Research (HGCR): Physics and Diagnostics of the Drivers of Solar Eruptions

Cheung, Rempel et al. (Nature Astronomy 2019)



A collaboration between LMSAL (PI: Cheung), NCAR, BAERI,
SAO & U Oslo, supported by NASA Grant NNX14AI14G



NOAA AR 12017:
one X-class ("Best Observed X-flare"), 3 M-class, and about two dozen C-class flares

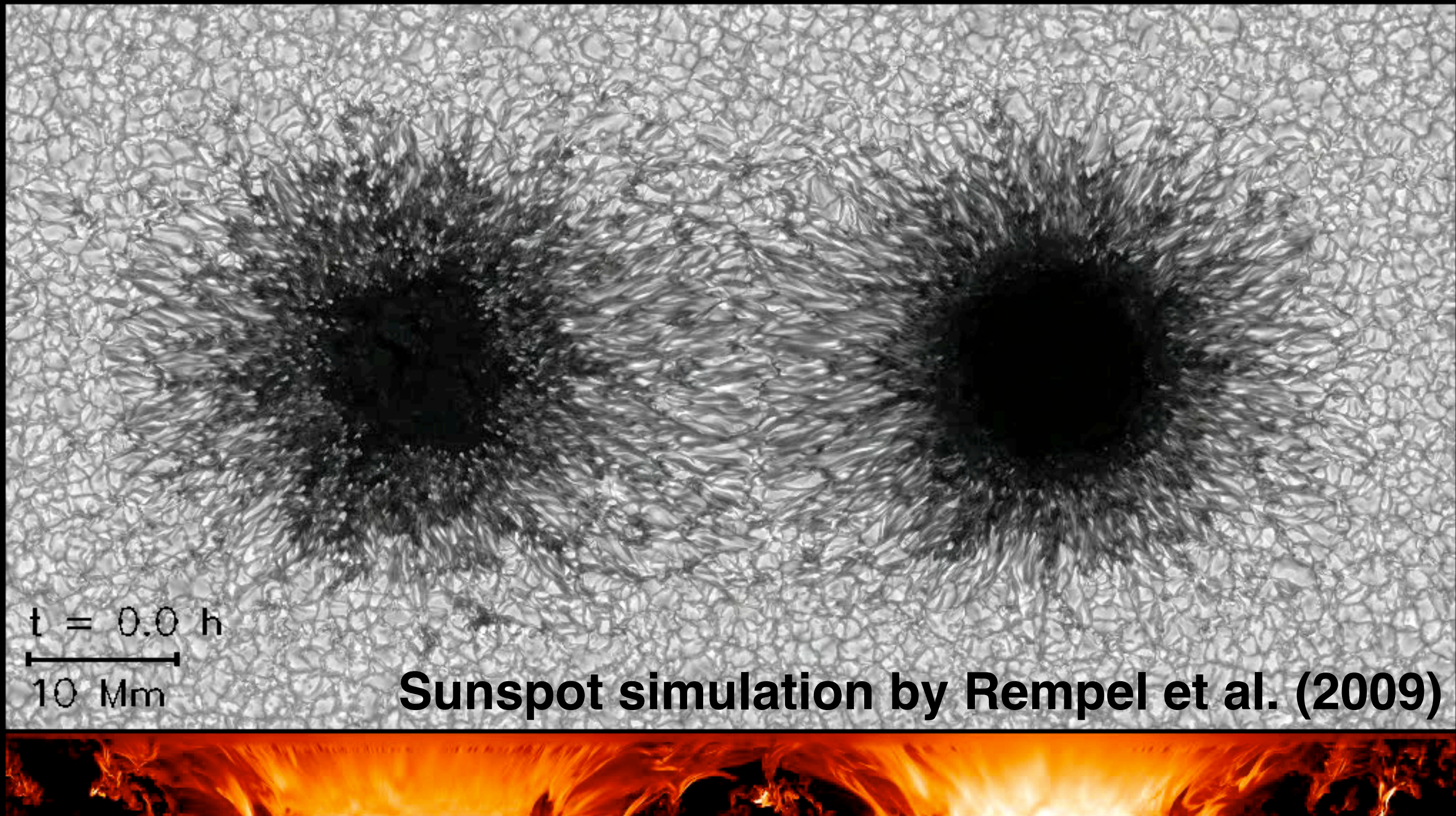
Sunquake: Judge et al. (2014)

Filament Eruption before X-flare: Kleint et al. (2015)

IRIS Fe XXI FUV spectra: Young et al. (2015)

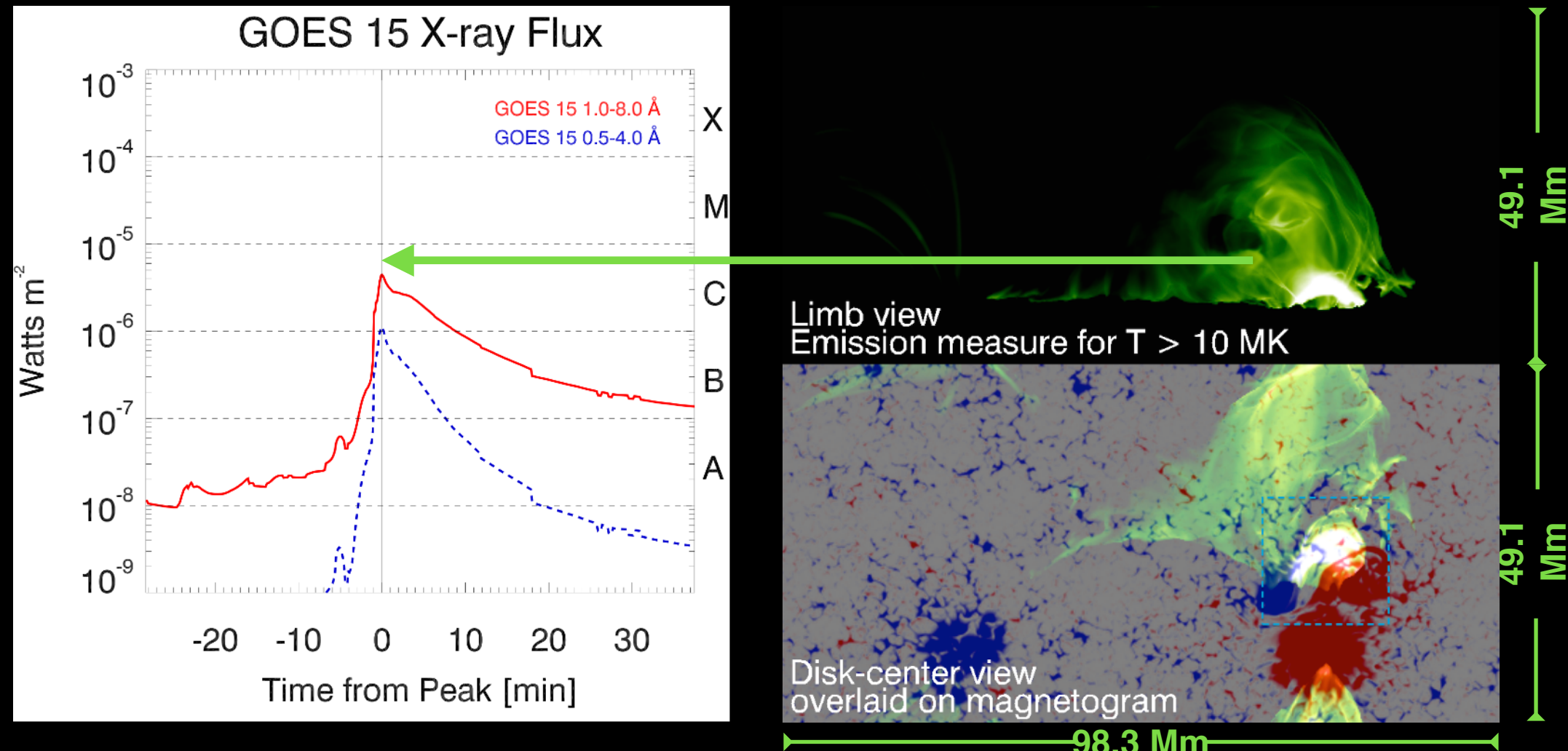
Chromospheric Evaporation: Li et al. (2015)

Sunspots Simulation with MURaM

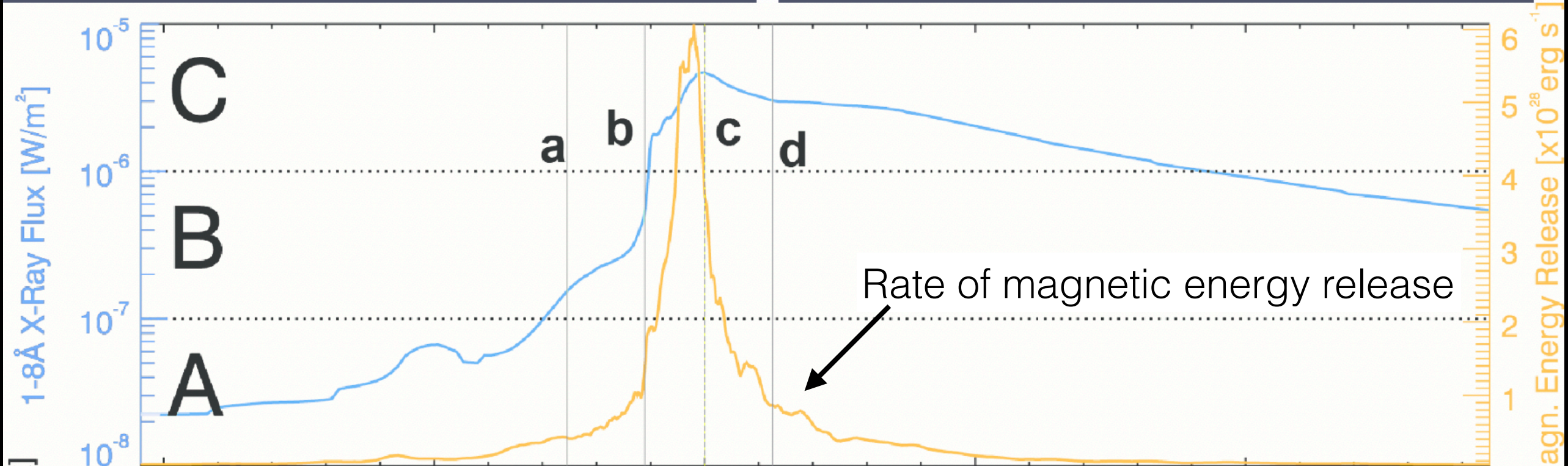
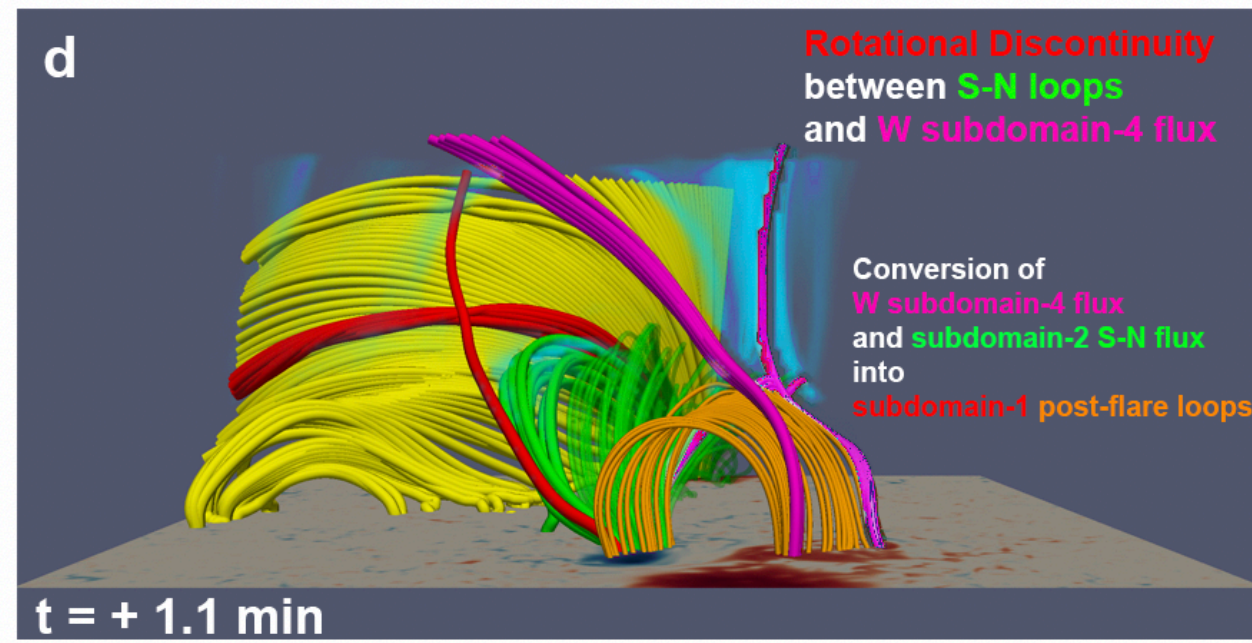
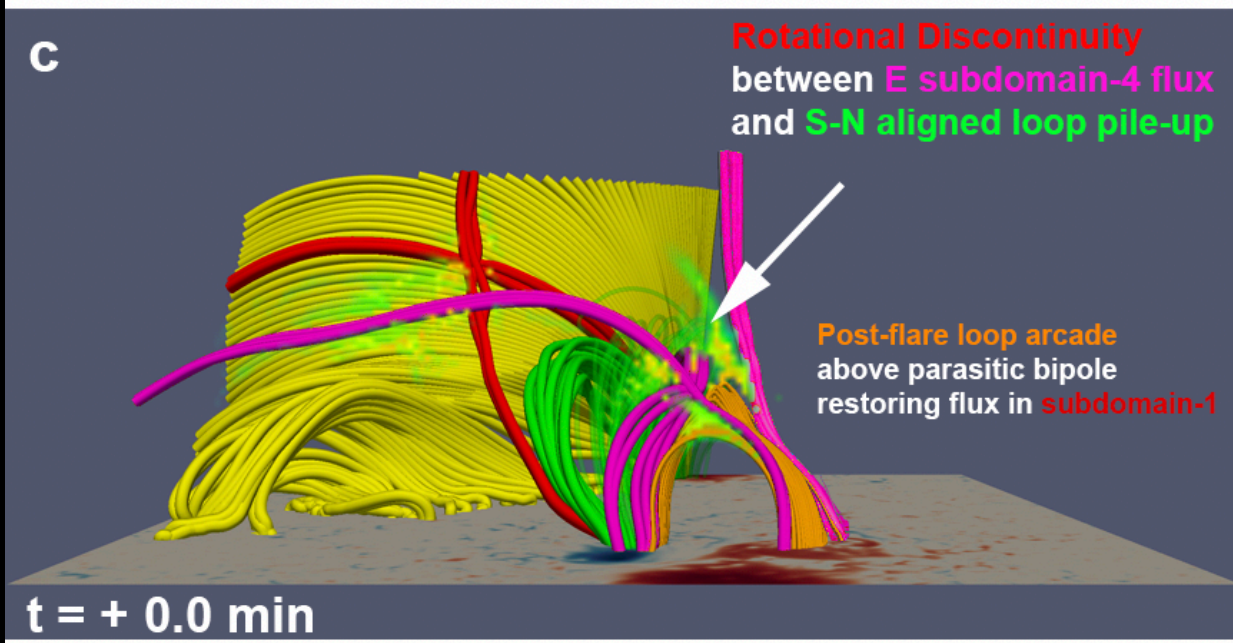
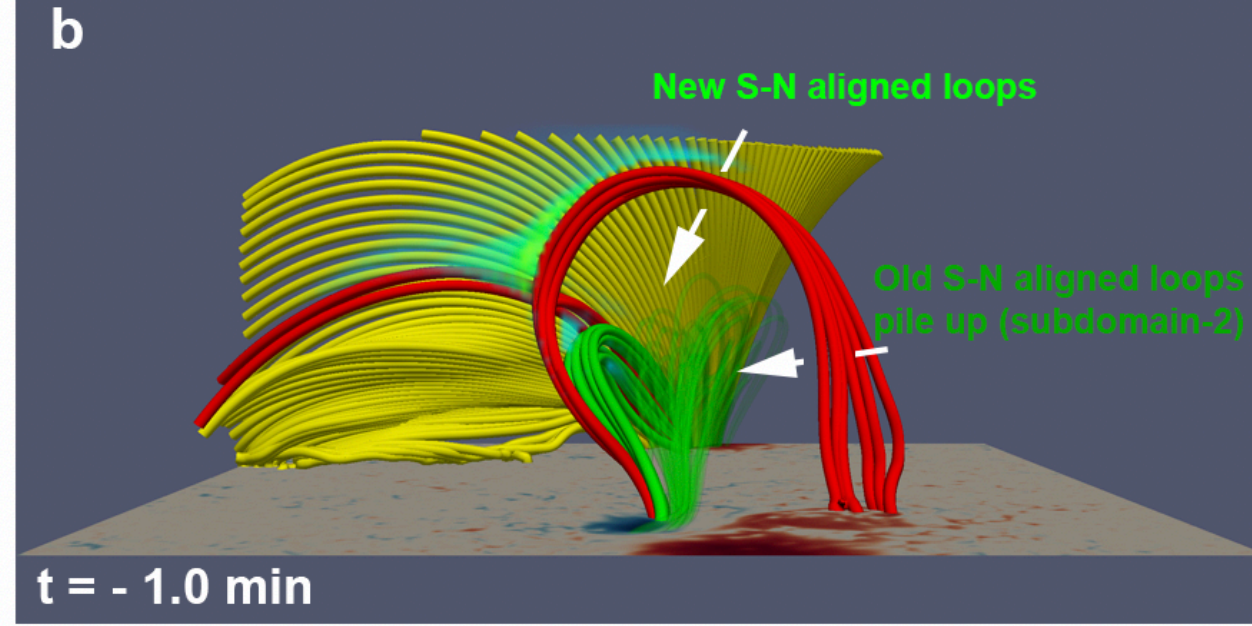
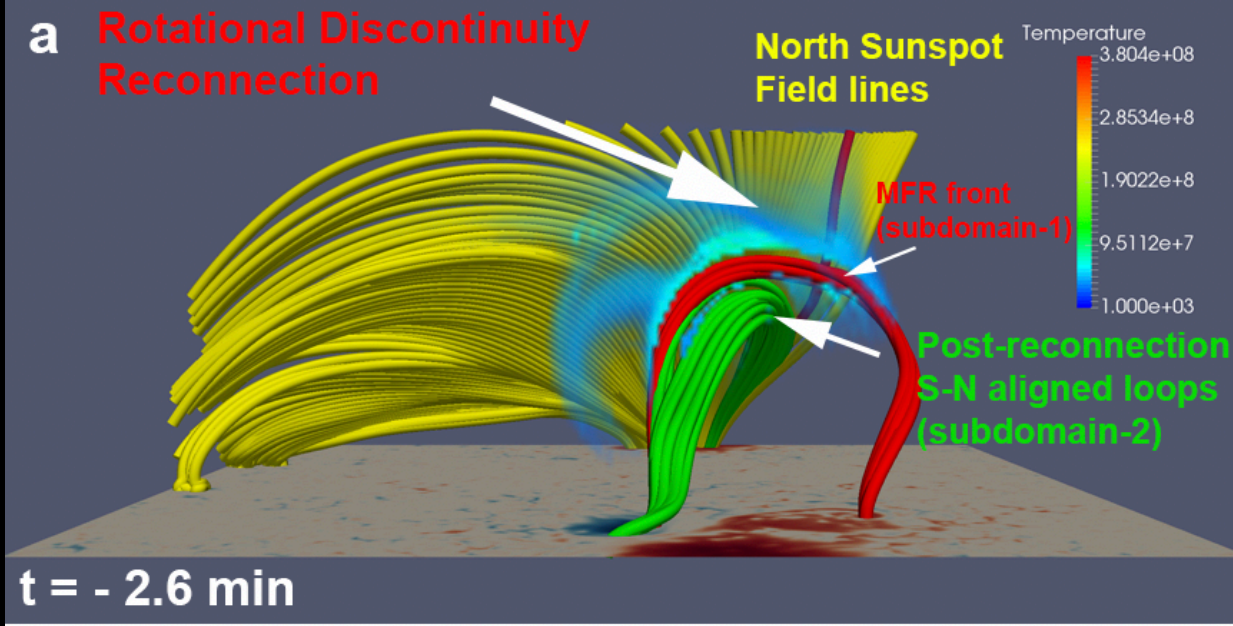


Top: Emergent gray intensity. Bottom: Vertical slice of $|B|$

Synthetic GOES X-ray Light Curves

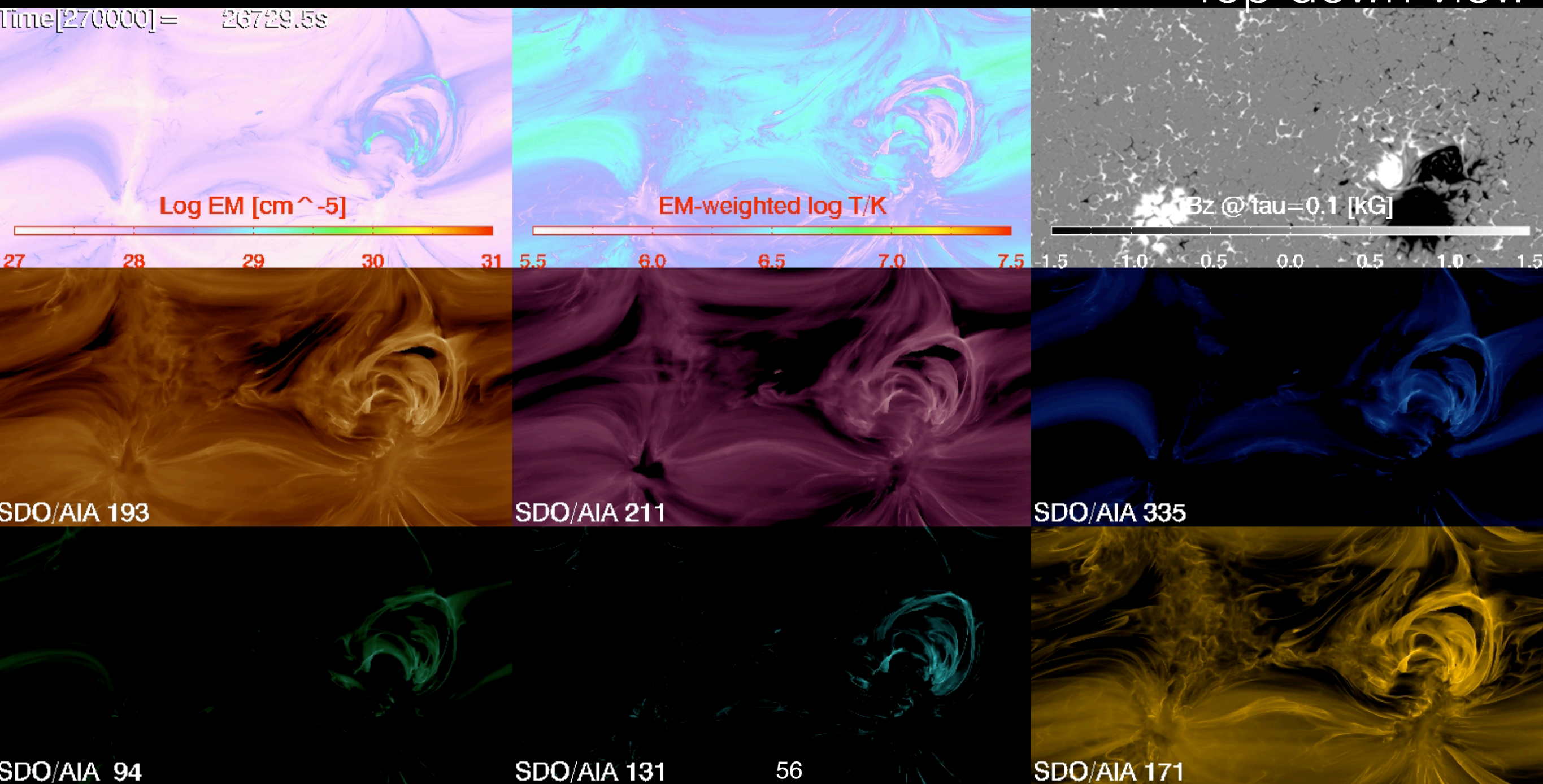


C4 flare if measured by detectors on GOES 15. The free magnetic energy (actual minus potential field) dropped by $\sim 5 \times 10^{30}$ erg ($\sim 10\%$) over 5 minutes.

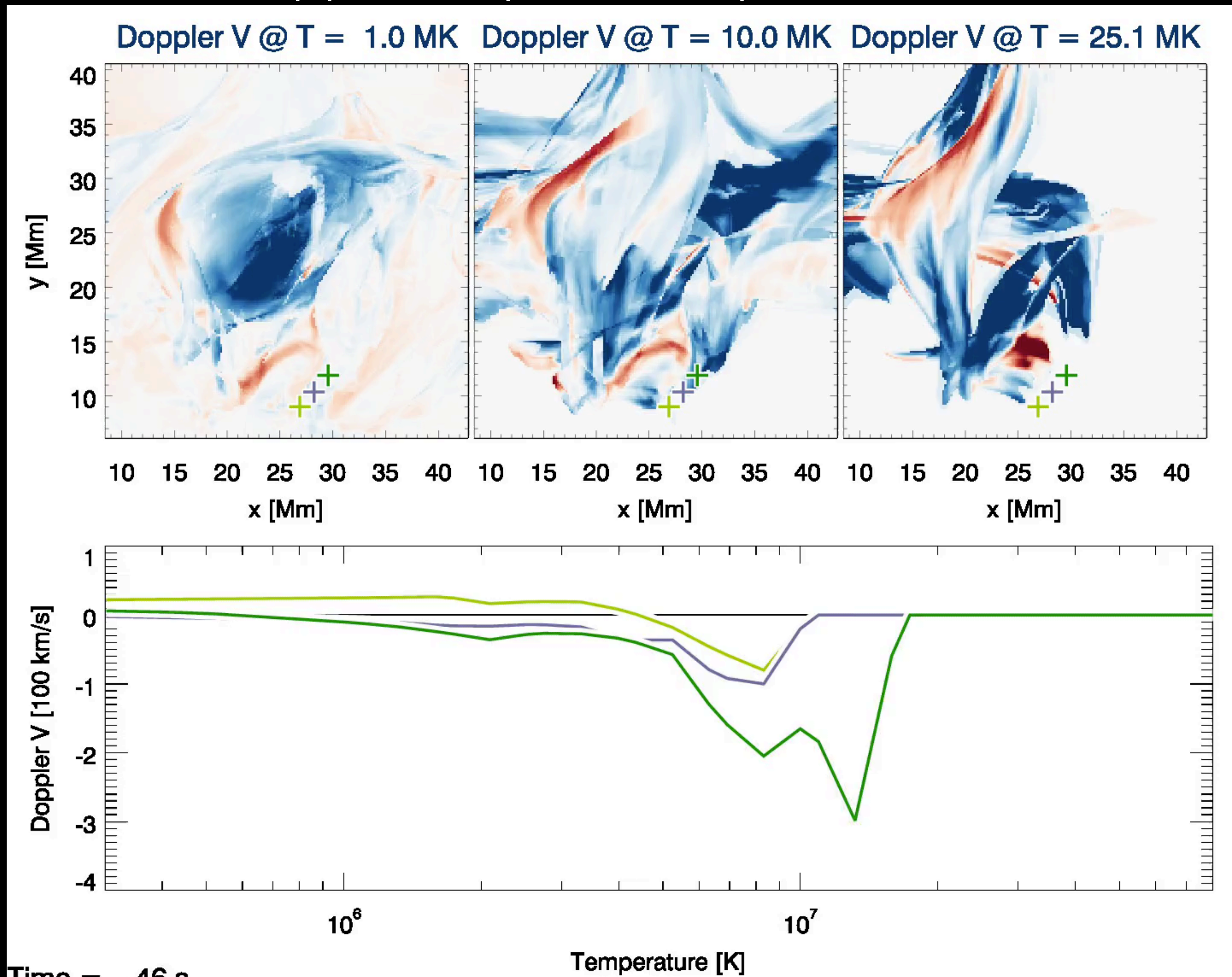


Synthetic SDO/AIA EUV Images

Top down view



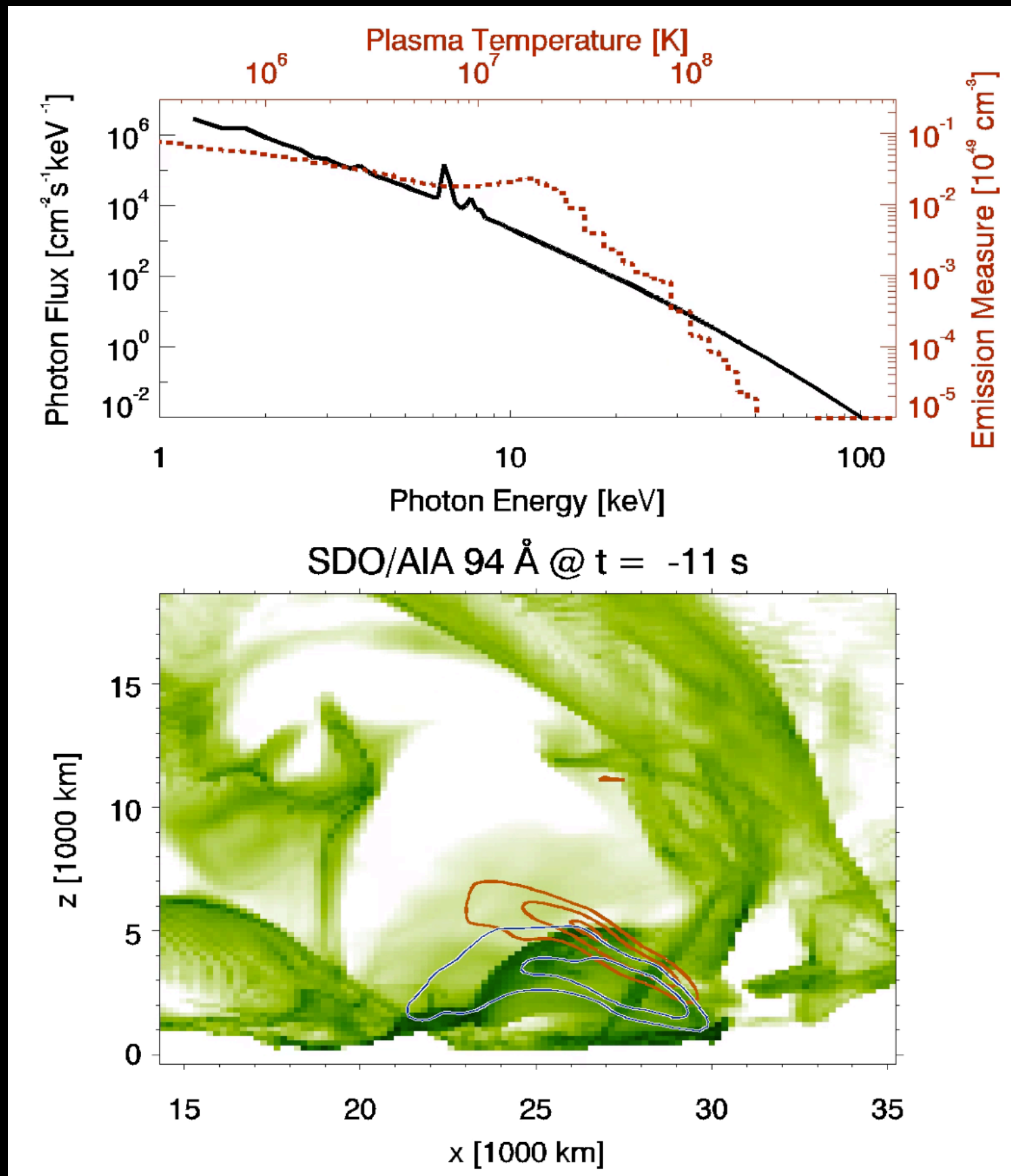
Synthetic Doppler Maps from Optically Thin Radiation



Using thermal bremsstrahlung, the model yields power law-like shapes for the X-ray spectrum.

The multi-thermal nature of the magnetic structure gives rise to the apparent non-thermal behavior.

Above-the-loop-top harder X-ray sources (> 25 keV) are located above softer loop sources.

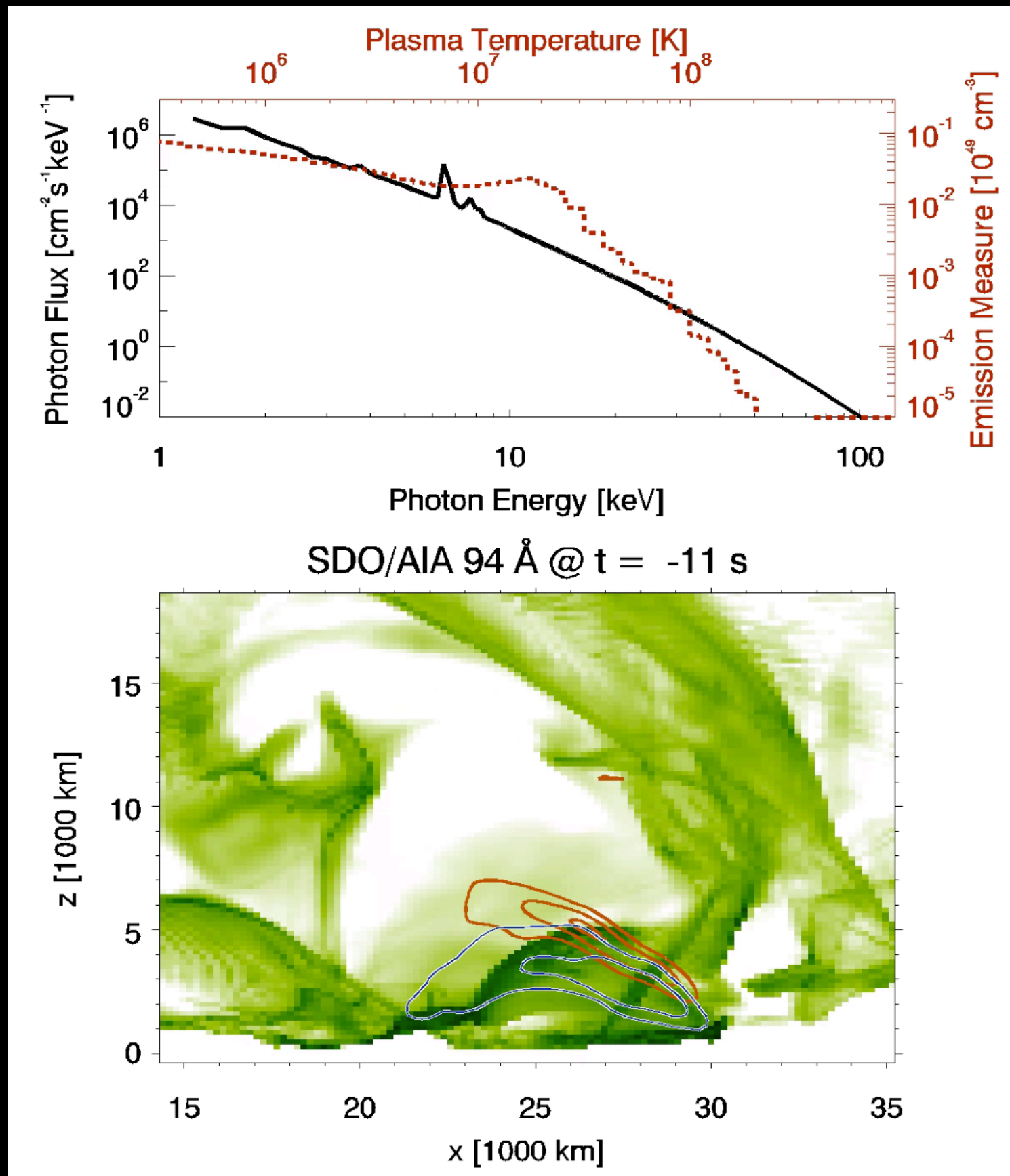


Hard x-rays ≥ 25 keV 6 \leq Soft x-rays ≤ 12 keV

Using thermal bremsstrahlung, the model yields power law-like shapes for the X-ray spectrum.

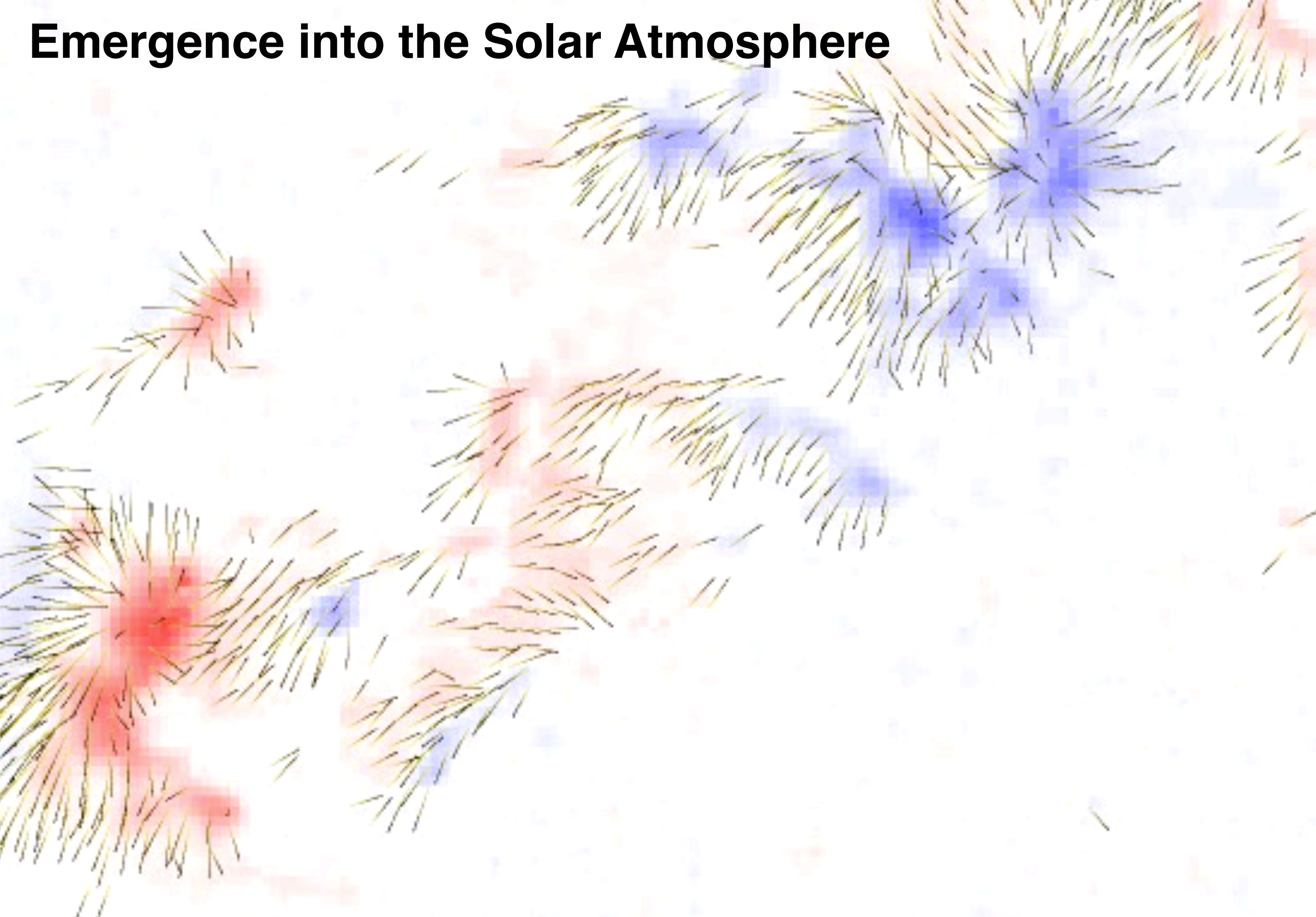
The multi-thermal nature of the magnetic structure gives rise to the apparent non-thermal behavior.

Above-the-loop-top harder X-ray sources (> 25 keV) are located above softer loop sources.



Hard x-rays ≥ 25 keV 6 \leq Soft x-rays ≤ 12 keV

Emergence into the Solar Atmosphere



Credit: SDO/HMI (visualization by Keiji Hayashi)

"Magnetograms" from a Magnetofriction* simulation

B_z at 2011-02-10T14:11

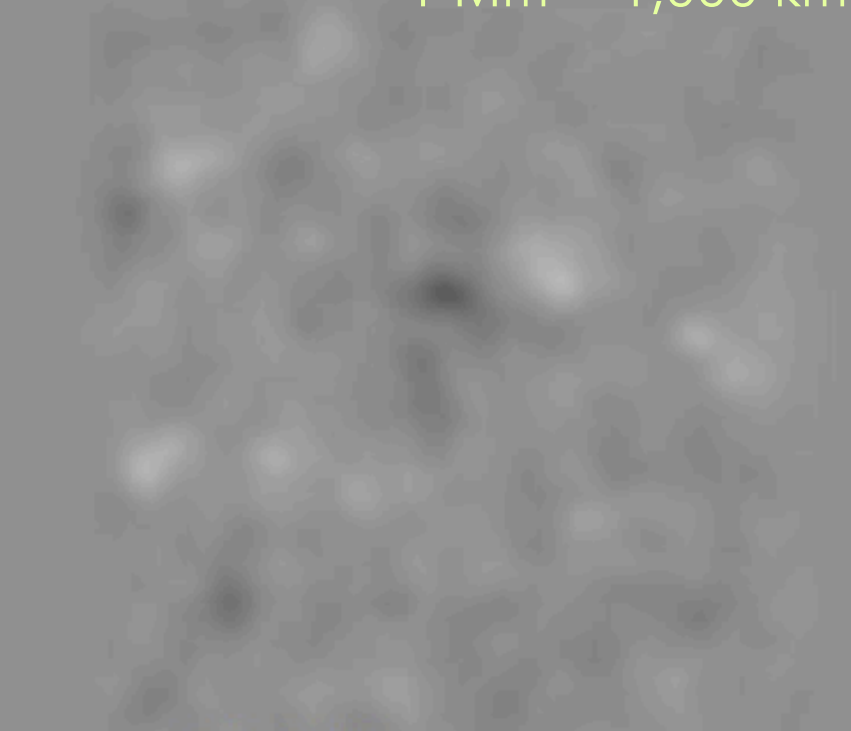
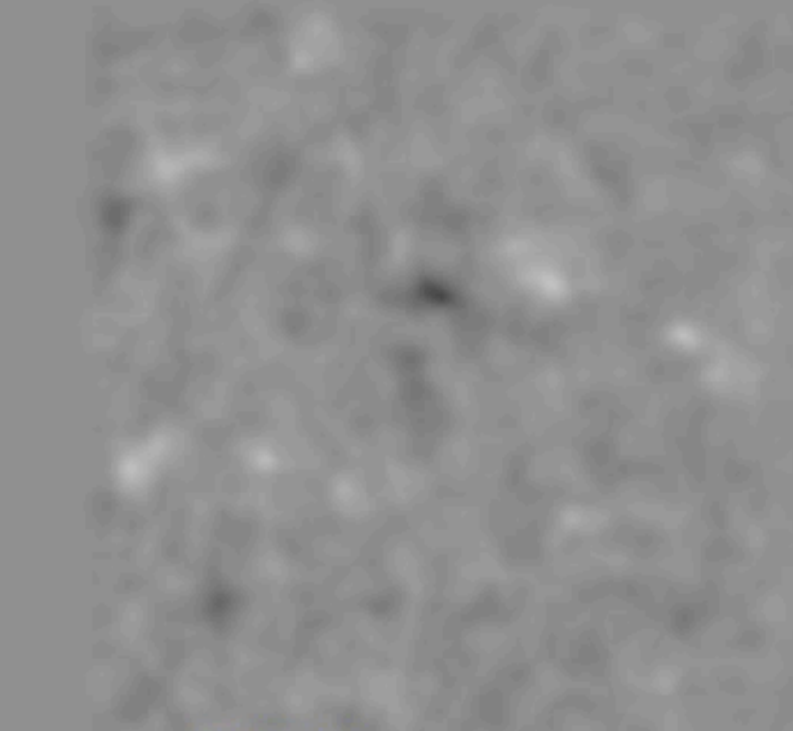
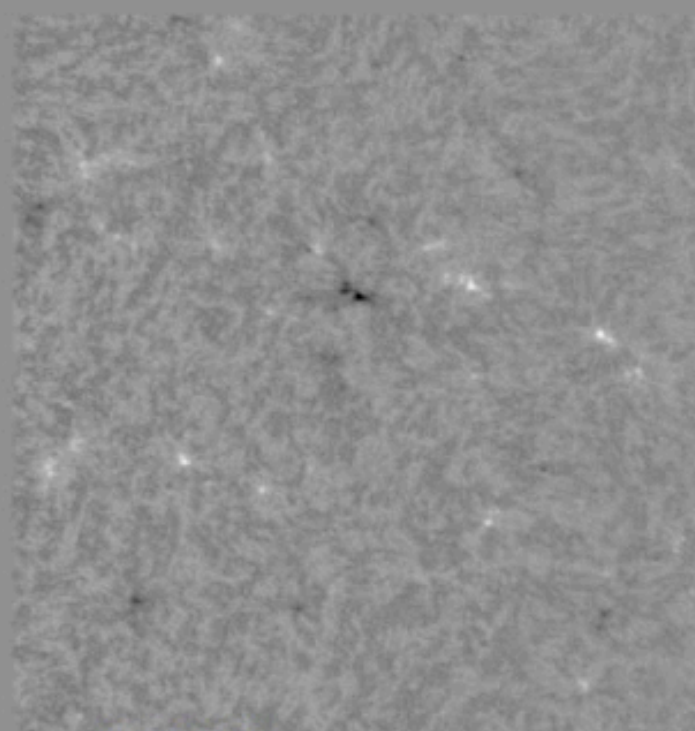
*Magnetofriction means assuming plasma \mathbf{v} to be proportional to the Lorentz force

$z = 8.1 \text{ Mm}$

$z = 54.2 \text{ Mm}$

$z = 135.4 \text{ Mm}$

1 Mm = 1,000 km



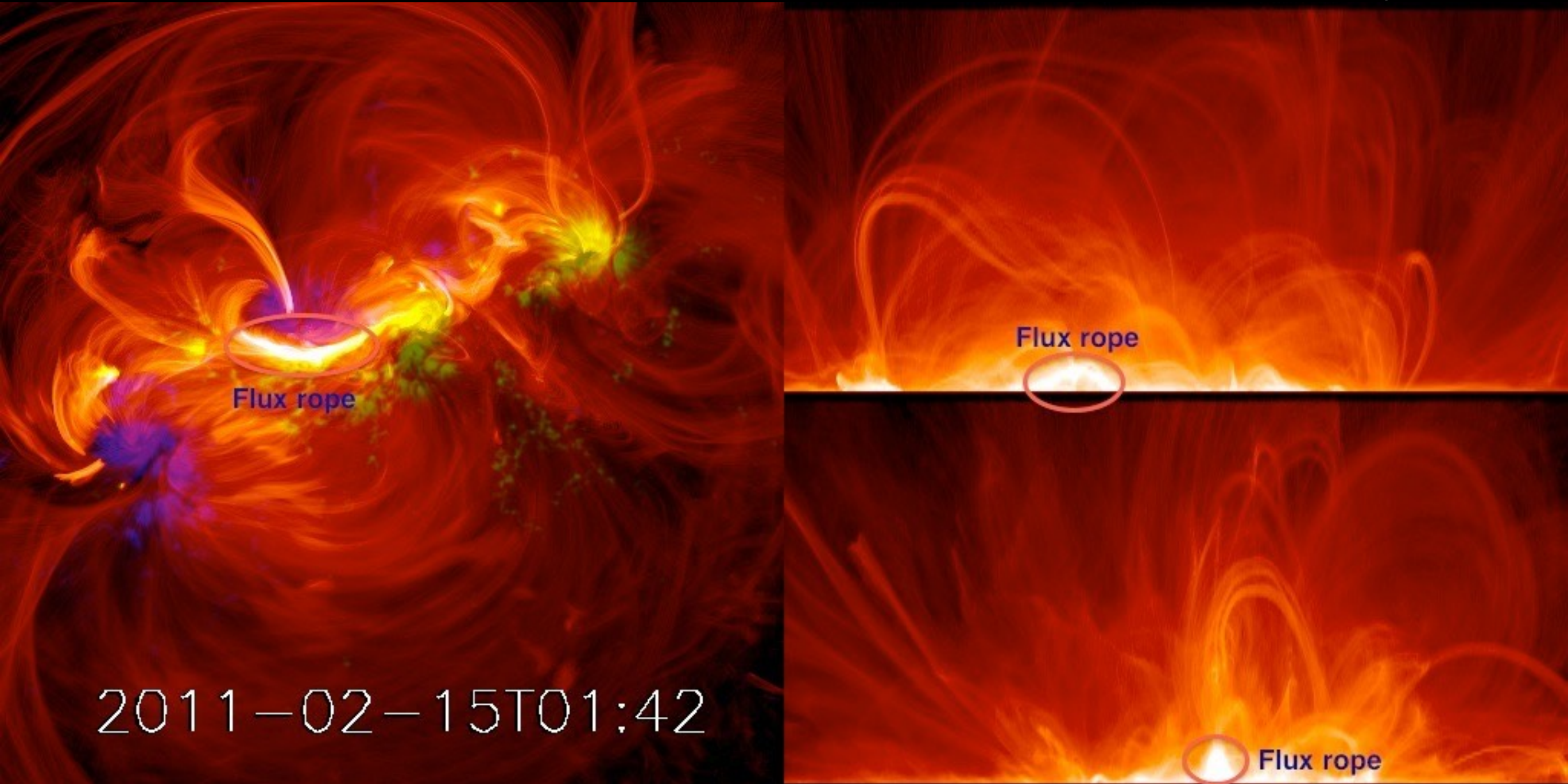
$z = 0.0 \text{ Mm}$

$z = 2.7 \text{ Mm}$

$z = 5.4 \text{ Mm}$

From the CGEM collaboration between UC Berkeley, Stanford and LMSAL (Fisher et al. 2015).

Visualization of field lines based on current density



There is no impulsive eruption at the time of the observed X-flare. However, moments before this time, a current-carrying flux rope is observed to form and is eventually ejected, though the rise time is on the order of hours.

Summary and Outlook

- The Sun is a natural laboratory for many astrophysical processes (e.g. heating mechanism of plasmas, acceleration of stellar winds, interpretation of radiative signatures). In particular, a lot of physical information is encoded at EUV wavelengths.
- SDO/AIA has excellent temperature coverage of the corona (quiescent and flaring), and provides critical remote sensing diagnostics to observations by the Daniel K Inouye Solar Telescope (DKIST).
- White light flares not well understood. Usually WL emission is assumed to be black-body radiation @ 10 kK. What is the WL contribution due to flare loops?
- MHD models of the solar corona increasingly applied to test exoplanet habitability (w.r.t. space weather impacts on life). Are these models valid for other stars?
- Synthetic observables in a data-inspired flare simulation (Cheung, Rempel et al. 2019) qualitatively match observations of flares. For example, non-thermal-like X-ray spectra can result from multithermal distribution of plasma (in our model).
- The SDO dataset is a treasure trove of information for physics-based and for ML models (Bobra & Mason 2018; e-book for ML for Heliophysics; Galvez et al. 2019: A ML Dataset for SDO).